

The Importance of Chromophore Rigidity on the Efficiency of Blue Thermally Activated Delayed Fluorescence Emitters

Nadzeya A. Kukhta,^a Andrei S. Batsanov,^a Martin R. Bryce,^{a,*} Andrew P. Monkman^{b,*}

^aDepartment of Chemistry, Durham University, South Road, Durham, DH1 3LE, UK.

^bDepartment of Physics, Durham University, South Road, Durham, DH1 3LE, UK.

KEYWORDS. Azepine, dual photoluminescence; conformer; DFT

ABSTRACT. Four new symmetrical donor–acceptor–donor (D–A–D)-type molecules are reported with diphenylamine (DPA) or 10,11-dihydro-5*H*-dibenz[*b,f*]azepine (Az) as electron donors and 9,9-dimethylthioxanthene-*S,S*-dioxide (TXO2) as the electron acceptor. The donors are attached at different positions on the acceptor core – either *para* or *meta* to the sulfone unit. This series provides new insights into the effects of chromophore rigidity/flexibility on the efficiency of TADF. The molecules have been characterized by X-ray crystallography, in-depth photophysical studies and by theoretical calculations. The clear differences observed in the photophysical properties when using DPA or Az as a donor are shown to originate from different

geometries of the donor unit which, in turn, influence the geometry of the nitrogen lone pair and the donating strength of the corresponding fragment. Thus, a *para*-substituted Az derivative demonstrated blue TADF in polar media, while the compounds with more flexible DPA units did not show delayed fluorescence. To obtain deep-blue emitters weaker donating units are needed. A more flexible donor unit leads to increased local excited state (donor) LE emission and reduced TADF. However, a certain amount of flexibility has to be present to ensure deep-blue TADF.

Introduction

Organic light emitting devices (OLEDs) with external quantum efficiencies (EQEs) >25% are now well established by using intramolecular charge transfer donor (D)–acceptor (A) type emitter molecules which harvest non-emissive triplet excited states and convert them to singlet states via thermally activated reverse intersystem crossing (rISC). The exploitation of triplet states via this mechanism leads to thermally activated delayed fluorescence (TADF) which was originally termed E-type delayed fluorescence.¹ TADF overcomes the spin-statistical limit of 25% on the singlet production yield arising from direct charge recombination² after electrical excitation. A plethora of various color TADF emitters have been reported recently.^{3–9} However, only a few deep-blue emitters possessing good color purity and high stability are known.^{5,8,10–14} The problems of instability, relevant color coordinates and color purity^{15–18} motivate the design of new blue emitters. However, the choice of the electron-donating units suitable for achieving efficient blue TADF is quite limited.^{5,19}

Efficient TADF requires a strong charge transfer (CT) interaction between the D and A units. Strong D and A moieties usually have a rigid molecular skeleton. However, the involvement of strong D and A fragments lowers the energies of ^1CT and ^3LE states,²⁰ which makes it difficult to obtain deep-blue emission, even though a vanishing ΔE_{ST} can be reached. Therefore, in order to design a deep-blue TADF emitter, careful tuning of D/A strength along with molecular geometry has to be considered. For instance, although fully conjugated 3,6-substituted carbazole is the most thermally and chemically stable donor utilized in deep-blue TADF emitters,^{10,21–24} its tendency for triplet-triplet annihilation,^{25,26} dimer formation^{27,28} and lack of steric control of the D–A dihedral angle^{23,29,30} make it a difficult chromophore to control in the design of new emitters. Diphenylamine (DPA) also suffers from the same issues in attaining the optimum molecular geometry which is crucial for HOMO/LUMO separation and a small ΔE_{ST} . Although there are several green, yellow and red TADF emitters with DPA donors,^{31–35} only a few inefficient blue TADF emitters utilizing the DPA unit have been reported.^{11,29} More control over the molecular geometry can be achieved using acridine (Ac) donors. A number of efficient blue TADF emitters employing acridine are known.^{9,36,37} However, due to the high electron-donating strength of acridine^{5,36} it is complicated to achieve deep-blue TADF. Thus, a fragment with moderate donating strength and conformational flexibility might offer a better solution. For this reason we were attracted to 10,11-dihydro-5*H*-dibenz[*b,f*]azepine (Az) which has been used in hole-transporting materials,^{38,39} but to the best of our knowledge has not previously been suggested as a component of TADF emitters. Taking into account the recent report on the ultralong phosphorescence of Az,⁴⁰ it is timely to investigate Az as the donor in TADF emitters.

This work presents a systematic study of non-conjugated arylamine donors for the design of blue TADF emitters with a D–A–D structure. We show that by manipulation of the rigidity of the

donor unit it is possible to achieve a trade-off between structural and photophysical properties leading to deep-blue TADF emitters. We present four derivatives of 9,9-dimethylthioxanthene-*S,S*-dioxide (TXO2) featuring Az and DPA donors attached at different positions on the acceptor core. A thorough photophysical investigation is supported by theoretical calculations. The benefits and drawbacks of this molecular design strategy are discussed. A comparison is also made with the literature compound 2,7-bis(9,9-dimethylacridin-10-yl)-9,9-dimethylthioxanthene-*S,S*-dioxide (***p*-DDMA-TXO2**).^{9,36} The importance of the control of molecular conformation in TADF emitters is emphasized. Unlike previous work which has focused on controlling the dihedral angle around the D–A bonds and sterically restricting D–A bond rotation by *ortho*-substitution,^{41–44} the present work concerns how conformational effects remote from the D–A bonds can affect the whole D–A–D chromophore.

Experimental section

The synthesis and structural characterization of the azepine and diphenylamine derivatives are given in detail in Section S1 of the Supporting Information. Two types of samples were studied in this work: solutions (10^{-3} to 10^{-5} M) and films produced in Zeonex matrix (5 wt%). All of the solutions were diluted in different solvents and stirred for several hours. To remove all of the oxygen dissolved in the solutions, and to perform the degassing test and delayed fluorescence measurements, the solutions were degassed by four freeze–pump–thaw cycles. Films in the Zeonex matrix were fabricated by drop-casting onto quartz substrates. Steady-state absorption and emission spectra were acquired using a UV-3600 Shimadzu spectrophotometer and a Jobin Yvon Horiba Fluoromax 3, respectively. Time-resolved spectra were obtained by exciting the sample with a Nd:YAG laser (EKSPLA), 10 Hz, 355 nm/266 nm or by using a nitrogen laser, 10 Hz, 337 nm. Phosphorescence, prompt fluorescence (PF), and delayed fluorescence (DF) spectra

and decays were recorded using nanosecond gated luminescence and lifetime measurements (from 800 ps to 1 s) with either a high energy pulsed Nd:YAG laser emitting at 355 nm (EKSPLA) or a N₂ laser emitting at 337 nm with pulse width 170 ps. Emission was focused onto a spectrograph and detected on a sensitive gated iCCD camera (Stanford Computer Optics) having sub-nanosecond resolution. PF/DF time resolved measurements were performed by exponentially increasing the gate and delay times. The delay and integration times are chosen in a way that the next delay is set at a time longer than the previous delay+integration time. Therefore, no spectral overlap exists between the spectra corresponding to successive delays. The curve obtained directly from this process does not represent the real luminescence decay. However, this is easily corrected by integrating the measured spectra and dividing the integral by the corresponding integration time. In this way, each experimental point represents a snap-shot of the number of photons emitted per second at a time $t = \text{delay} + (\text{integration time})/2$. The luminescence decay is then obtained by plotting each experimental point against time, and fitting with sum of exponentials when required. In this way we are able to collect the entire emission spectrum decaying over 8 decades in time and in a single experiment. For initial development of these methods see previously published literature.⁴⁵ Computations were performed with the Gaussian 09 package⁴⁶ using different density functional theory (DFT) methods. The isolated molecules were optimized at the rBMK/6-31G (d) level in the gas phase. The spectroscopic properties of the molecules were calculated by means of time dependent DFT (TDDFT)^{47,48} calculations employing 6-31G (d) basis set.

X-ray crystallography. Diffraction experiments (Table S1) were carried out on a Bruker 3-circle D8 Venture diffractometer with a PHOTON 100 CMOS area detector and I μ S microsources with focusing mirrors, using APEX3 v.2016.1-0 software (© Bruker, 2016).

Crystals were cooled to 120 K using Cryostream (Oxford Cryosystems) open-flow N₂ gas cryostats. ***m*-DAz-TXO2**, ***p*-DDPA-TXO2**, ***m*-DDPA-TXO2** and its hexane/DCM solvate were studied with Mo-*K*α radiation, while Cu-*K*α radiation was used for two weakly diffracting solvates of ***p*-DAz-TXO2** with DCM and acetone, respectively. Of these, ***p*-DAz-TXO2**·CH₂Cl₂ was also studied (at 100 K) using synchrotron radiation (I19 beamline at Diamond Light Source, double crystal Si(111) monochromator); the data were collected on a dual air-bearing fixed- γ diffractometer with a Dectris Pilatus 2M pixel-array photon-counting detector⁴⁹ and converted to Bruker format using `cbf_to_sfrm.py` program.⁵⁰ Reflection intensities were integrated with SAINT 8.38A program (© Bruker, 2017) and corrected for absorption by SADABS program⁵¹ based on Laue equivalents and multiple scans. The structures of ***m*-DAz-TXO2**, ***p*-DAz-TXO2**·Me₂CO and ***p*-DAz-TXO2**·CH₂Cl₂ were solved by dual-space intrinsic phasing methods using SHELXT 2018/2⁵² or (for the latter) SHELXD programs,⁵³ other structures were solved by direct methods using SHELXS 2013/1 program.⁵⁴ All structures were refined by full-matrix least-squares using SHELXL software⁵⁵ on OLEX2 platform.⁵⁶ Full data (including structure factors) in CIF format is available as ESI and have been deposited with the Cambridge Structural Database, CCDC-1872344 to 1872350.

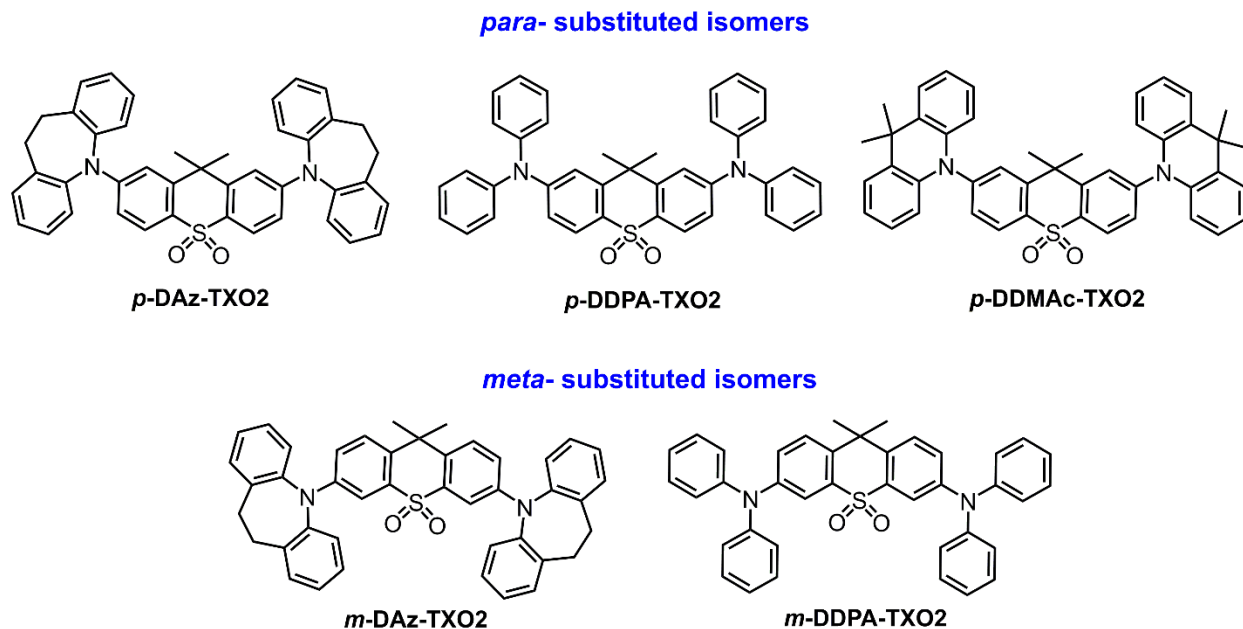
Each structure contains one symmetrically independent (host) molecule, except the unsolvated phase of ***m*-DDPA-TXO2** which has two molecules, of very similar conformation. The crystals of ***m*-DAz-TXO2** and ***p*-DDPA-TXO2** also contain no solvent. In the solvated form of ***m*-DDPA-TXO2**, the host molecule occupies a general position, while the *n*-hexane molecule lies astride a crystallographic inversion center and is partly replaced (with ca. 6% probability) by two DCM molecules related by the same inversion center. ***p*-DAz-TXO2** was crystallized and studied as two 1:1 solvates, with either DCM or acetone. Two independent determinations of the former

structure at 100 and 120 K gave essentially the same molecular geometries, the average of which is discussed below. Although the structure of the acetone solvate was determined with low resolution, it is sufficient for comparison of the molecular conformation with the other structures.

Results and discussion

1. Molecular design. 9,9-Dimethylthioxanthene-*S,S*-dioxide (TXO2) was chosen as the electron acceptor due to its stability and high triplet energy:⁹ furthermore, the *S,S*-dioxide group is known to promote a high intersystem crossing (ISC) rate, which in turn is helpful for increasing reverse ISC (rISC) in D–A conjugates.^{57,58} The choice of the donors was dictated by the requirement of a high triplet energy which is the case for 10,11-dihydro-5*H*-dibenz[*b,f*]azepine (Az) and diphenylamine (DPA) units.^{40,59} Furthermore, as these donors have differing molecular flexibility, the effects of the geometry of the nitrogen lone pair electrons can also be probed. While the phenyl rings are free to rotate in DPA, they are fused by the ethylene linker in Az. The influence of the linking position of the D–A units (*para*- vs *meta*- with respect to the sulfone group) was also studied. The chemical structures of the new Az and DPA compounds are presented on Scheme 1, along with the previously reported dimethylacridine analog (*p*-DDMAc-TXO2)^{9,36} for comparison.

The synthetic procedures for the Az and DPA compounds are reported in the SI. Palladium-catalyzed Buchwald-Hartwig coupling⁶⁰ was employed to link the D and A fragments. The identity and high purity of all the materials was confirmed by a combination of NMR spectroscopy, accurate mass spectrometry, elemental analysis and X-ray crystallography.



Scheme 1. Chemical structures of the new 10,11-dihydro-5*H*-dibenz[*b,f*]azepine (Az) and diphenylamine (DPA) derivatives, and the previously reported dimethylacridine (Ac) analog

2. *Crystal structures.* X-Ray molecular structures (Figures 1 and S1, Tables 1 and S1) revealed interesting differences between the Az and DPA derivatives on the one hand, and *para-/meta-* isomers on the other, in the solid state. Thus, while the TXO2 moiety is always folded, the angle between its arene ring planes is much wider in *m-* than in *p-*derivatives (including those reported earlier).^{61,62} In DPA derivatives each N atom is planar-trigonal, with the three arene rings around it twisted in a usual propeller-like fashion. In seven out of eight cases, the twist angle between the N atom plane and the adjacent TXO2 arene ring is $\geq 32^\circ$. The corresponding angles for phenyl rings vary widely and rather irregularly, according to crystal packing. Neither these angles nor the bond distances around the N atom suggest any preferred π -conjugation of its lone pair with TXO2 (or phenyls) in both forms of *m-DDPA-TXO2*. In *p-DDPA-TXO2*, shorter N-

C(TXO2) bonds and smaller (12.4°) twist at one (but not the other!) of these bonds may indicate intrinsically stronger conjugation, but this may be an effect of crystal packing.

On the contrary, the Az conformation is remarkably stable. In each case, it has a quasi-axial conformation with respect to the TXO2: *anti* in ***m*-DAz-TXO2** and *syn* in *both* solvates of ***p*-DAz-TXO2** which have very different crystal packing (the acetone molecule of crystallization occupies the intramolecular cleft, which in the DCM solvate is filled by an azepine moiety of another host molecule). The N atoms are nearly (although not exactly) planar, the conformation about the N-C(TXO2) bond is nearly eclipsed, while the large twists (62-87°) about the N-C(Az) bonds preclude any kind of conjugation. These differences in crystal structure translate into differences in the photophysical properties.

Table 1. X-ray molecular geometry

Compound	<i>m</i> -DAz-TXO2	<i>p</i> -DDPA-TXO2	<i>m</i> -DDPA-TXO2	<i>m</i> -DDPA-TXO2 ·solv.	<i>p</i> -DAz-TXO2 ·CH ₂ Cl ₂ *	<i>p</i> -DAz-TXO2 ·Me ₂ CO
TXO2 fold / °	149.0	134.5	149.3, 155.2	143.1	131.9	126
Az orientation	<i>Anti</i>	---	---	---	<i>Syn</i>	<i>Syn</i>
Twist N-C(TXO2) / °	7.3, 2.1	32.2, 12.4	33.1-47.2	35.4, 32.0	5.1, 0.6	14, 1
N-C(TXO2) / Å	1.393(3)	1.403(2)	1.420(2)	1.412(2)	1.390(4)	1.373(14)
N-C(Ph) / Å	---	1.413-1.434(2)	1.417-1.433(2)	1.414-1.438(2)	---	---
N-C(Az) / Å	1.437(3)	---	---	---	1.441(4)	1.45(2)
Twist N-C(Ph) / °	---	31.9-62.6	29.0-54.4	21.3-58.9	---	---
Twist N-C(Az) / °	62.1-82.7	---	---	---	65.6-85.0	80-87
Azepine fold / °	113.4, 120.5				114.0, 118.0	118.5, 121.5

*Mean of two determinations (at 100 and 120 K)

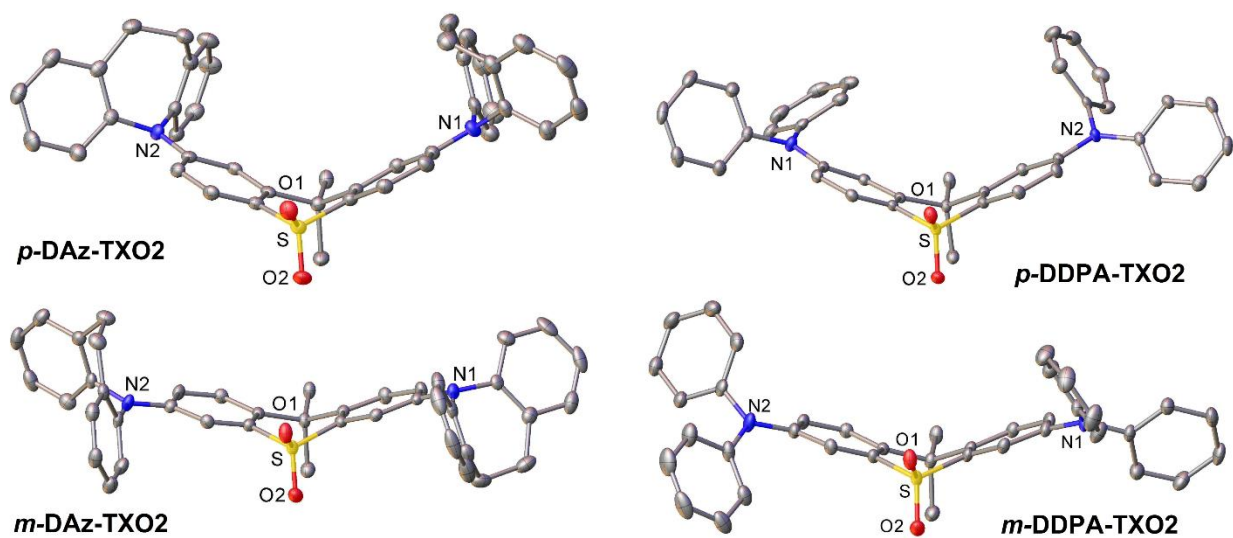


Figure 1. X-Ray crystal structures of the Az and DPA derivatives.

3. *Geometry optimization, theoretical absorption spectra.* In order to better understand the structural diversity in this series of D–A–D compounds, the geometry of the donating units, i.e. DPA, Az and Ac, along with the HOMO/LUMO wave function distributions and the theoretical absorption, were calculated (Figure S2). The BMK functional was chosen for the geometry optimization and prediction of the optical properties of all the studied molecules as it was shown to be pertinent for the description of the low energy band in absorption of D–A CT compounds.^{63–65} Upon restraining the rotation between two adjacent phenyl rings by means of an alkyl linker, the donors show relative planarization of the core in the order DPA < Az < Ac, with the dihedral angle decreasing from 25.31° to 0.04°. This leads in turn to an increase of the HOMO energy, proving that Ac is the strongest donor of the three. The trend is also observed in the theoretical UV/Vis spectra of the units (Figure S2 (b)): the spectral profile of the Ac absorption is the most red-shifted and features the lowest oscillator strength of the $S_0 \rightarrow S_1$ transition ($f = 0.0459$). The Az donor presents an intermediate case: due to the partial restraint of

the phenyl rotation it features a higher HOMO than that of DPA, and the highest oscillator strength of the first transition ($f = 0.4394$).

The overall geometry of the D–A–D derivatives is determined by the folded skeleton of the TXO2 acceptor, as well as the shape and position of the donor substituents (Figure 2). Generally, the DPA unit features a propeller shape with freely rotating phenyl rings. The torsional angles at the N–C bridging bonds are 31.6° for *p*-DDPA-TXO2 and 34.7° for *m*-DDPA-TXO2, respectively. On the contrary, for *p*-DAz-TXO2 and *m*-DAz-TXO2, where the Az unit possesses only limited flexibility this angle reaches a high value of 77.94° in *m*-DAz-TXO2. Overall, the *meta*-substituted derivatives show larger angles than the *para*-isomers (by $3\text{--}6^\circ$) presumably due to slightly interrupted conjugation in the *meta*-isomers. The optimized geometry of *p*-DDMAc-TXO2 is also presented for comparison (Figure S3). As expected, the methylene bridge in 9,9-dimethylacridine ensures a planar conformation of the donor, translating into the almost orthogonal (89°) arrangement of the D and A fragments.

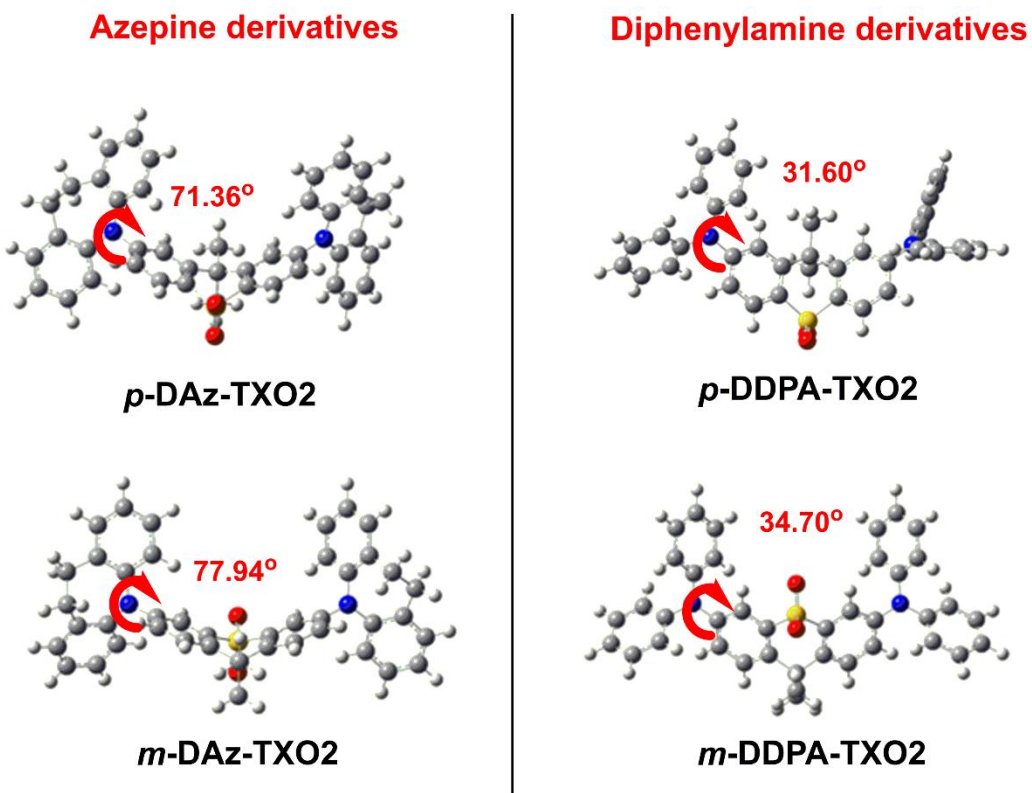


Figure 2. Optimized geometries of the Az and DPA derivatives (rBMK/6-31G(d)) in the ground state.

The differences in molecular geometry lead to a diversity in optical properties. To illustrate this, the UV/Vis absorption spectra were simulated at the TD-DFT rBMK/6-31G(d) level of theory (Figure S4). While the onset of absorption of all the derivatives is at 400 nm, major differences are observed in the spectral profiles of the Az- and DPA-based compounds. The absorption of ***p*-DAz-TXO2** and ***m*-DAz-TXO2** clearly features two well-resolved bands. In turn, the spectra of ***p*-DDPA-TXO2** and ***m*-DDPA-TXO2** have a broad Gaussian shape. Generally, the absorption of the *para*-substituted derivatives is red-shifted and has higher oscillator strengths compared to the *meta*- isomers. To reveal the nature of the lowest energy band (LEB), a selected set of pertinent excited states ($S_0 \rightarrow S_{1-3}$) were calculated, in which hole and electron distributions are described

by means of natural transition orbitals (NTOs)⁶⁶ (Figures 3 and S5). Thus, for ***p*-DAz-TXO2** the highest and lowest occupied NTO (HONTO and LUNTO, respectively) are localized on the donating (Az) and accepting (TXO2) parts of the molecule in the first two transitions. This observation agrees with the highest oscillator strength of $S_0 \rightarrow S_1$ ($f = 0.1558$) and indicates well-pronounced CT character of the LEB. However, a certain HONTO/LUNTO overlap in the case of two first excitations, and a delocalized donor $S_0 \rightarrow S_3$ transition (with small overlap into the acceptor) implies partial locally excited (LE) character to the transitions. On the contrary, the HONTO and LUNTO of $S_0 \rightarrow S_{1,2}$ are clearly delocalized across the DPA and TXO2 fragments in ***p*-DDPA-TXO2**. High oscillator strength (0.7031 and 0.2338 for $S_0 \rightarrow S_1$ and $S_0 \rightarrow S_2$, respectively) and delocalized wave functions are unmistakable features of LE excitations. A comparison of the *meta*-isomers ***m*-DDPA-TXO2** and ***m*-DAz-TXO2**, reveals a certain degree of CT character in the latter. However, the small oscillator strengths of the transitions and stronger wave function localization on the donor unit make the CT much less pronounced for the *meta* isomer than for ***p*-DAz-TXO2**. Similar dependencies of the CT/LE character for *meta* and *para* isomers of D–A–D molecules were previously discussed.^{26,33,41} However, Matulaitis et al. reported higher CT character and more efficient TADF in the *meta*-substituted isomer of a carbazole-triazine D–A system.⁶⁷

The acridine-based ***p*-DDMAc-TXO2** is quite different. The absorption spectrum features two well-resolved high energy bands with LE character and a very broad low intensity LEB onset at 420 nm, obviously of CT origin (Figure S4 (e)). Unlike ***p*-DAz-TXO2**, for ***p*-DDMAc-TXO2** all three first singlet HONTOs and LUNTOs of DDMA-TXO2 (Figure S6) are well separated with very minor orbital overlap, and S_1 and S_2 are degenerated. Such NTO distribution provides additional proof of a strong CT character of **DDMAc-TXO2**. However, due to the orthogonality

of the D and A units in *p*-DDMAc-TXO2, the oscillator strength values of the $S_0 \rightarrow S_{1-3}$ transitions are extremely small (0.0002-0.0008), which should translate into low PLQY, but this is not observed experimentally in hosts of certain polarity.⁹

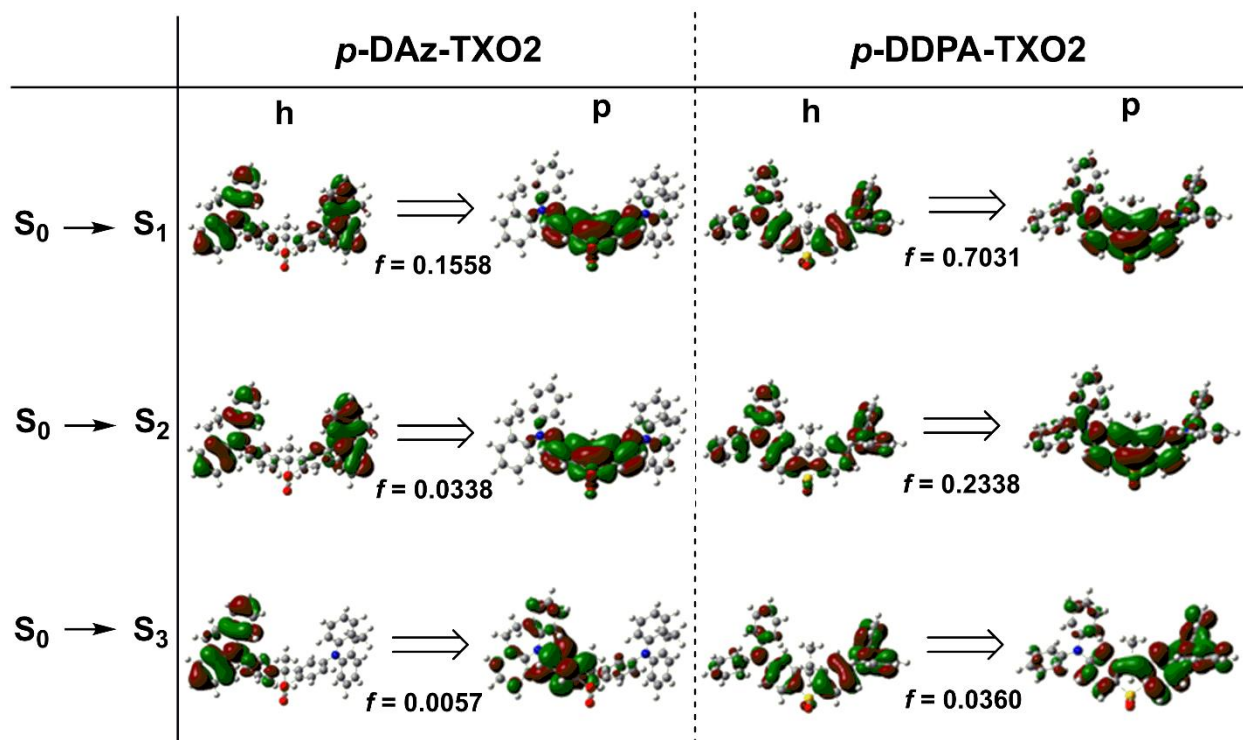


Figure 3. Natural transition orbitals (NTOs) corresponding to the first three singlet transitions in the absorption of *p*-DAz-TXO2 and *p*-DDPA-TXO2 (TD-DFT rBMK/6-31G(d))

To gain an insight into the nature of triplet emission, the NTOs of the T_1 state were calculated for the Az and DPA derivatives (Figure S7). Delocalization of the HONTO/LUNTO electron density distribution of *p*-DDPA-TXO2 and *m*-DDPA-TXO2 throughout the whole molecule explains the lower triplet energies (3.17 and 3.21 eV, respectively) when compared to those of the Az derivatives (3.31 and 3.64 eV). In contrast, the localized triplet of *m*-DAz-TXO2 (mostly on the D units) and the HONTO/LUNTO of *p*-DAz-TXO2 (involving both D and A units) is the origin of phosphorescence in these two compounds. In the case of *p*-DDMAc-TXO2 the

phosphorescence originates solely from the triplets of the acridine donor (Figure S6). This points to the role of increasing D–A dihedral angle in localizing the triplet states in the D and A fragments.

Table 2. Important parameters of the Az and DPA derivatives

Compound	S ₁ ^a / [eV]	T ₁ ^a / [eV]	ΔE _{ST} ^a / [eV]	S ₁ ^b / [eV]	T ₁ ^b / [eV]	S ₁ ^c / [eV]	ΔE _{ST} ^c / [eV]
<i>p</i> -DAz-TXO2	3.64	3.31	0.33	3.87	3.17	3.20	0.03
<i>m</i> -DAz-TXO2	3.99	3.64	0.35	3.61	3.01	3.26	0.25
<i>p</i> -DDPA-TXO2	3.88	3.17	0.71	3.43	3.01	3.30	0.29
<i>m</i> -DDPA-TXO2	3.90	3.21	0.69	3.32	2.94	3.28	0.32

^a Calculated using TD rBMK/6.31G(d); ^b estimated from the onset of PL (Phos) spectra, measured in Zeonex; ^c estimated from the onset of PL spectra measured in chloroform.

Finally, singlet/triplet energy diagrams (Table 2, Figure S8) clearly show the trends in ΔE_{ST}: *p*-DAz-TXO2 and *m*-DAz-TXO2 possess much smaller S₁-T₁ gaps (0.33 and 0.35 eV, respectively) than the DPA analogs (0.71 and 0.69 eV). Remarkably, the rigid acridine donor results in almost degenerate S₁₋₂, on the one hand, and T₁₋₃, on the other, giving rise to a negligible ΔE_{ST} of 0.043 eV in *p*-DDMAc-TXO2.

4. Optical and photophysical properties

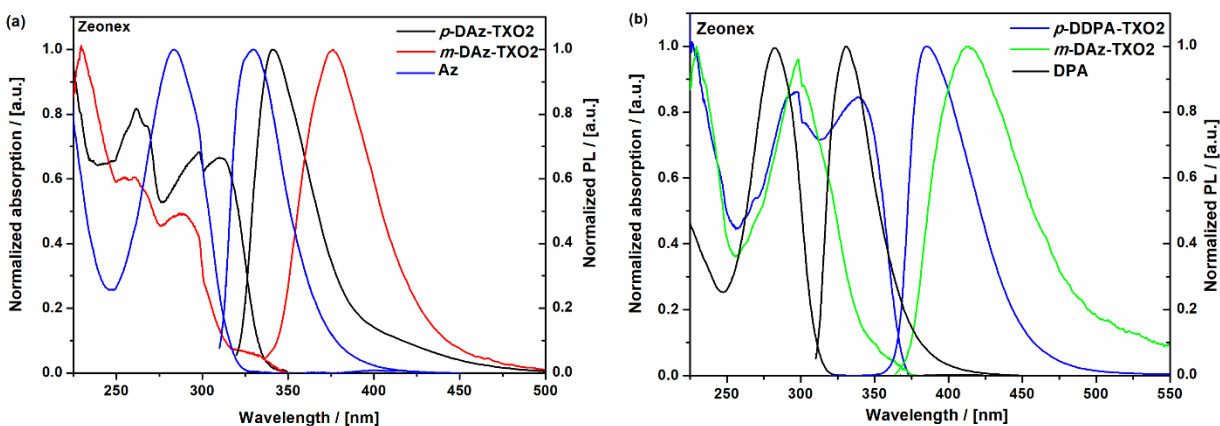
Absorption. The UV/Vis absorption of the molecular dispersions of the target compounds in Zeonex extends to 380 nm (Figure 4 (a, b)). As the D and A units absorb until 300 nm,⁹ the new bands at λ_{max} 294-340 nm clearly arise from the excitation throughout the whole molecule. The low energy bands red-shift with increasing solvent polarity (Figures 4 (b, c), S9 (a, b)). This observation, along with the NTO analysis, suggests that the LEBs are of mixed π-π* and n-π* character with a certain degree of CT for *p*-DAz-TXO2 and *m*-DAz-TXO2, and mainly π-π* character for the DPA derivatives. Two trends can be clearly seen in the absorption data. Firstly, DPA-based *p*-DDPA-TXO2 and *m*-DDPA-TXO2 absorb at longer wavelengths compared to the

Az analogs, in agreement with the theoretically predicted spectra (Figure S4) and delocalized NTOs (Figures 3 and S5). Secondly, the LEB intensity is higher for the *para*-substituted ***p*-DAz-TXO2** and ***p*-DDPA-TXO2**, compared with their *meta*-substituted analogs where mixing with π - π^* transitions enhances the oscillator strength.^{41,68}

Steady-state photoluminescence. The differences in absorption spectra translate into diverse emissive properties. Zeonex films of the azepine derivatives exhibit deep violet PL with $\lambda_{\text{max}} = 340\text{-}375$ nm, and onsets at 318 and 340 nm for ***p*-DAz-TXO2** and ***m*-DAz-TXO2**, respectively, upon excitation at 310 nm (Figure 4 (a), Table 2). However, the λ_{max} values of ***p*-DDPA-TXO2** and ***m*-DDPA-TXO2** are red-shifted to 385 and 412 nm with onsets at 361 and 362 nm, respectively. Interestingly, the PL of the *para*-isomers in Zeonex is blue-shifted compared to the *meta*-isomers for both Az and DPA derivatives: we assume this is due to different molecular packing in the thin films.

The Az and DPA molecules all show positive solvatochromism⁶⁹ in their emission spectra (Figures 4 (c, d) and S9 (a, b)). Notably, ***p*-DAz-TXO2** and ***m*-DAz-TXO2** exhibit much larger Stokes' shifts (154 and 140 nm, respectively) than the DPA derivatives (92 and 130 nm for ***p*-DDPA-TXO2** and ***m*-DDPA-TXO2**) consistent with much stronger CT in the Az compounds. Interestingly, both ***p*-DAz-TXO2** and ***m*-DAz-TXO2** feature dual emission. A peak at 340-387 nm dominates in very low polarity solvent and red shifts with increasing polarity: the small shift is indicative of very weak CT character. This peak decreases in intensity with increasing solvent polarity and it differs from the emission of the azepine donor (Figures 4 (c) and S9 (a)). The onset of this emission shifts by 15 nm. A second, much stronger CT emission is also observed at longer wavelengths. This band is not present in MCH solution in ***m*-DAz-TXO2**, nor is it seen in Zeonex films of either ***p*-DDPA-TXO2** or ***m*-DDPA-TXO2**. However, in bis[2-

(diphenylphosphino)phenyl] ether oxide (DPEPO) film this band dominates in both ***p*-DAz-TXO2** and ***m*-DAz-TXO2** and shows the concomitant red shift due to the higher polarity of DPEPO compared to Zeonex. Moreover, there is also a low intensity highly red-shifted emission band which is clearer in ***m*-DAz-TXO2**, the *meta*-coupled analog. The absence of CT bands in both Zeonex and DPEPO is due to the cumulative effect of planarization of the molecule and hindrance to intermolecular packing of the emitters. This behavior is a clear signature of twisted intramolecular charge transfer (TICT)⁷⁰ where the dihedral angles measured by X-ray analysis are much less than 90°. Therefore, to stabilize the CT state one of the donors must rotate to near 90° about the N-C bond.⁷¹ In the solid state, this rotation of the bulky azepine donor is sufficiently hindered that the majority of CT states are not stabilized. Dual CT emission has been previously described for a D–A–D molecule in terms of different conformations of the phenothiazine D units which have different degrees of charge transfer and different local triplet states.⁴¹ The flexibility of the azepine donor unit would readily allow different conformers (see Figure 8). This dual CT emission in both ***p*-DAz-TXO2** and ***m*-DAz-TXO2** is not observed with the DPA molecules as they cannot have such types of conformations.



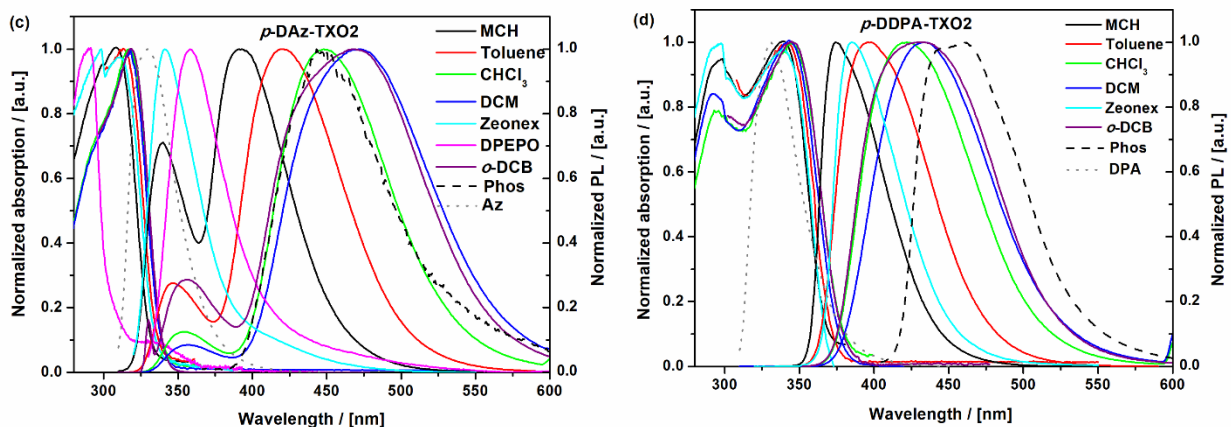
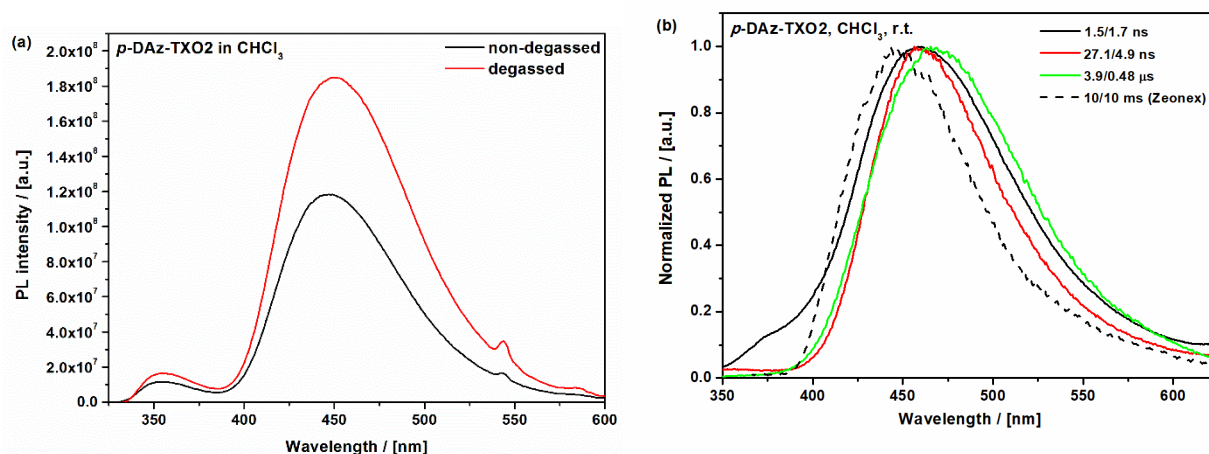


Figure 4. (a, b) UV/Vis absorption and photoluminescence of all the derivatives measured in Zeonex; (c, d) UV/Vis absorption and photoluminescence of *p*-DAz-TXO2 and *p*-DDPA-TXO2 measured in various solvents ($\lambda_{\text{ex}} = 310$ nm) along with photoluminescence of Az and DPA units and phosphorescence of *p*-DAz-TXO2 and *p*-DDPA-TXO2.

Time-resolved photoluminescence. Phosphorescence spectra of the Az and DPA derivatives in Zeonex were recorded at 80 K (Figure S9 (c, d), Table 2). Generally, the azepine derivatives exhibit phosphorescence at higher energies compared to the DPA analogs. The triplet energies obtained from the onsets of the phosphorescence spectra are 3.17 eV for *p*-DAz-TXO2, 3.01 eV for *m*-DAz-TXO2 and *p*-DDPA-TXO2, and 2.94 eV for *m*-DDPA-TXO2. While phosphorescence of *m*-DDPA-TXO2 has a very similar profile to that of the DPA donor, the triplet emission of the Az derivatives seems to be a superposition of phosphorescence spectra of both D and A units. These observations are consistent with the triplet NTOs (Figure 3) and are in line with other D–A–D TADF materials.⁷²

To estimate the contribution of triplet excited states to the overall emission, the PL intensity in oxygen-saturated and deoxygenated solvents was recorded (Table S2). A negligible dependence on oxygen was observed in *p*-DDPA-TXO2 and *m*-DDPA-TXO2. In contrast, the azepine

derivatives exhibited up to 2.1-fold PL intensity enhancement upon the deoxygenation of the solutions, especially in CHCl_3 (Figure 5 (a)). Time-resolved spectra were recorded (Nd-YAG laser, $\lambda_{\text{ex}} = 355 \text{ nm}$) for the solutions of *p*-DAz-TXO2 in CHCl_3 . The weak high energy CT peak observed in the steady-state PL, disappears at early time delay, as previously observed in other D–A molecules⁷³ leaving only the low energy CT state in PF. However, as the unrelaxed ¹CT state is used to estimate ΔE_{ST} ,⁹ the singlet/triplet energy gap (of this low energy CT state) was found to be 0.05 eV for the chloroform solution of *p*-DAz-TXO2 (Figure 5). The ΔE_{ST} increases to 0.15 eV due to the CT stabilization over the first 20-30 ns (Figure 5 (b)). Given a small ΔE_{ST} value, the delayed emission (DF) was observed with further time delay starting from 2 μs (Figure 5 (c, d)). The dependence of the DF intensity on the excitation laser fluence was recorded (Figure 5 (e)). The slope of 1.067 clearly identifies a monomolecular mechanism, i.e. TADF. We note that the Az-based emitters in this study lack photostability in chloroform, but not in the other solvents. During the photophysical measurements the chloroform solutions changed color, and the PL spectra after the time-dependent measurements did not correlate with the original steady-state PL spectra of the freshly-prepared solutions. Presumably this is due to the decomposition of the azepine donor.



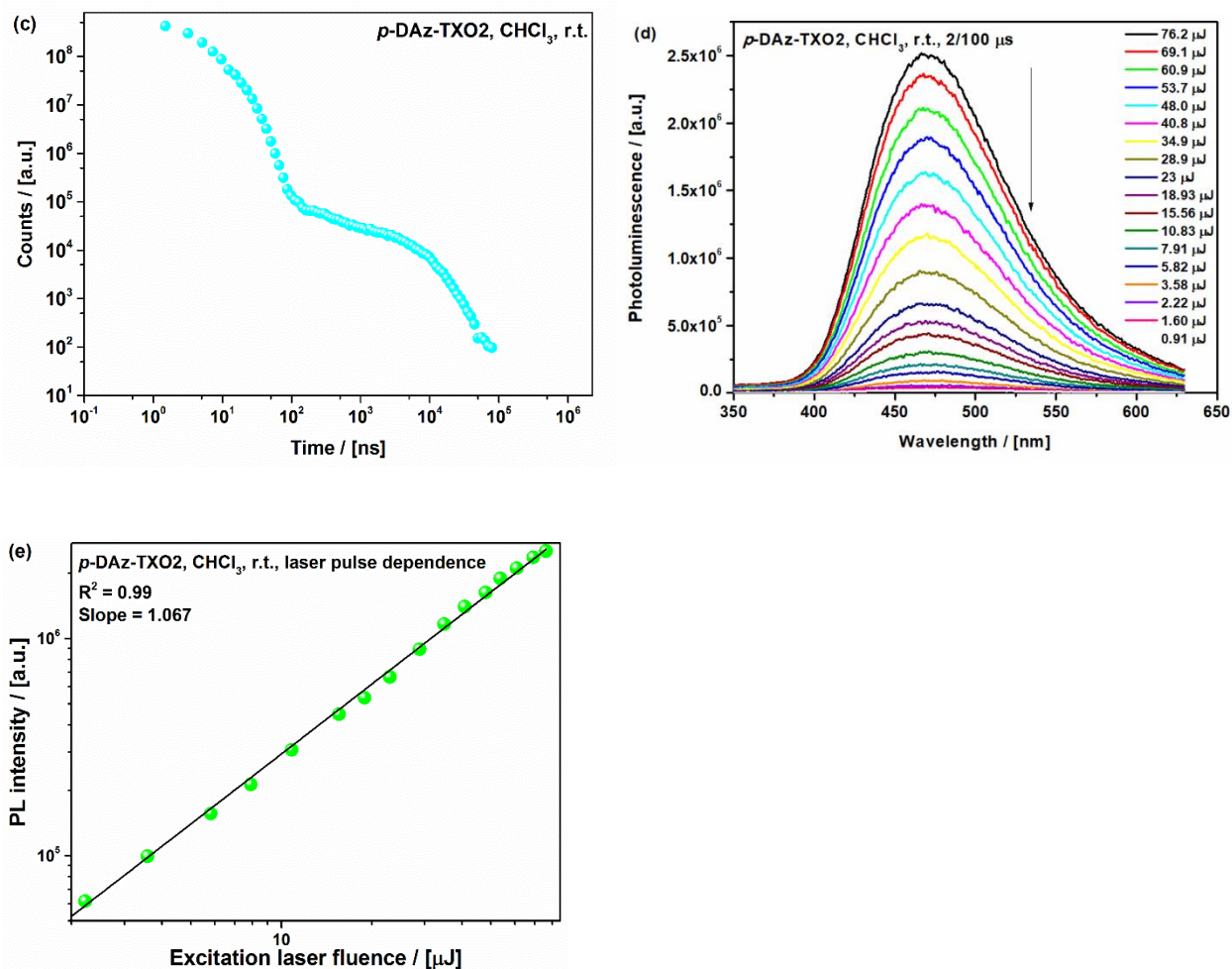


Figure 5. (a) Steady-state PL spectra of oxygen-equilibrated and deoxygenated CHCl₃ solutions of *p*-DAz-TXO₂; (b) time-resolved (Nd-YAG laser, $\lambda_{\text{ex}} = 355$ nm) PL spectra (c) PL decay curve; (d, e) dependence of the PL intensity on the excitation laser fluence (deoxygenated solutions in CHCl₃).

Although showing only a minor DF/PF increment of 1.31, *p*-DAz-TXO₂ also exhibited TADF in *o*-DCB solution with no observed photodegradation (Figure S10). Thus, a small intensity peak at 355 nm gradually disappeared with the increase of time delay, presumably due to the CT stabilization, and weak TADF was observed at 458 nm. Surprisingly, in spite of the highest PL enhancement (2.1 times), no DF was observed in a toluene solution of *p*-DAz-TXO₂ (Figure

S11). Furthermore, no DF was observed for the *meta*-isomer ***m*-DAz-TXO2**, even though significant DF/PF increments were obtained in various solvents (Table S1). No DF was observed for the DPA derivatives (Figure S9). This is consistent with the previously reported absence of DF in other *meta*-linked D–A–D systems.³³

The DF behavior of ***p*-DAz-TXO2** in the solid state was investigated by time-resolved emission decay measurements on 5 wt% ***p*-DAz-TXO2** films in DPEPO host (Figure 6). DPEPO was chosen due to its suitable polarity,⁹ thus, observation of the DF was expected. Although UV emission peaking at 359 nm, originating presumably from mixed LE and CT states, was observed in steady-state measurements (Figure 4 (c)), the apparent red shift of the PL in the time-resolved measurements is due to the cut-off filter used to block 355 nm excitation light reaching the iCCD detector. The CT state was stabilized at longer time delay when the D–A dihedral angle had reached $\approx 90^\circ$. Thus, the singlet/triplet energy gap moved from 0.56 eV at early PF times to 0.22 eV when the CT had stabilized. DF is observed at λ_{max} 447 nm, with onset 3.26 eV. A TADF mechanism was confirmed by the power dependence of the decays (Figure 6c), and slope 1.17 of the laser pulse dependence (Figure 6d). TADF of much weaker intensity was observed for ***p*-DAz-TXO2** in diphenyl-4-triphenylsilylphenyl-phosphine oxide (TSPO1) host (Figure S13). No DF was observed for ***m*-DAz-TXO2**, ***p*-DDPA-TXO2** and ***m*-DDPA-TXO2** in DPEPO host (Figure S12).

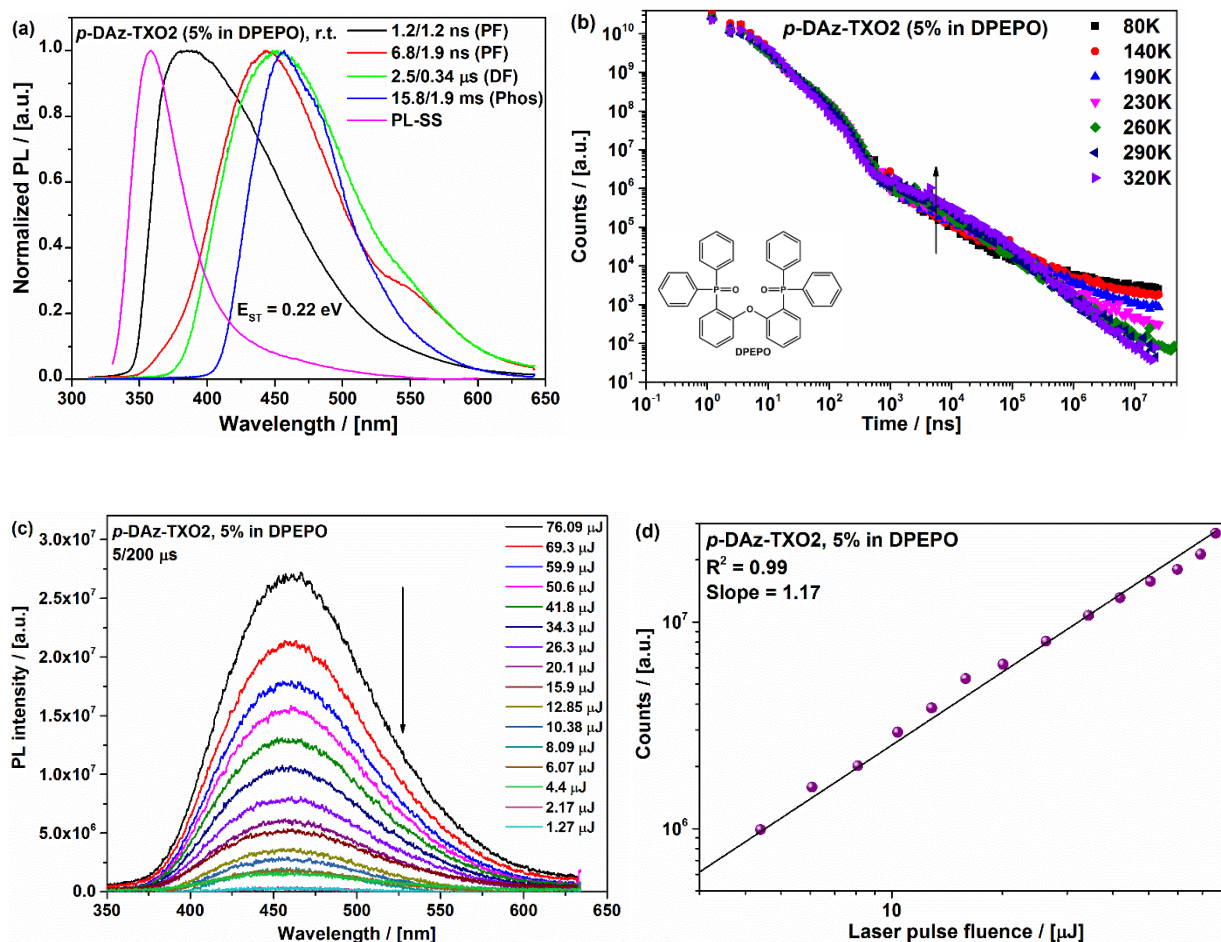


Figure 6. (a) Time-resolved (Nd-YAG laser, $\lambda_{\text{ex}} = 355$ nm) PL spectra of *p*-DAz-TXO2 in DPEPO (b) PL decay curves along with the chemical structure of DPEPO; (c, d) dependence of the PL intensity on the excitation laser fluence (deoxygenated film in DPEPO).

Conformational isomerism. Dual emission, observed in the steady-state measurements for the azepine derivatives (Figures 4 (c) and S9 (a)) along with their much weaker TADF compared to *p*-DDMac-TXO2,⁹ can be explained by the conformational isomerism of the flexible azepine unit, which will not occur with the more rigid acridine unit. In contrast, much more flexible DPA derivatives can adopt a large number of different potential conformers with almost barrier-less interconversion due to the free rotation about the N-C bonds, thus leading to a single peak in the

emission. To illustrate the conformers in the azepine derivatives, DFT methods were employed. The energies of the conformational twist around the N-C bond for ***p*-DAz-TXO2** at the rBMK/6-31G(d) theory level is shown in Figure 7(a). The breaks in the curve refer to the steric hindrance occurring with the drastic twist of the azepine moiety (70-110° and 250-290°). Such breaks were not observed in the conformational curves of D-A-D phenothiazine and phenoxazine derivatives⁷⁴ which comprise six-membered rings as opposed to the seven-membered azepine. While twists by 20° demand negligible energy at room temperature, up to 1 eV is required to twist the azepine donor by 40° relative to the acceptor plane. Such twists can be facilitated upon optical excitation. Here it should be noted that due to the absence of local minima (energy of conformers at 0, 180, 360° is identical) optimization of the twisted structures was impossible, therefore only twist energies for the non-optimized structures are provided. This explains the overestimated values of the twist energies. Figure 7(b) presents the molecular geometry of a possible close-to-planar twisted conformer with a torsion angle of 31.36° between the D and A units. In this structure the HOMO and LUMO are much more delocalized throughout the molecule when compared to the optimized structure in Figure 2, which is similar to the X-ray results ($\alpha = 71.36^\circ$). The delocalized HOMO and LUMO enables favorable mixing of CT and LE states, explaining the dual emission in the steady-state measurements of ***p*-DAz-TXO2**. However, the excited state geometry (Figure 7 (c)) relaxes to almost orthogonal chromophore orientation ($\alpha=83^\circ$), giving rise to the DF.

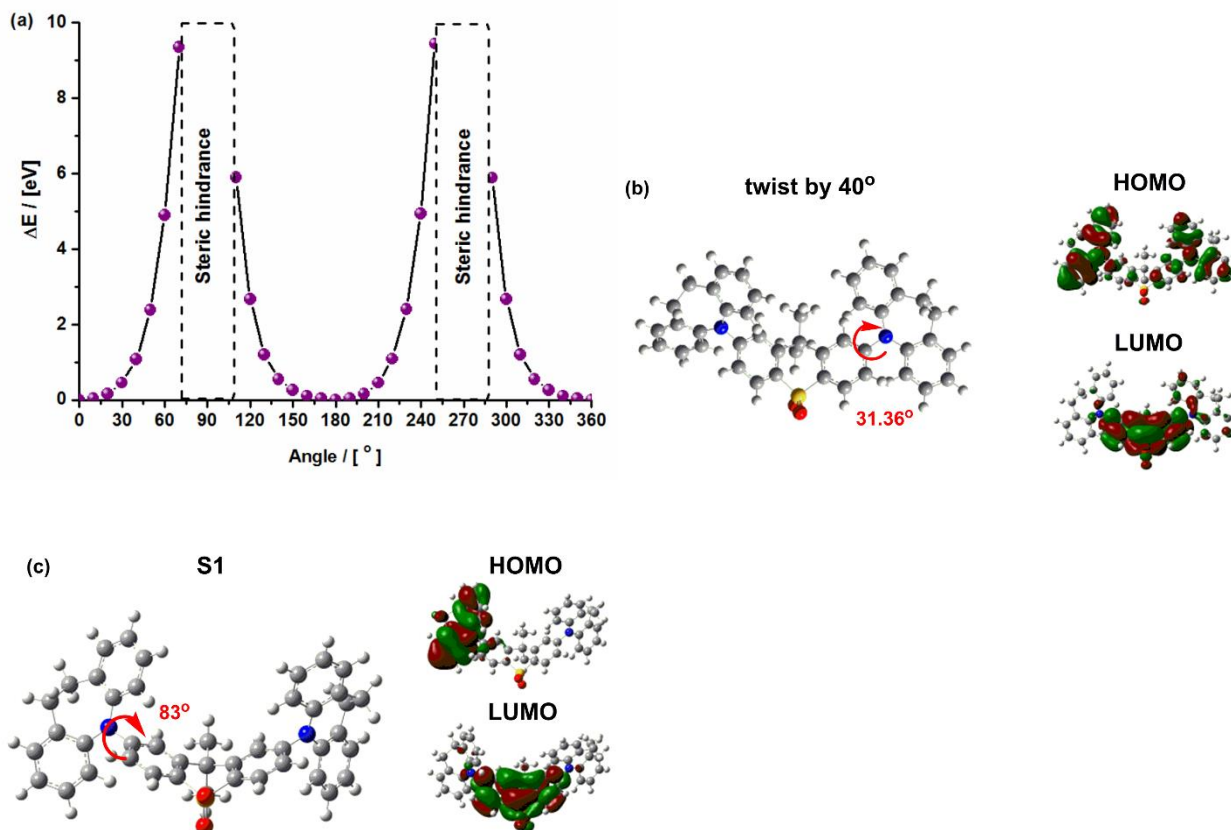


Figure 7. (a) Theoretically predicted dependence of the conformational change energy on the D–A twist angle (rBMK/6-31G(d)) upon the twist of a single azepine donor; molecular geometry along with HOMO and LUMO of (b) a possible conformer (one azepine donor twisted by 40°); (c) S₁ excited state geometry and HOMO/LUMO maps of *p*-DAz-TXO2.

Interestingly, the dependence of the conformational twist energy on the dihedral angle has an asymmetrical parabolic profile (Figure 7 (a)). This is because *p*-DAz-TXO2 possesses C_s symmetry and lacks an inversion center. Thus, the almost barrier-less motion of the CH₂-CH₂ bridge of the azepine (*syn/anti*) results in at least four ground state conformers (Figure 8) possessing different dipole moments and triplet energy values. (The difference in energy for the optimized structures in Figure 8 is about 0.003 eV). Depending on the twist direction of the Az unit, the conjugation changes between the D and A fragments. This is seen in a change in

HOMO/LUMO distribution of the conformers. Furthermore, as there are two donor units in the molecule, multiple twists to the opposite sides relative to the plane of TXO2 acceptor should be expected. Hence, combination of the barrier-less folding of the azepine unit with the N-C bond twist leads to the superposition of various conformers, some of which have more decoupled electron wavefunctions, while the others have mixed states. Thus, due to the extremely small energy barrier, various interchanging conformers can be present both in solution and solid state.

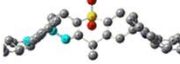
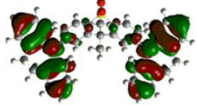
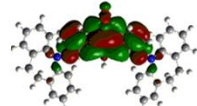
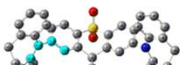
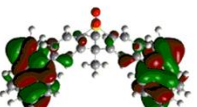
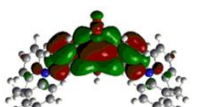
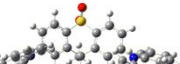
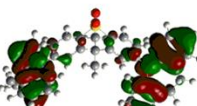
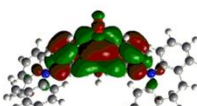

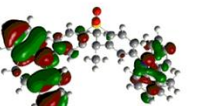
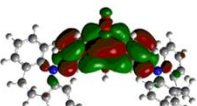
Conformer	Twist angle / [°]	HOMO	LUMO	Dipole moment / [D]	T ₁ / [eV]
 anti / anti	109			5.1027	3.3065
 syn / syn	71			5.1173	3.3100
 anti / syn	109 / 71			5.0558	3.3091
 syn / anti	71 / 109			5.1241	3.3127

Figure 8. Four possible ground state conformers of *p*-DAz-TXO2 formed upon the folding of the azepine CH₂-CH₂ bridge in either one or both azepine donors (rBMK/6-31G(d)). The degree of precision of the calculated dipole moments and triplet energies was kept purposely to show the difference between the conformers.

This assumption was confirmed experimentally. The red shift of the phosphorescence of ***p*-DAz-TXO2** with increasing host polarity (Figure S14) suggests the existence of several triplet states due to the conformational changes. This shift in triplet energy cannot be explained simply by polarity changes as the data for DPEPO and TSPO1 are very similar, and triplet energy does not generally shift with polarity, unlike singlet emission (fluorescence).⁷² This feature in turn may explain the discrepancy in ΔE_{ST} values and TADF efficiency observed in the azepine derivatives in various media. As discussed in recent literature,⁴⁰ Az shows ultralong phosphorescence due to the formation of H-aggregates. However, we assume that the appearance of ground state dimers is unlikely in the case of the D–A–D molecules presented here, because of their steric bulk and twisted structures. The possibility of ground state dimers of ***p*-DAz-TXO2** is discussed in S4 of the SI (Figures S15-17).

Conclusions and outlook

Clear differences have been observed in photophysical properties when using diphenylamine (DPA) or 10,11-dihydro-5*H*-dibenz[*b,f*]azepine (Az) as a donor in a series of D–A–D molecules, where A is 9,9-dimethylthioxanthene-*S,S*-dioxide (TXO2). These differences are shown to originate from divergent geometry, and hence rigidity, of the donor unit. This, in turn, influences the geometry of the nitrogen electron lone pair and the donating strength of the corresponding fragment. A combination of geometrical and electronic effects causes conformational changes which affect the CT formation and hence the TADF efficiency. Comparing the results of the TXO2 acceptor substituted by various donors shows that the efficiency of TADF enhances in the series DPA < Az < Ac. The high efficiency of the acridine-based emitters originates in the

relative planarity of acridine, which ensures nearly perpendicular D–A orientation and strong CT. However, these advantages of Ac make it difficult to obtain deeper-blue TADF emitters using Ac as it is a strong rigid donor. In contrast, the DPA moiety has an extremely flexible structure that prevents pertinent HOMO/LUMO decoupling, and might show TADF only in combination with strong acceptors. The Az fragment represents an intermediate case, combining sufficiently strong electron donor strength and relative flexibility. However, the Az systems require suitably polar media to show efficient TADF.

These results shed new light on important issues to consider in designing TADF emitters. Firstly, the electron donating/accepting strength should be carefully balanced: to achieve TADF of a certain emission color chromophores of similar strength must be utilized. Thus, for deep-blue emitters weaker units are needed to ensure a wide HOMO/LUMO gap. Secondly, the relative rigidity of the D and A units has a direct link to the possible conformational changes and the relative electron donating/accepting strength. Generally, a more flexible donor unit will lead to a larger amount of LE emission, meaning the absence of, or only weak, TADF. However, a certain amount of flexibility has to be present to ensure deep-blue TADF. It should be noted that for flexible donors, appropriate hosts have to be developed in order to control the conformational changes and provide sustainable polarity to form a stable CT state.

ASSOCIATED CONTENT

Supporting Information. The Supporting Information is available free of charge on the ACS Publications website at DOI:xxxxxxxx

Synthesis and characterization details of the new molecules; methods and results for the photophysics and calculations (PDF). X-ray crystallographic data (CCDC 1872344-1872350) (cif); computational atomic coordinates (xyz).

AUTHOR INFORMATION

Corresponding Authors

*E-Mail: m.r.bryce@durham.ac.uk

*E-Mail: a.p.monkman@durham.ac.uk

Author Contributions

The manuscript was written through contributions of all authors. All authors have given approval to the final version of the manuscript.

Notes

The authors declare no competing financial interest.

ACKNOWLEDGMENT

We thank EPSRC grant EP/L02621X/1 and EU Horizon 2020 grant agreement number 732013 (HyperOLED) for funding. The Diamond Light Source is thanked for the award of instrument time on Station I19 (MT 11145) and the instrument scientists for their kind support.

REFERENCES

- (1) Parker, C. A.; Hatchard, C. G. Triplet-Singlet Emission in Fluid Solutions. Phosphorescence of Eosin. *Trans. Faraday Soc.* **1961**, *57*, 1894.
- (2) Baldo, M. A.; O'Brien, D. F.; You, Y.; Shoustikov, A.; Sibley, S.; Thompson, M. E.; Forrest, S. R. Highly Efficient Phosphorescent Emission from Organic Electroluminescent Devices. **1998**, *395*, 151–154.
- (3) Tanaka, H.; Shizu, K.; Miyazaki, H.; Adachi, C. Efficient Green Thermally Activated Delayed Fluorescence (TADF) from a Phenoxazine-Triphenyltriazine (PXZ-TRZ) Derivative. *Chem. Commun. (Camb)*. **2012**, *48*, 11392–11394.
- (4) Jankus, V.; Data, P.; Graves, D.; McGuinness, C.; Santos, J.; Bryce, M. R.; Dias, F. B.; Monkman, A. P. Highly Efficient TADF OLEDs: How the Emitter-Host Interaction Controls Both the Excited State Species and Electrical Properties of the Devices to Achieve Near 100% Triplet Harvesting and High Efficiency. *Adv. Funct. Mater.* **2014**, *24*, 6178–6186.
- (5) Im, Y.; Kim, M.; Cho, Y. J.; Seo, J.-A.; Yook, K. S.; Lee, J. Y. Molecular Design Strategy of Organic Thermally Activated Delayed Fluorescence Emitters. *Chem. Mater.* **2017**, *29*, 1946–1963.
- (6) Tachibana, H.; Aizawa, N.; Hidaka, Y.; Yasuda, T. Tunable Full-Color Electroluminescence from All-Organic Optical Upconversion Devices by Near-Infrared Sensing. *ACS Photonics* **2017**, *4*, 223–227.
- (7) Kawasumi, K.; Wu, T.; Zhu, T.; Chae, H. S.; Van Voorhis, T.; Baldo, M. A.; Swager, T.

- M. Thermally Activated Delayed Fluorescence Materials Based on Homoconjugation Effect of Donor-Acceptor Triptycenes. *J. Am. Chem. Soc.* **2015**, *137*, 11908–11911.
- (8) Sun, J. W.; Baek, J. Y.; Kim, K.-H.; Moon, C.-K.; Lee, J.-H.; Kwon, S.-K.; Kim, Y.-H.; Kim, J.-J. Thermally Activated Delayed Fluorescence from Azasiline Based Intramolecular Charge-Transfer Emitter (DTPDDA) and a Highly Efficient Blue Light Emitting Diode. *Chem. Mater.* **2015**, *27*, 6675–6681.
- (9) dos Santos, P. L.; Ward, J. S.; Bryce, M. R.; Monkman, A. P. Using Guest–Host Interactions To Optimize the Efficiency of TADF OLEDs. *J. Phys. Chem. Lett.* **2016**, *7*, 3341–3346.
- (10) Wu, S.; Aonuma, M.; Zhang, Q.; Huang, S.; Nakagawa, T.; Kuwabara, K.; Adachi, C. High-Efficiency Deep-Blue Organic Light-Emitting Diodes Based on a Thermally Activated Delayed Fluorescence Emitter. *J. Mater. Chem. C* **2014**, *2*, 421–424.
- (11) Jürgensen, N.; Kretzschmar, A.; Höfle, S.; Freudenberg, J.; Bunz, U. H. F.; Hernandez-Sosa, G. Sulfone-Based Deep Blue Thermally Activated Delayed Fluorescence Emitters: Solution-Processed Organic Light-Emitting Diodes with High Efficiency and Brightness. *Chem. Mater.* **2017**, *29*, 9154–9161.
- (12) Tao, Y.; Yuan, K.; Chen, T.; Xu, P.; Li, H.; Chen, R.; Zheng, C.; Zhang, L.; Huang, W. Thermally Activated Delayed Fluorescence Materials towards the Breakthrough of Organoelectronics. *Adv. Mater.* **2014**, *26*, 7931–7958.
- (13) Wong, M. Y.; Zysman-Colman, E. Purely Organic Thermally Activated Delayed Fluorescence Materials for Organic Light-Emitting Diodes. *Adv. Mater.* **2017**, *29*,

1605444.

- (14) Liu, Y.; Li, C.; Ren, Z.; Yan, S.; Bryce, M. R. All-Organic Thermally Activated Delayed Fluorescence Materials for Organic Light-Emitting Diodes. *Nat. Rev. Mater.* **2018**, *3*, 18020.
- (15) Wu, Z.; Luo, J.; Sun, N.; Zhu, L.; Sun, H.; Yu, L.; Yang, D.; Qiao, X.; Chen, J.; Yang, C.; et al. High-Performance Hybrid White Organic Light-Emitting Diodes with Superior Efficiency/Color Rendering Index/Color Stability and Low Efficiency Roll-Off Based on a Blue Thermally Activated Delayed Fluorescent Emitter. *Adv. Funct. Mater.* **2016**, *26*, 3306–3313.
- (16) Kim, M.; Jeon, S. K.; Hwang, S.-H.; Lee, J. Y. Stable Blue Thermally Activated Delayed Fluorescent Organic Light-Emitting Diodes with Three Times Longer Lifetime than Phosphorescent Organic Light-Emitting Diodes. *Adv. Mater.* **2015**, *27*, 2515–2520.
- (17) Noguchi, Y.; Kim, H.-J.; Ishino, R.; Goushi, K.; Adachi, C.; Nakayama, Y.; Ishii, H. Charge Carrier Dynamics and Degradation Phenomena in Organic Light-Emitting Diodes Doped by a Thermally Activated Delayed Fluorescence Emitter. *Org. Electron.* **2015**, *17*, 184–191.
- (18) Sandanayaka, A. S. D.; Matsushima, T.; Adachi, C. Degradation Mechanisms of Organic Light-Emitting Diodes Based on Thermally Activated Delayed Fluorescence Molecules. *J. Phys. Chem. C* **2015**, *119*, 23845–23851.
- (19) Bui, T.-T.; Goubard, F.; Ibrahim-Ouali, M.; Gigmes, D.; Dumur, F. Recent Advances on Organic Blue Thermally Activated Delayed Fluorescence (TADF) Emitters for Organic

- Light-Emitting Diodes (OLEDs). *Beilstein J. Org. Chem.* **2018**, *14*, 282–308.
- (20) Etherington, M. K.; Gibson, J.; Higginbotham, H. F.; Penfold, T. J.; Monkman, A. P. Revealing the Spin-Vibronic Coupling Mechanism of Thermally Activated Delayed Fluorescence. *Nat. Commun.* **2016**, *7*, 1–7.
- (21) Liu, W.; Zheng, C.-J.; Wang, K.; Chen, Z.; Chen, D.-Y.; Li, F.; Ou, X.-M.; Dong, Y.-P.; Zhang, X.-H. Novel Carbazol-Pyridine-Carbonitrile Derivative as Excellent Blue Thermally Activated Delayed Fluorescence Emitter for Highly Efficient Organic Light-Emitting Devices. *ACS Appl. Mater. Interfaces* **2015**, *7*, 18930–18936.
- (22) Lee, Y. H.; Park, S.; Oh, J.; Woo, S.-J.; Kumar, A.; Kim, J.-J.; Jung, J.; Yoo, S.; Lee, M. H. High-Efficiency Sky Blue to Ultradeep Blue Thermally Activated Delayed Fluorescent Diodes Based on *Ortho* -Carbazole-Appended Triarylboron Emitters: Above 32% External Quantum Efficiency in Blue Devices. *Adv. Opt. Mater.* **2018**, *6*, 1800385.
- (23) Liang, J.-J.; Li, Y.; Yuan, Y.; Li, S.-H.; Zhu, X.-D.; Barlow, S.; Fung, M.-K.; Jiang, Z.-Q.; Marder, S. R.; Liao, L.-S. A Blue Thermally Activated Delayed Fluorescence Emitter Developed by Appending a Fluorene Moiety to a Carbazole Donor with *Meta* -Linkage for High-Efficiency OLEDs. *Mater. Chem. Front.* **2018**, *2*, 917–922.
- (24) Rajamalli, P.; Rota Martir, D.; Zysman-Colman, E. Pyridine-Functionalized Carbazole Donor and Benzophenone Acceptor Design for Thermally Activated Delayed Fluorescence Emitters in Blue Organic Light-Emitting Diodes. *J. Photonics Energy* **2018**, *8*, 032106.
- (25) Klöpffer, W.; Fischer, D. Triplet Energy Transfer in Solid Solutions and Films of

- Poly(Vinyl Carbazole). *J. Polym. Sci. Polym. Symp.* **2007**, *40*, 43–56.
- (26) Kukhta, N. A.; Matulaitis, T.; Volyniuk, D.; Ivaniuk, K.; Turyk, P.; Stakhira, P.; Grazulevicius, J. V.; Monkman, A. P. Deep-Blue High-Efficiency TTA OLED Using *Para* - and *Meta* -Conjugated Cyanotriphenylbenzene and Carbazole Derivatives as Emitter and Host. *J. Phys. Chem. Lett.* **2017**, *8*, 6199–6205.
- (27) Saiful, I. S. M.; Heinze, P.; Ohba, Y.; Yamauchi, S.; Yamamoto, M.; Tohda, Y.; Tani, K. Interplanar Interactions in the Excited Triplet States of Carbazole Dimers by Means of Time-Resolved EPR Spectroscopy. *Mol. Phys.* **2006**, *104*, 1535–1542.
- (28) Jankus, V.; Monkman, A. P. Is Poly(Vinylcarbazole) a Good Host for Blue Phosphorescent Dopants in PLEDs? Dimer Formation and Their Effects on the Triplet Energy Level of Poly(N-Vinylcarbazole) and Poly(N-Ethyl-2-Vinylcarbazole). *Adv. Funct. Mater.* **2011**, *21*, 3350–3356.
- (29) Zhang, Q.; Li, J.; Shizu, K.; Huang, S.; Hirata, S.; Miyazaki, H.; Adachi, C. Design of Efficient Thermally Activated Delayed Fluorescence Materials for Pure Blue Organic Light Emitting Diodes. *J. Am. Chem. Soc.* **2012**, *134*, 14706–14709.
- (30) Huang, B.; Qi, Q.; Jiang, W.; Tang, J.; Liu, Y.; Fan, W.; Yin, Z.; Shi, F.; Ban, X.; Xu, H.; et al. Thermally Activated Delayed Fluorescence Materials Based on 3,6-Di-Tert-Butyl-9-((Phenylsulfonyl)Phenyl)-9H-Carbazoles. *Dye. Pigment.* **2014**, *111*, 135–144.
- (31) Ohkuma, H.; Nakagawa, T.; Shizu, K.; Yasuda, T.; Adachi, C. Thermally Activated Delayed Fluorescence from a Spiro-Diazafluorene Derivative. *Chem. Lett.* **2014**, *43*, 1017–1019.

- (32) Sohna, S.; Kohb, B. H.; Baek, Y. J. ; Byun, H. C.; Lee, J. H.; Shin, D.-S.; Ahn, H.; Lee, H.-K.; Hwang, J.; Jung, S. et al. Synthesis and Characterization of Diphenylamine Derivative Containing Malononitrile for Thermally Activated Delayed Fluorescent Emitter. *Dyes Pigm.* **2017**, *140*, 14–21.
- (33) Dias, F. B.; Bourdakos, K. N.; Jankus, V.; Moss, K. C.; Kamtekar, K. T.; Bhalla, V.; Santos, J.; Bryce, M. R.; Monkman, A. P. Triplet Harvesting with 100% Efficiency by Way of Thermally Activated Delayed Fluorescence in Charge Transfer OLED Emitters. *Adv. Mater.* **2013**, *25*, 3707–3714.
- (34) Choi, J.; Ahn, D.-S.; Oang, K. Y.; Cho, D. W.; Ihee, H. Charge Transfer-Induced Torsional Dynamics in the Excited State of 2,6-Bis(Diphenylamino)Anthraquinone. *J. Phys. Chem. C* **2017**, *121*, 24317–24323.
- (35) Shizu, K.; Tanaka, H.; Uejima, M.; Sato, T.; Tanaka, K.; Kaji, H.; Adachi, C. Strategy for Designing Electron Donors for Thermally Activated Delayed Fluorescence Emitters. *J. Phys. Chem. C* **2015**, *119*, 1291–1297.
- (36) Lee, I.; Lee, J. Y. Molecular Design of Deep Blue Fluorescent Emitters with 20% External Quantum Efficiency and Narrow Emission Spectrum. *Org. Electron.* **2016**, *29*, 160–164.
- (37) Lin, T.-A.; Chatterjee, T.; Tsai, W.-L.; Lee, W.-K.; Wu, M.-J.; Jiao, M.; Pan, K.-C.; Yi, C.-L.; Chung, C.-L.; Wong, K.-T.; et al. Sky-Blue Organic Light Emitting Diode with 37% External Quantum Efficiency Using Thermally Activated Delayed Fluorescence from Spiroacridine-Triazine Hybrid. *Adv. Mater.* **2016**, *28*, 6976–6983.
- (38) Jhulki, S.; Moorthy, J. N. Small Molecular Hole-Transporting Materials (HTMs) in

- Organic Light-Emitting Diodes (OLEDs): Structural Diversity and Classification. *J. Mater. Chem. C* **2018**, *6*, 8280–8325.
- (39) Thompson, M. E.; Douglas, L.; O'Brien, D.; Koene, B. E.; Forrest, S. R. OLEDs Containing Thermally Stable Glassy Organic Hole Transporting Materials. US09058305. **1998**.
- (40) Sun, C.; Ran, X.; Wang, X.; Cheng, Z.; Wu, Q.; Cai, S.; Gu, L.; Gan, N.; Shi, H.; An, Z.; et al. Twisted Molecular Structure on Tuning Ultralong Organic Phosphorescence. *J. Phys. Chem. Lett.* **2018**, *9*, 335–339.
- (41) Etherington, M. K.; Franchello, F.; Gibson, J.; Northey, T.; Santos, J.; Ward, J. S.; Higginbotham, H. F.; Data, P.; Kurowska, A.; dos Santos, P. L.; et al. Regio- and Conformational Isomerization Critical to Design of Efficient Thermally-Activated Delayed Fluorescence Emitters. *Nat. Commun.* **2017**, *8*, 14987.
- (42) Huang, R.; Ward, J. S.; Kukhta, N. A.; Avó, J.; Gibson, J.; Penfold, T.; Lima, J. C.; Batsanov, A. S.; Berberan-Santos, M. N.; Bryce, M. R. et al. The Influence of Molecular Conformation on the Photophysics of Organic Room Temperature Phosphorescent Luminophores. *J. Mater. Chem. C* **2018**, *6*, 9238-9247 .
- (43) Higginbotham, H. F.; Yi, C.-L.; Monkman, A. P.; Wong, K.-T. Effects of Ortho-Phenyl Substitution on the RISC Rate of D–A Type TADF Molecules. *J. Phys. Chem. C* **2018**, *122*, 7627–7634.
- (44) Park, H. J.; Han, S. H.; Lee, J. Y. A Directly Coupled Dual Emitting Core Based Molecular Design of Thermally Activated Delayed Fluorescent Emitters. *J. Mater. Chem.*

- C* **2017**, *5*, 12143–12150.
- (45) Rothe, C.; Monkman, A. P. Triplet Exciton Migration in a Conjugated Polyfluorene. *Phys. Rev. B* **2003**, *68*, 075208.
- (46) Frisch, M. J.; Trucks, G. W.; Schlegel, H. B.; Scuseria, G. E.; Robb, M. A.; Cheeseman, J. R.; Scalmani, G.; Barone, V.; Petersson, G. A.; Nakatsuji, H. et al. Gaussian 09, Revision B.02. *Gaussian 09, Revision A.02*. 2009.
- (47) Gross, E.; Kohn, W. Local Density-Functional Theory of Frequency-Dependent Linear Response. *Phys. Rev. Lett.* **1985**, *55*, 2850–2852.
- (48) Thanthiriwatte, K. S.; Gwaltney, S. R. Excitation Spectra of Dibenzoborole Containing Pi-Electron Systems: Controlling the Electronic Spectra by Changing the $p_{\pi}-\pi^*$ Conjugation. *J. Phys. Chem. A* **2006**, *110*, 2434–2439.
- (49) Allan, D. .; Nowell, H.; Barnett, S.; Warren, M.; Wilcox, A.; Christensen, J.; Saunders, L.; Peach, A.; Hooper, M.; Zaja, L.; et al. A Novel Dual Air-Bearing Fixed- χ Diffractometer for Small-Molecule Single-Crystal X-Ray Diffraction on Beamline I19 at Diamond Light Source. *Crystals* **2017**, *7*, 336.
- (50) Johnson, N.; Waddell, P.; Clegg, W.; Probert, M.; Johnson, N. T.; Waddell, P. G.; Clegg, W.; Probert, M. R. Remote Access Revolution: Chemical Crystallographers Enter a New Era at Diamond Light Source Beamline I19. *Crystals* **2017**, *7*, 360.
- (51) Krause, L.; Herbst-Irmer, R.; Sheldrick, G. M.; Stalke, D. Comparison of Silver and Molybdenum Microfocus X-Ray Sources for Single-Crystal Structure Determination. *J.*

- Appl. Crystallogr.* **2015**, *48*, 3–10.
- (52) Sheldrick, G. M. *SHELXT* – Integrated Space-Group and Crystal-Structure Determination. *Acta Crystallogr. Sect. A Found. Adv.* **2015**, *71*, 3–8.
- (53) Schneider, T. R.; Sheldrick, G. M. Substructure Solution with SHELXD. *Acta Crystallogr. D. Biol. Crystallogr.* **2002**, *58*, 1772–1779.
- (54) Sheldrick, G. M. A Short History of *SHELX*. *Acta Crystallogr. Sect. A Found. Crystallogr.* **2008**, *64*, 112–122.
- (55) Sheldrick, G. M. Crystal Structure Refinement with *SHELXL*. *Acta Crystallogr. Sect. C Struct. Chem.* **2015**, *71*, 3–8.
- (56) Dolomanov, O. V.; Bourhis, L. J.; Gildea, R. J.; Howard, J. A. K.; Puschmann, H. *OLEX2*: A Complete Structure Solution, Refinement and Analysis Program. *J. Appl. Crystallogr.* **2009**, *42*, 339–341.
- (57) Ward, J. S.; Nobuyasu, R. S.; Batsanov, A. S.; Data, P.; Monkman, A. P.; Dias, F. B.; Bryce, M. R. The Interplay of Thermally Activated Delayed Fluorescence (TADF) and Room Temperature Organic Phosphorescence in Sterically-Constrained Donor–acceptor Charge-Transfer Molecules. *Chem. Commun.* **2016**, *52*, 2612–2615.
- (58) Huang, R.; Avó, J.; Northey, T.; Channing-Pearce, E.; dos Santos, P. L.; Ward, J. S.; Data, P.; Etherington, M. K.; Fox, M. A.; Penfold, T. J.; et al. The Contributions of Molecular Vibrations and Higher Triplet Levels to the Intersystem Crossing Mechanism in Metal-Free Organic Emitters. *J. Mater. Chem. C* **2017**, *5*, 6269–6280.

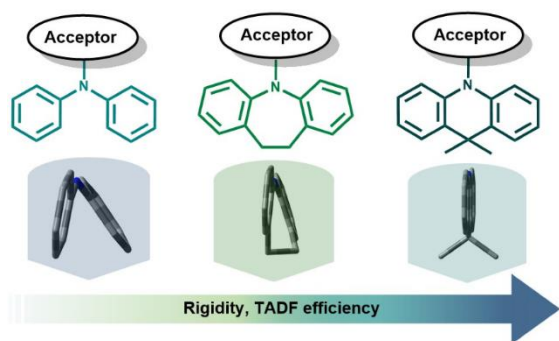
- (59) Adams, J. E.; Mantulin, W. W.; Huber, J. R. Effect of Molecular Geometry on Spin-Orbit Coupling of Aromatic Amines in Solution. Diphenylamine, Iminobibenzyl, Acridan, and Carbazole. *J. Am. Chem. Soc.*, **1973**, *95*, 5477–5481.
- (60) Heravi, M. M.; Kheilkordi, Z.; Zadsirjan, V.; Heydari, M.; Malmir, M. Buchwald-Hartwig Reaction: An Overview. *J. Organomet. Chem.* **2018**, *861*, 17–104.
- (61) dos Santos, P. L.; Ward, J. S.; Data, P.; Batsanov, A. S.; Bryce, M. R.; Dias, F. B.; Monkman, A. P. Engineering the Singlet-Triplet Energy Splitting in a TADF Molecule. *J. Mater. Chem. C* **2016**, *4*, 3815–3824.
- (62) dos Santos, P. L.; Ward, J. S.; Batsanov, A. S.; Bryce, M. R.; Monkman, A. P. Optical and Polarity Control of Donor-Acceptor Conformation and Their Charge-Transfer States in Thermally Activated Delayed-Fluorescence Molecules. *J. Phys. Chem. C* **2017**, *121*, 16462–16469.
- (63) Kukhta, N. A.; da Silva Filho, D. A.; Volyniuk, D.; Gražulevičius, J. V.; Sini, G. Can Fluorenone-Based Compounds Emit in the Blue Region? Impact of the Conjugation Length and the Ground State Aggregation. *Chem. Mater.* **2017**, *29*, 1695–1707.
- (64) Brédas, J.-L. Organic Electronics: Does a Plot of the HOMO–LUMO Wave Functions Provide Useful Information? *Chem. Mater.* **2017**, *29*, 477–478.
- (65) Boese, A. D.; Martin, J. M. L. Development of Density Functionals for Thermochemical Kinetics. *J. Chem. Phys.* **2004**, *121*, 3405–3416.
- (66) Martin, R. L. Natural Transition Orbitals. *J. Chem. Phys.* **2003**, *118*, 4775–4777.

- (67) Matulaitis, T.; Imbrasas, P.; Kukhta, N. A.; Baronas, P.; Bučiūnas, T.; Banevičius, D.; Kazlauskas, K.; Gražulevičius, J. V.; Juršėnas, S. Impact of Donor Substitution Pattern on the TADF Properties in the Carbazolyl-Substituted Triazine Derivatives. *J. Phys. Chem. C* **2017**, *121*, 23618–23625.
- (68) Marian, C. M. A New Pathway for the Rapid Decay of Electronically Excited Adenine. *J. Chem. Phys.* **2005**, *122*, 104314.
- (69) Reichardt, C. *Solvents and Solvent Effects in Organic Chemistry*; Wiley-VCH Verlag GmbH & Co. KGaA: Weinheim, FRG, 2002.
- (70) Sasaki, S.; Drummen, G. P. C.; Konishi, G. Recent Advances in Twisted Intramolecular Charge Transfer (TICT) Fluorescence and Related Phenomena in Materials Chemistry. *J. Mater. Chem. C* **2016**, *4*, 2731–2743.
- (71) Haberhauer, G. Planarized and Twisted Intramolecular Charge Transfer: A Concept for Fluorophores Showing Two Independent Rotations in Excited State. *Chem. - A Eur. J.* **2017**, *23*, 9288–9296.
- (72) dos Santos, P. L.; Ward, J. S.; Congrave, D. G.; Batsanov, A. S.; Eng, J.; Stacey, J. E.; Penfold, T. J.; Monkman, A. P.; Bryce, M. R. Triazatruxene: A Rigid Central Donor Unit for a D–A₃ Thermally Activated Delayed Fluorescence Material Exhibiting Sub-Microsecond Reverse Intersystem Crossing and Unity Quantum Yield via Multiple Singlet–Triplet State Pairs. *Adv. Sci.* **2018**, *5*, 1–9.
- (73) dos Santos, P. L.; Etherington, M. K.; Monkman, A. P. Chemical and Conformational Control of the Energy Gaps Involved in the Thermally Activated Delayed Fluorescence

Mechanism. *J. Mater. Chem. C* **2018**, *6*, 4842–4853.

- (74) Ward, J. S.; Nobuyasu, R. S.; Fox, M. A.; Batsanov, A. S.; Santos, J.; Dias, F. B.; Bryce, M. R. Bond Rotations and Heteroatom Effects in Donor-Acceptor-Donor Molecules: Implications for Thermally Activated Delayed Fluorescence and Room Temperature Phosphorescence. *J. Org. Chem.* **2018**, acs.joc.8b02187.

ToC Graphic



Supporting information

The Importance of Chromophore Rigidity on the Efficiency of Blue Thermally Activated Delayed Fluorescence Emitters

Nadzeya A. Kukhta,^a Andrei S. Batsanov,^a Martin R. Bryce,^{a,*} Andrew P. Monkman^{b,*}

^a*Department of Chemistry, Durham University, South Road, Durham, DH1 3LE, UK.*

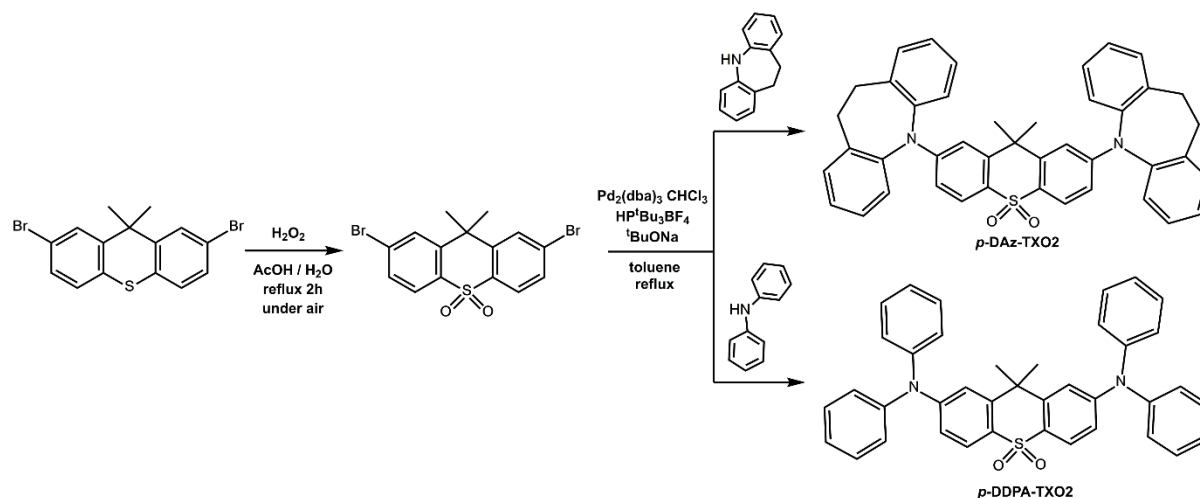
^b*Department of Physics, Durham University, South Road, Durham, DH1 3LE, UK.*

S1. Synthesis and characterization

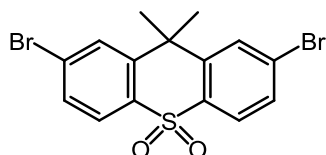
All reactions were carried out under an argon atmosphere unless otherwise stated. Starting materials were purchased commercially and were used as received. Solvents were dried using an Innovative Technology solvent purification system and were stored in ampoules under argon. TLC analysis was carried out using Merck Silica gel 60 F254 TLC plates and spots were visualized using a TLC lamp emitting at 365, 312 or 254 nm. Silica gel column chromatography was performed using silica gel 60 purchased from Sigma Aldrich. ¹H and ¹³C NMR spectroscopy was carried out on Bruker AV400, Varian VNMRS 500 and 700, and Varian Inova 500 NMR spectrometers. Residual solvent peaks were referenced as described in the literature,¹ and all NMR data was processed in MestReNova V10. Melting points were carried out on a Stuart SMP40 machine with a ramping rate of 4 °C min⁻¹. Videos were replayed manually to accurately determine the melting point. High resolution mass spectrometry was carried out on a Waters LCT Premier XE using ASAP ionization. Samples were analyzed directly as solids using N₂ at 350 °C. Elemental analysis was performed on an Exeter Analytical E-440 machine. Any stated use of hexane refers to a mix isomers grade.

Synthesis and characterization

Synthesis of *para*-isomers



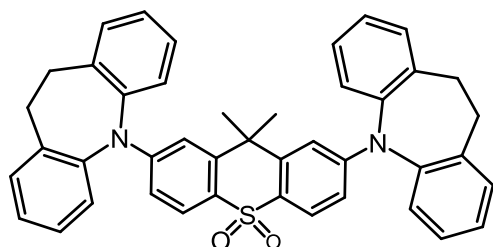
- 2,7-Dibromo-9,9-dimethylthioxanthene-*S,S*-dioxide



2,7-Dibromo-9,9-dimethylthioxanthene-*S,S*-dioxide was prepared according to the procedure described in literature² starting from 2,7-dibromo-9,9-dimethylthioxanthene (5.0 g). White solid (4.2 g, yield 77%).

^1H NMR (400 MHz, CDCl_3) δ : 8.05 (d, 2H, $J = 8.31$ Hz), 7.89 (d, 2H, $J = 1.79$ Hz), 7.69 (dd, 2H, $J = 8.26$ Hz, $J = 1.81$ Hz), 1.90 (s, 6H). ^{13}C NMR (101 MHz, CDCl_3) δ : 147.2, 135.6, 130.9, 129.0, 128.1, 125.9, 39.5, 30.5.

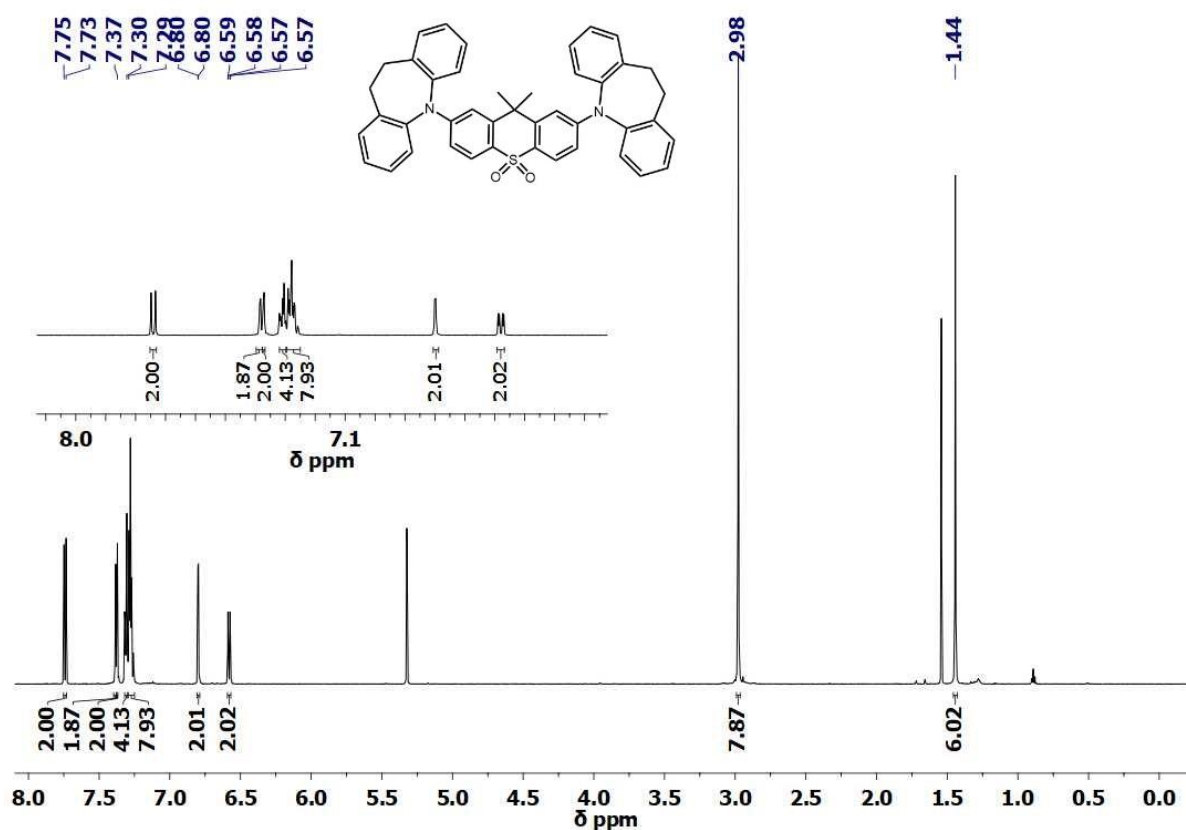
- 2,7-Bis(10,11-dihydro-5*H*-dibenzo[*b,f*]azepin-5-yl)-9,9-dimethyl-9*H*-thioxanthene 10,10-dioxide (***p*-DAZ-TXO2**)

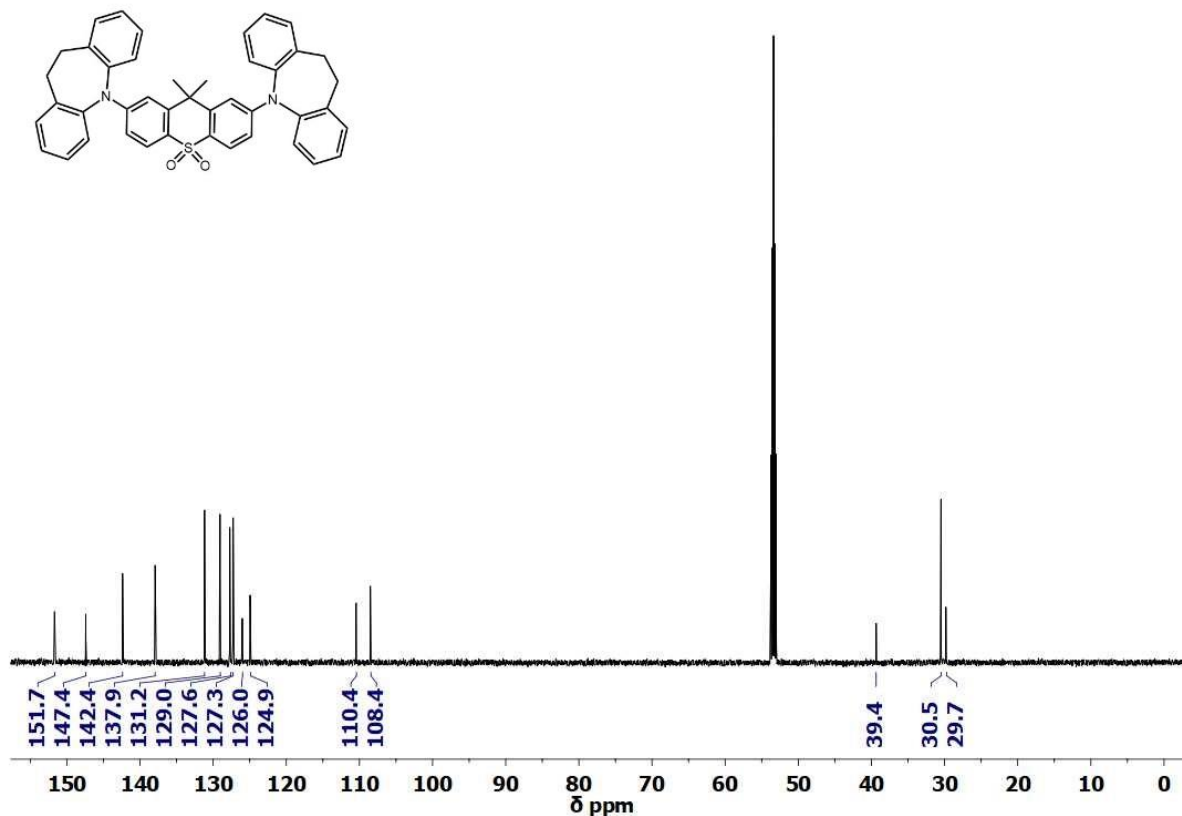


2,7-Dibromo-9,9-dimethylthioxanthene-*S,S*-dioxide (0.50 g, 1.28 mmol, 1 eq.) and 10,11-dihydro-5*H*-dibenzo[*b,f*]azepine (0.52 g, 2.60 mmol, 2.2 eq.) were dried under vacuum for 30 min in a two-neck round-bottomed 100 mL flask fitted with a reflux condenser. The flask was back-filled with argon for 30 min, then $\text{Pd}_2(\text{dba})_3 \cdot \text{CHCl}_3$ (66 mg, 0.06 mmol, 0.05 eq.) and $\text{HP}^t\text{-Bu}_3\text{BF}_4$ (37 mg, 0.13 mmol, 0.1 eq.) and toluene (30 mL) were added and the reaction

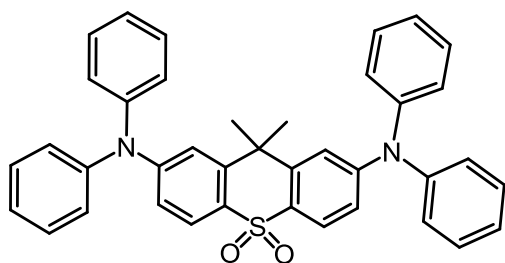
mixture was bubbled with argon for 30 min. *t*-BuONa (0.37 g, 3.84 mmol, 3 eq.) was added under a high flow of argon and the reaction was heated then to 115°C (DrySyn kit temperature) with stirring for 17 h. After being cooled to room temperature, the reaction mixture was extracted with CHCl₃. Afterwards the organic layer was dried over MgSO₄ and filtered. The solvent was removed under reduced pressure and the crude mixture was purified by silica gel chromatography with gradient elution from 50% v/v CHCl₃/hexane switching to 100% CHCl₃ in 10% increasing increments. Removal of solvent under reduced pressure resulted in product as a yellow solid. Recrystallization from a boiling mixture of diethyl ether and hexane (5/1 v/v) gave pure product as a cream-white crystalline solid (0.36 g, 44% yield).

¹H NMR (400 MHz, CD₂Cl₂) δ: 7.74 (d, 2H, *J* = 8.80 Hz), 7.38 (d, 2H, *J* = 2.11 Hz), 7.37-7.38 (m, 4H), 7.30-7.32 (m, 4H), 7.26-7.29 (m, 8H), 6.80 (d, 2H, *J* = 2.32 Hz), 6.58 (dd, 2H, *J* = 8.79 Hz, *J* = 2.36 Hz), 2.98 (s, 8H), 1.44 (s, 6H). ¹³C NMR (101 MHz, CD₂Cl₂) δ: 151.7, 147.4, 142.4, 137.9, 131.2, 129.1, 127.7, 127.3, 126.0, 124.9, 110.5, 108.5, 39.4, 30.5, 29.8. HRMS-ASAP+ *m/z* calculated for C₄₃H₃₆N₂O₂S [M]⁺ 644.2497, found: 644.2517. Anal. Calc. for C₄₃H₃₆N₂O₂S: C, 80.09; H, 5.63; N, 4.34. Found: C, 80.07; H, 5.59; N, 4.26. m.p. 232-234 °C.





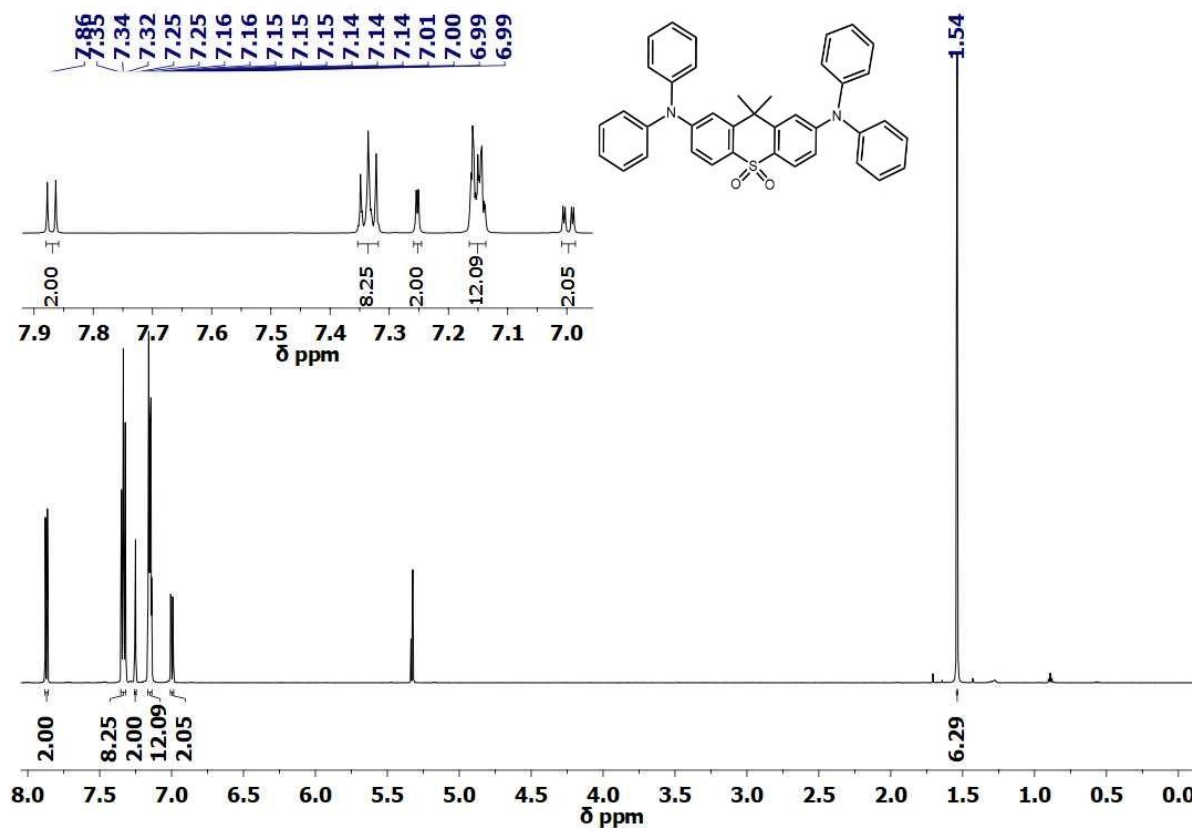
- 2,7-Bis(diphenylamino)-9,9-dimethyl-9H-thioxanthene-10,10-dioxide (*p*-DDPA-TXO2)

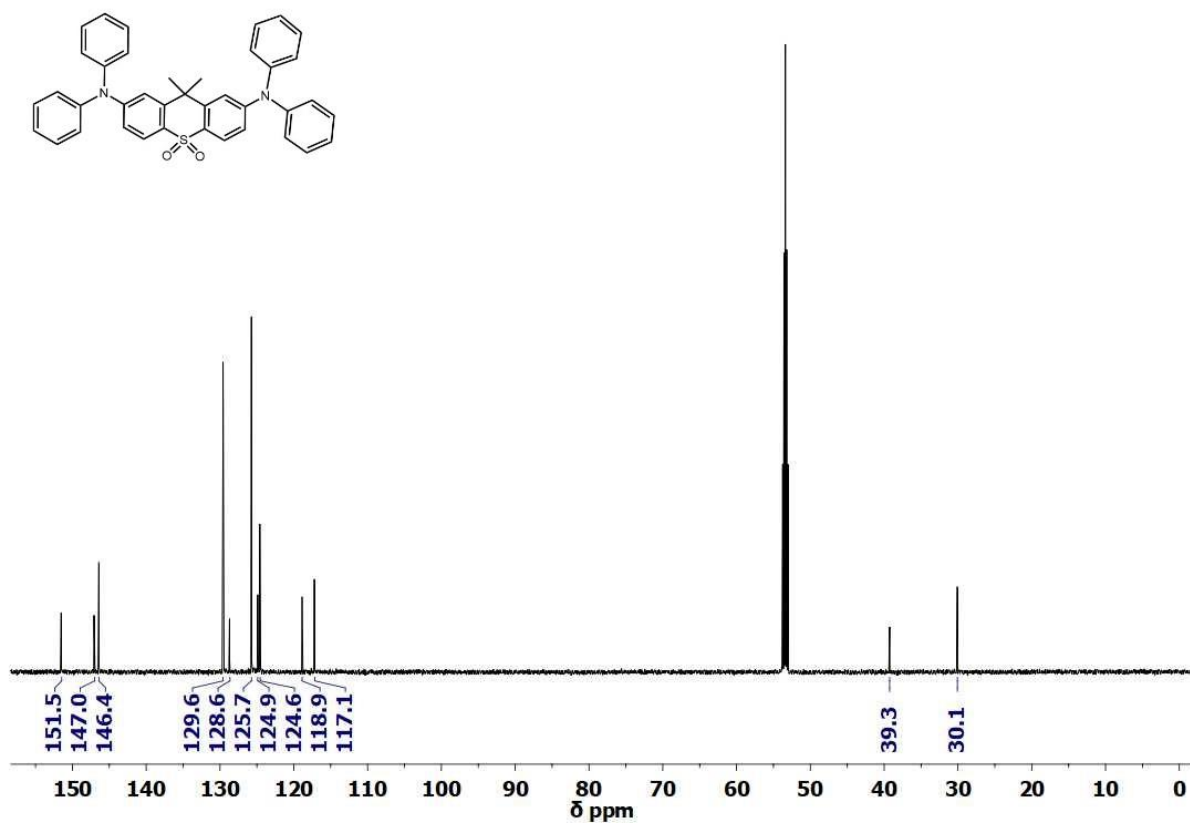


2,7-Dibromo-9,9-dimethylthioxanthene-*S,S*-dioxide (0.50 g, 1.28 mmol, 1 eq.) and diphenylamine (0.44 g, 2.60 mmol, 2.2 eq.) were dried under vacuum for 30 min in a two-neck round-bottomed 100 mL flask fitted with a reflux condenser. The flask was back-filled with argon for 30 min, then $\text{Pd}_2(\text{dba})_3 \cdot \text{CHCl}_3$ (66 mg, 0.06 mmol, 0.05 eq.) and $\text{HP}t\text{-Bu}_3\text{BF}_4$ (37 mg, 0.13 mmol, 0.1 eq.) and toluene (30 mL) were added and the reaction mixture was bubbled with argon for 30 min. *t*-BuONa (0.37 g, 3.84 mmol, 3 eq.) was added under a high flow of argon and the reaction was then heated to 115 °C (DrySyn kit temperature) with stirring for 17 h. After being cooled to room temperature, the reaction mixture was extracted with CHCl_3 . Afterwards the organic layer was dried over MgSO_4 and filtered. The solvent was removed under reduced pressure and the crude mixture was purified by silica gel chromatography with gradient elution from 50% v/v CHCl_3 /hexane switching to 100% CHCl_3 in 10% increasing increments. Removal of solvent under reduced pressure resulted in

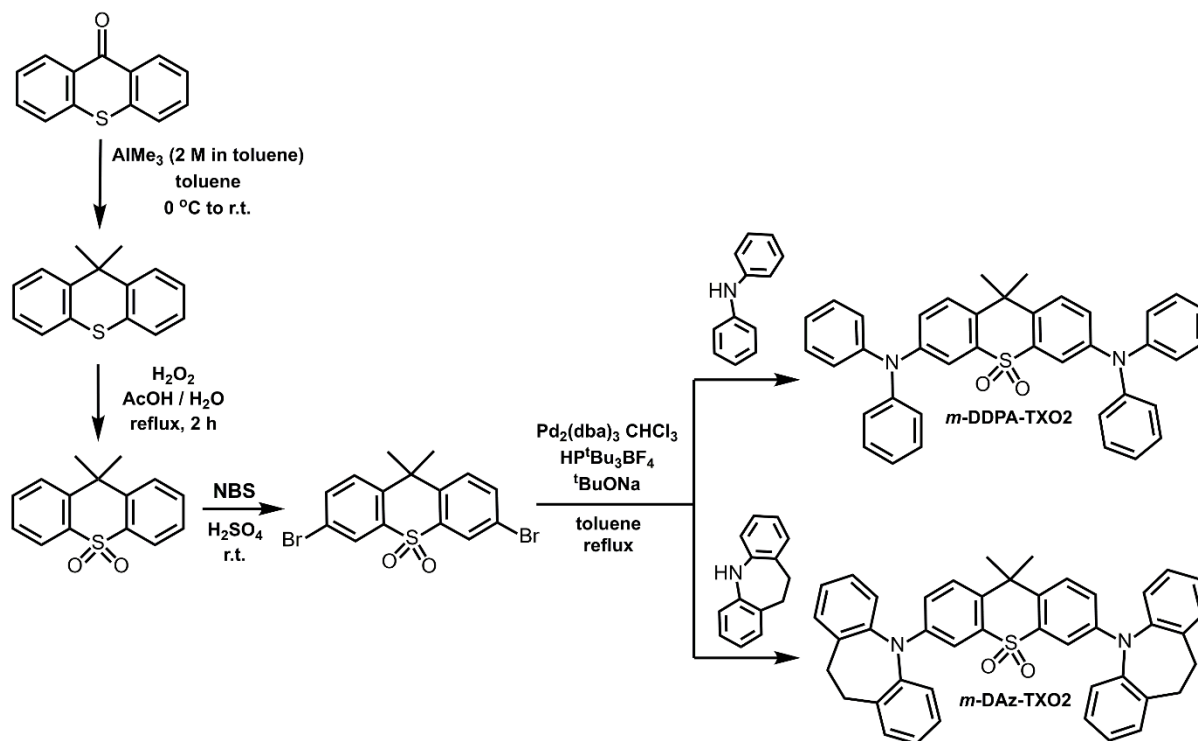
product as a yellow solid. Precipitation from dichloromethane solution to cold hexane gave pure product as a white solid (0.36 g, 33% yield).

^1H NMR (400 MHz, CD_2Cl_2) δ : 7.87 (d, 2H, $J = 8.64$ Hz), 7.33 (t, 8H, $J = 7.22$ Hz), 7.25 (d, 2H, $J = 2.19$ Hz), 7.14-7.17 (m, 12H), 7.00 (dd, 2H, $J = 8.64$ Hz, $J = 2.17$ Hz), 1.51 (s, 6H).
 ^{13}C NMR (101 MHz, CD_2Cl_2) δ : 151.5, 147.1, 146.4, 129.6, 128.7, 125.4, 124.9, 124.6, 118.9, 117.2, 39.3, 30.1. HRMS-ASAP+ m/z calculated for $\text{C}_{39}\text{H}_{32}\text{N}_2\text{O}_2\text{S}$ $[\text{M}]^+$ 592.2184, found: 592.2188. Anal. Calc. for $\text{C}_{39}\text{H}_{32}\text{N}_2\text{O}_2\text{S}$: C, 79.03; H, 5.44; N, 4.73. Found: C, 78.67; H, 5.46; N, 4.69. m.p. 243-245 $^\circ\text{C}$.

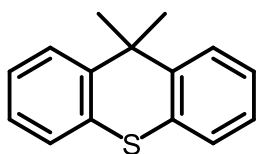




Synthesis of meta-isomers



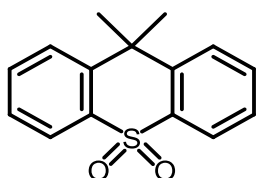
- 9,9-Dimethyl-9*H*-thioxanthene



9,9-Dimethyl-9*H*-thioxanthene was prepared according the literature³ starting from thioxanthene-9-one (5.0 g) and obtained as a colorless oil (4.9 g, yield 94%).

¹H NMR (400 MHz, CD₂Cl₂) δ: 7.61 (dd, 2H, *J* = 7.93 Hz, *J* = 1.40 Hz), 7.50 (dd, 2H, *J* = 7.54, *J* = 1.50 Hz), 7.33 (td, 2H, *J* = 7.32 Hz, *J* = 1.51 Hz), 7.25 (td, 2H, *J* = 7.44 Hz, *J* = 1.42 Hz), 1.73 (s, 6H). ¹³C NMR (101 MHz, CD₂Cl₂) δ: 142.3, 132.8, 127.1, 126.6, 126.0, 124.7, 40.3, 24.8.

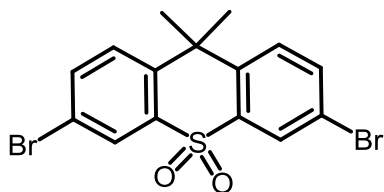
- 9,9-Dimethylthioxanthene-*S,S*-dioxide⁴



To a stirring solution of 9,9-dimethylthioxanthene-*S,S*-dioxide (2.0 g, 8.98 mmol) in AcOH (60 mL) was slowly added H₂O₂ (35 wt% in H₂O, 50 mL). The reaction mixture was refluxed for 2 h and left to cool to room temperature, resulting in the crystallization of pure product, collected by filtration and washed with water and MeOH. White crystalline solid (2.10 g, yield 91%).

¹H NMR (400 MHz, CDCl₃) δ: 8.22 (dd, 2H, *J* = 7.73 Hz, *J* = 1.45 Hz), 7.77 (dd, 2H, *J* = 8.01 Hz, *J* = 1.13 Hz), 7.62 (td, 2H, *J* = 7.35 Hz, *J* = 1.56 Hz), 7.53 (td, 2H, *J* = 7.57 Hz, *J* = 1.13 Hz), 1.91 (s, 6H). ¹³C NMR (101 MHz, CDCl₃) δ: 145.8, 136.8, 132.8, 127.5, 125.7, 124.3, 39.2, 30.9.

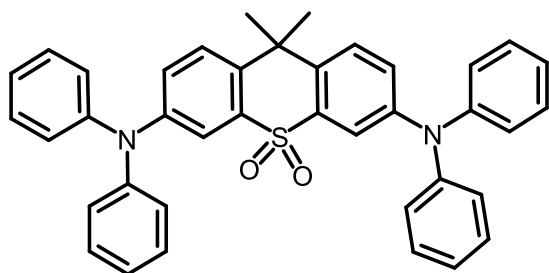
- 3,6-Dibromo-9,9-dimethylthioxanthene-*S,S*-dioxide⁵



9,9-Dimethylthioxanthene-*S,S*-dioxide (1.59 g, 5.81 mmol) was dissolved in concentrated H₂SO₄ (35 mL) and *N*-bromosuccinimide (2.06 g, 11.6 mmol) was added slowly over 1 h. The reaction mixture was stirred vigorously for a further 24 h at room temperature. After that, the reaction mixture was poured over ice, resulting in a white precipitate. The resulting solid was recrystallized from ethanol. White crystals (1.50 g, yield 62%).

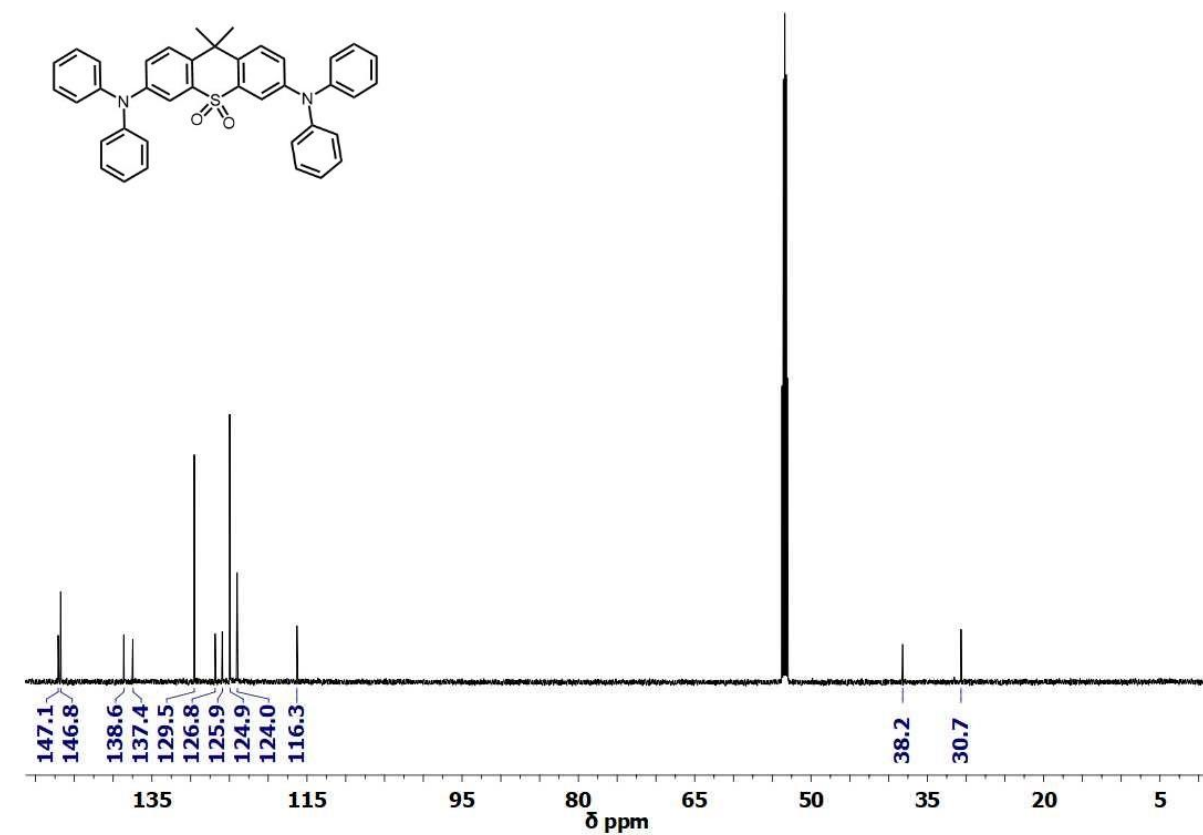
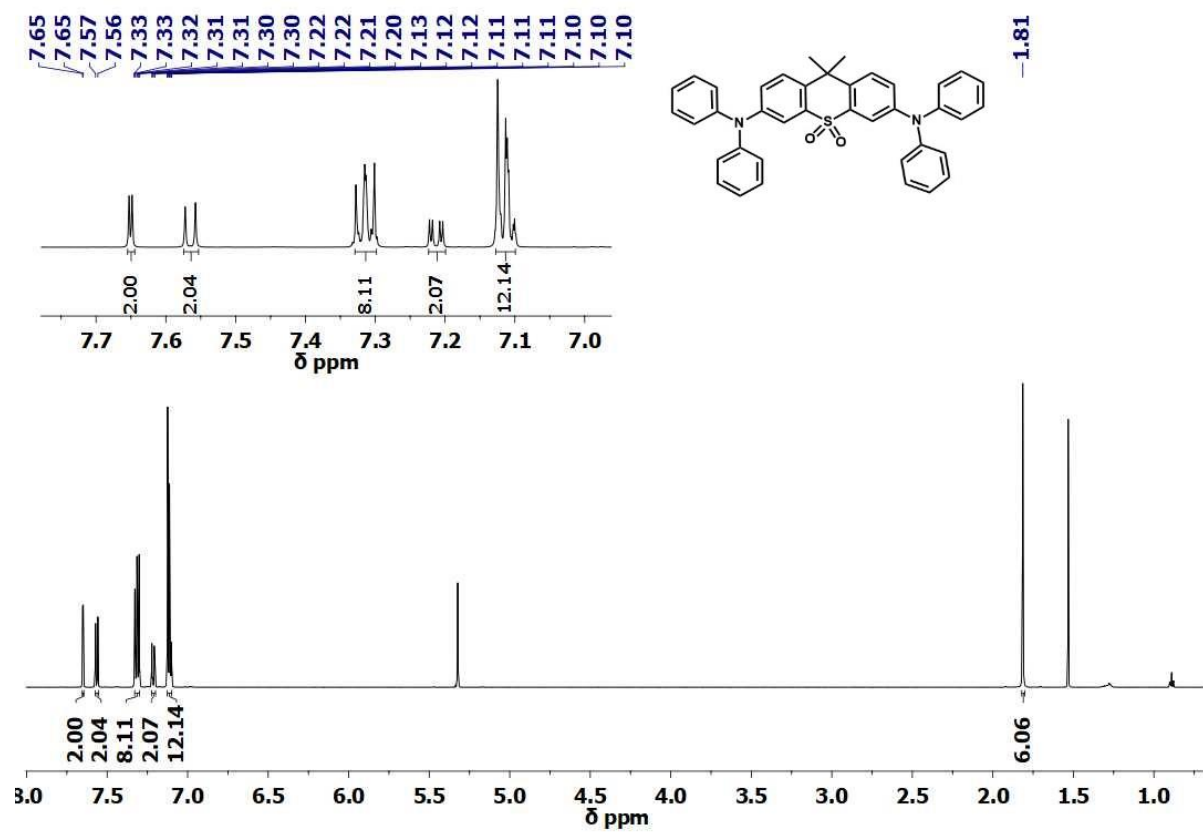
^1H NMR (400 MHz, CDCl_3) δ : 8.31 (d, 2H, $J = 2.16$ Hz), 7.74 (dd, 2H, $J = 8.59$ Hz, $J = 2.21$ Hz), 7.63 (d, 2H, $J = 8.66$ Hz), 1.87 (s, 6H). ^{13}C NMR (101 MHz, CDCl_3) δ : 144.2, 137.9, 135.8, 127.5, 127.2, 121.5, 39.1, 30.4.

- 3,6-Bis(diphenylamino)-9,9-dimethyl-9H-thioxanthene-10,10-dioxide (***m*-DDPA-TXO2**)

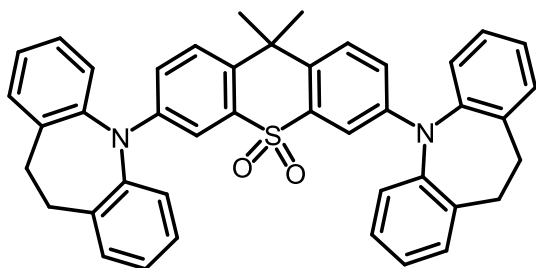


3,6-Dibromo-9,9-dimethylthioxanthene-*S,S*-dioxide (0.50 g, 1.28 mmol, 1 eq.) and diphenylamine (0.44 g, 2.60 mmol, 2.2 eq.) were dried under vacuum for 30 min in a two-neck round-bottomed 100 mL flask fitted with a reflux condenser. The flask was back-filled with argon for 30 min, then $\text{Pd}_2(\text{dba})_3 \cdot \text{CHCl}_3$ (66 mg, 0.06 mmol, 0.05 eq.) and $\text{HP}t\text{-Bu}_3\text{BF}_4$ (37 mg, 0.13 mmol, 0.1 eq.) and toluene (25 mL) were added and the reaction mixture was bubbled with argon for 30 min. $t\text{-BuONa}$ (0.37 g, 3.84 mmol, 3 eq.) was added under a high flow of argon and the reaction was then heated to 115 °C (DrySyn kit temperature) with stirring for 17 h. After being cooled to room temperature, the reaction mixture was extracted with CHCl_3 . Afterwards the organic layer was dried over MgSO_4 and filtered. The solvent was removed under reduced pressure and the crude mixture was purified by silica gel chromatography with gradient elution from 50% v/v CHCl_3 /hexane switching to 100% CHCl_3 in 10% increasing increments. Removal of solvent under reduced pressure resulted in product as a white solid. Precipitation from dichloromethane solution to cold hexane gave pure product as a white solid (0.40 g, 38% yield).

^1H NMR (400 MHz, CD_2Cl_2) δ : 7.65 (d, 2H, $J = 2.62$ Hz), 7.56 (d, 2H, $J = 8.80$ Hz), 7.30-7.33 (m, 8H), 7.21 (dd, 2H, $J = 8.79$ Hz, $J = 2.64$ Hz), 7.10-7.13 (m, 12H), 1.81 (s, 6H). ^{13}C NMR (101 MHz, CD_2Cl_2) δ : 147.1, 146.8, 138.6, 137.4, 129.5, 126.8, 125.9, 124.9, 124.0, 116.3, 38.2, 30.7. HRMS-ASAP+ m/z calculated for $\text{C}_{39}\text{H}_{32}\text{N}_2\text{O}_2\text{S}$ $[\text{M}]^+$ 592.2184, found: 592.2188. Anal. Calc. for $\text{C}_{39}\text{H}_{32}\text{N}_2\text{O}_2\text{S}$: C, 79.03; H, 5.44; N, 4.73. Found: C, 78.62; H, 5.42; N, 4.64. m.p. 258-260 °C.

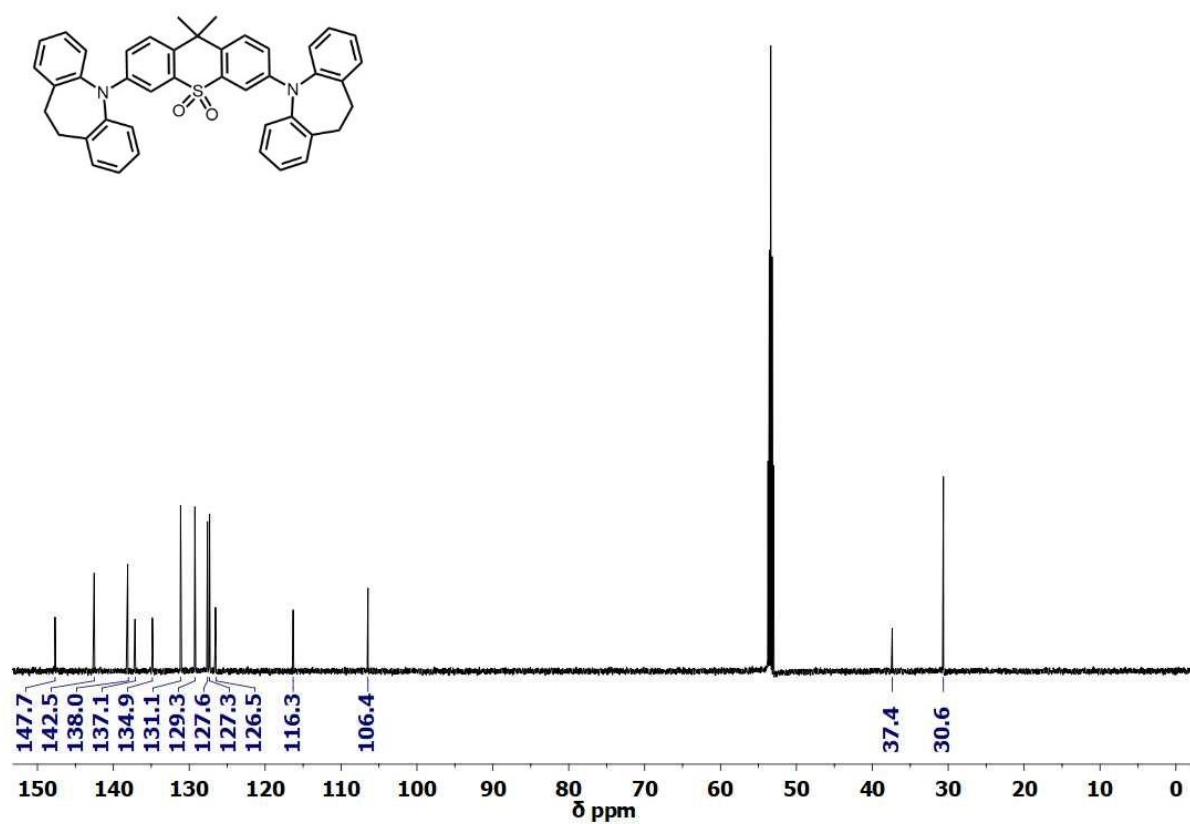
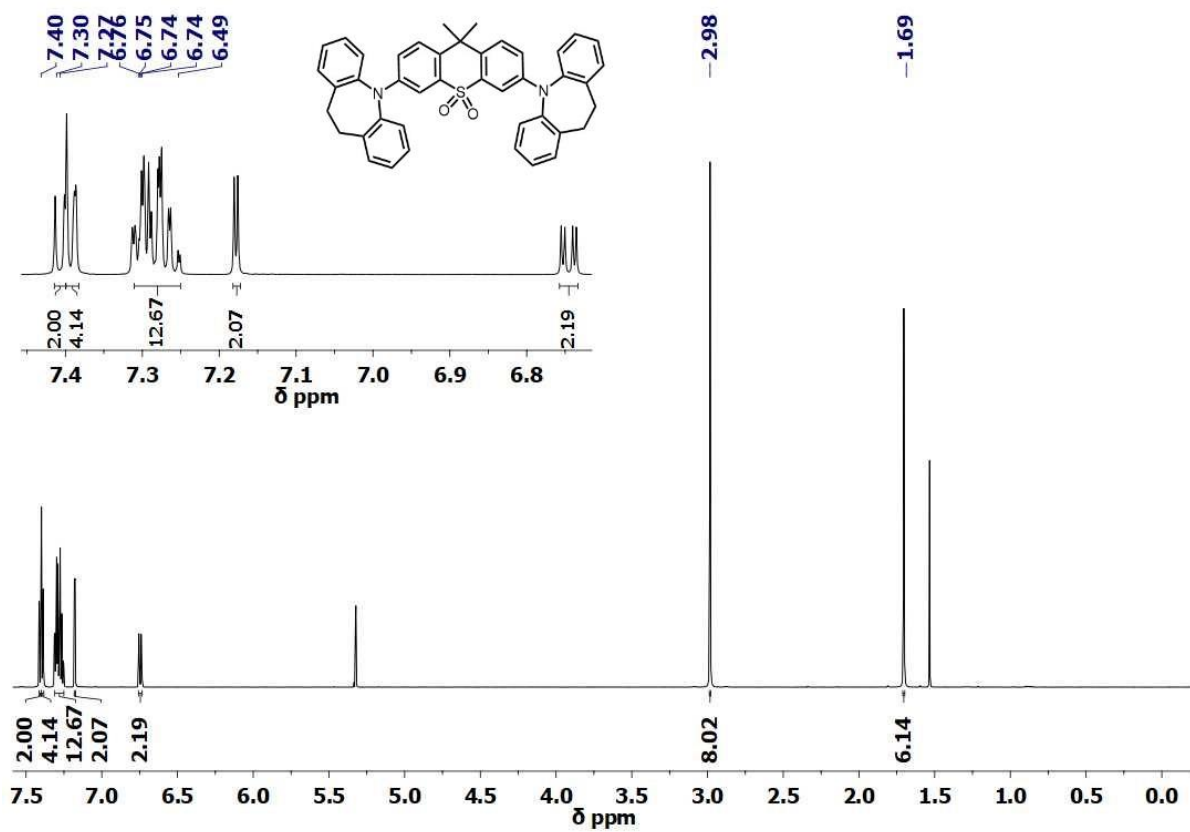


- 3,6-Bis(10,11-dihydro-5*H*-dibenzo[*b,f*]azepin-5-yl)-9,9-dimethyl-9*H*-thioxanthene-10,10-dioxide (***m*-DAz-TXO2**)



3,6-Dibromo-9,9-dimethylthioxanthene-*S,S*-dioxide (0.50 g, 1.28 mmol, 1 eq.) and 10,11-dihydro-5*H*-dibenz[*b,f*]azepine (0.52 g, 2.60 mmol, 2.2 eq.) were dried under vacuum for 30 min in a two-neck round-bottomed 100 mL flask fitted with a reflux condenser. The flask was back-filled with argon for 30 min, then Pd₂(dba)₃·CHCl₃ (66 mg, 0.06 mmol, 0.05 eq.) and HP*t*-Bu₃BF₄ (37 mg, 0.13 mmol, 0.1 eq.) and toluene (30 mL) were added and the reaction mixture was bubbled with argon for 30 min. *t*-BuONa (0.37 g, 3.84 mmol, 3 eq.) was added under a high flow of argon and the reaction was then heated to 115 °C (DrySyn kit temperature) with stirring for 17 h. After being cooled to room temperature, the reaction mixture was extracted with CHCl₃. Afterwards the organic layer was dried over MgSO₄ and filtered. The solvent was removed under reduced pressure and the crude mixture was purified by silica gel chromatography with gradient elution from 50% v/v CHCl₃/hexane switching to 100% CHCl₃ in 10% increasing increments. Removal of solvent under reduced pressure resulted in product as a white solid. Precipitation from dichloromethane solution to cold hexane gave pure product as a white solid (0.42 g, 51% yield).

¹H NMR (400 MHz, CD₂Cl₂) δ: 7.41 (d, 2H, *J* = 7.15 Hz), 7.38-7.40 (m, 4H), 7.25-7.31 (m, 12H), 7.18 (d, 2H, *J* = 2.83 Hz), 6.75 (dd, 2H, *J* = 8.94 Hz, *J* = 2.84 Hz), 2.88 (s, 8H), 1.70 (s, 6H). ¹³C NMR (101 MHz, CD₂Cl₂) δ: 147.7, 142.5, 138.11, 137.1, 134.8, 131.1, 129.2, 127.6, 127.3, 126.5, 116.3, 106.4, 37.4, 30.6. HRMS-ASAP+ *m/z* calculated for C₃₉H₃₂N₂O₂S [M]⁺ 644.2497, found: 644.2525. Anal. Calc. for C₄₃H₃₆N₂O₂S: C, 80.09; H, 5.63; N, 4.34. Found: C, 80.17; H, 5.62; N, 4.55. m.p. 342-344 °C.



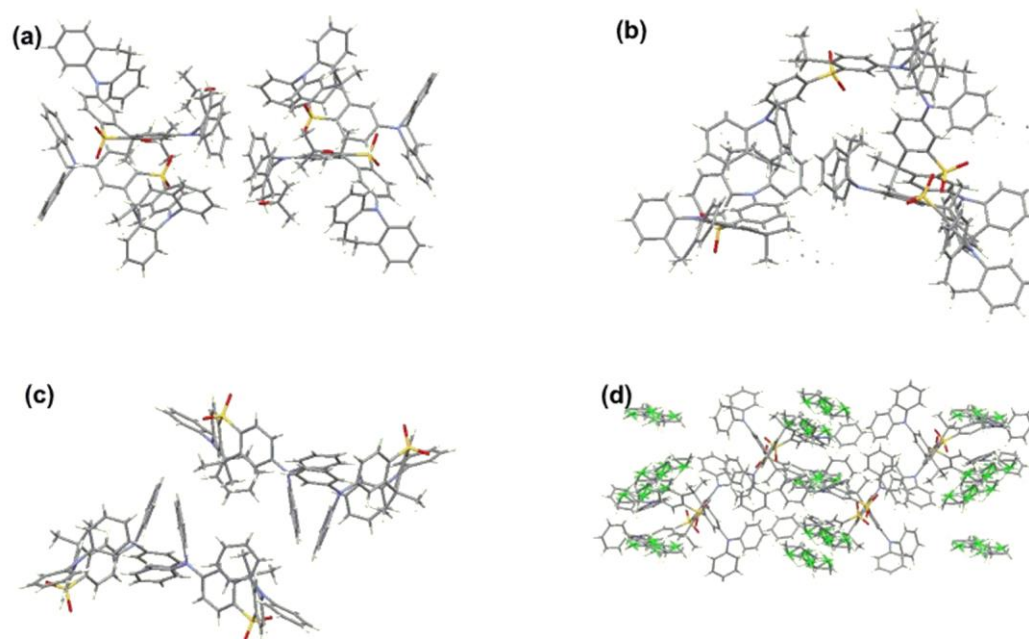


Figure S1. X-Ray packing patterns of (a) *p*-DAz-TXO₂, (b) *m*-DAz-TXO₂, (c) *p*-DDPA-TXO₂, and (d) *m*-DDPA-TXO₂

Table S1. Crystal data and experimental details of *p*-DAz-TXO2, *m*-DAz-TXO2, *p*-DDPA-TXO2 and *m*-DDPA-TXO2

Compound	<i>m</i> -DAz-TXO2	<i>p</i> -DDPA-TXO2	<i>m</i> -DDPA-TXO2	<i>m</i> -DDPA-TXO2	<i>p</i> -DAz-TXO2	<i>p</i> -DAz-TXO2	<i>p</i> -DAz-TXO2
CCDC	1872344	1872345	1872346	1872347	1872348	1872349	1872350
Formula	C ₄₃ H ₃₆ N ₂ O ₂ S	C ₃₉ H ₃₂ N ₂ O ₂ S	C ₃₉ H ₃₂ N ₂ O ₂ S	C ₃₉ H ₃₂ N ₂ O ₂ S ·0.44C ₆ H ₁₄ ·0.06CH ₂ Cl ₂	C ₄₃ H ₃₆ N ₂ O ₂ S ·CH ₂ Cl ₂	C ₄₃ H ₃₆ N ₂ O ₂ S ·CH ₂ Cl ₂	C ₃₉ H ₃₆ N ₂ O ₂ S ·Me ₂ CO
<i>D</i> _{calc.} / g cm ⁻³	1.270	1.320	1.295	1.263	1.357	1.344	1.286
μ /mm ⁻¹	0.137	0.148	0.145	0.146	0.261	2.482	1.145
Formula Weight	644.80	592.72	592.72	635.73	729.72	729.72	702.87
Size/mm ³	0.15×0.13×0.13	0.28×0.24×0.11	0.22×0.21×0.17	0.38×0.13×0.08	0.1×0.01×0.01	0.53×0.10×0.04	0.20×0.02×0.02
<i>T</i> /K	120	120	120	120	100	120	120
Crystal System	orthorhombic	monoclinic	triclinic	orthorhombic	orthorhombic	orthorhombic	monoclinic
Space Group	<i>P</i> 2 ₁ 2 ₁ 2 ₁ (no. 19)	<i>P</i> 2 ₁ / <i>c</i> (no. 14)	<i>P</i> -1 (no. 2)	<i>Pbca</i> (no. 61)	<i>Pbca</i> (no. 61)	<i>Pbca</i> (no. 61)	<i>P</i> 2 ₁ / <i>n</i> (no. 14)
<i>a</i> /Å	12.9552(4)	13.3299(7)	12.4874(6)	12.8953(6)	16.8912(6)	16.9973(7)	11.721(4)
<i>b</i> /Å	12.9939(4)	18.6530(10)	13.7988(7)	16.0322(7)	11.3960(4)	11.4060(5)	11.304(4)
<i>c</i> /Å	20.0294(7)	12.4216(7)	18.8029(9)	32.3384(14)	37.1194(14)	37.2160(16)	27.587(10)
α /°	90	90	76.4901(19)	90	90	90	90
β /°	90	105.1270(19)	75.1590(18)	90	90	90	96.745(6)
γ /°	90	90	83.1146(19)	90	90	90	90
<i>V</i> /Å ³	3371.72(19)	2981.5(3)	3039.0(3)	6685.6(5)	7145.2(4)	7215.1(5)	3630(2)
<i>Z</i>	4	4	4	8	8	8	4
Wavelength/Å	0.71073	0.71073	0.71073	0.71073	0.6889	1.54184	1.54184
Radiation type	Mo- <i>K</i> _α	Mo- <i>K</i> _α	Mo- <i>K</i> _α	Mo- <i>K</i> _α	synchrotron	Cu- <i>K</i> _α	Cu- <i>K</i> _α
2 θ _{max} /°	52	55	57.4	52	52.2	133.4	87.6
Reflections measured	51913	54619	54215	101608	49066	67345	8524
unique	6624	6852	15690	6559	8004	6263	2692
with <i>I</i> > 2 σ (<i>I</i>)	6056	5466	11430	5276	5620	4865	1189
<i>R</i> _{int}	0.045	0.051	0.041	0.057	0.101	0.073	0.182
Parameters, restraints	446, 3	402, 0	802, 0	451, 2	465, 0	465, 0	405, 265
$\Delta\rho$ / eÅ ⁻³	0.20, -0.25	0.38, -0.43	0.41, -0.50	0.36, -0.36	0.62, -1.15	0.40, -0.53	0.34, -0.31
Goodness of fit	1.046	1.023	1.035	1.034	1.041	1.064	0.976
<i>R</i> ₁ , <i>wR</i> ₂ (all data)	0.035, 0.071	0.056, 0.097	0.071, 0.109	0.053, 0.091	0.113, 0.273	0.075, 0.134	0.214, 0.211
<i>R</i> ₁ , <i>wR</i> ₂ [<i>I</i> > 2 σ (<i>I</i>)]	0.030, 0.069	0.039, 0.089	0.043, 0.099	0.037, 0.083	0.085, 0.242	0.053, 0.125	0.081, 0.159

S2. Theoretical investigation

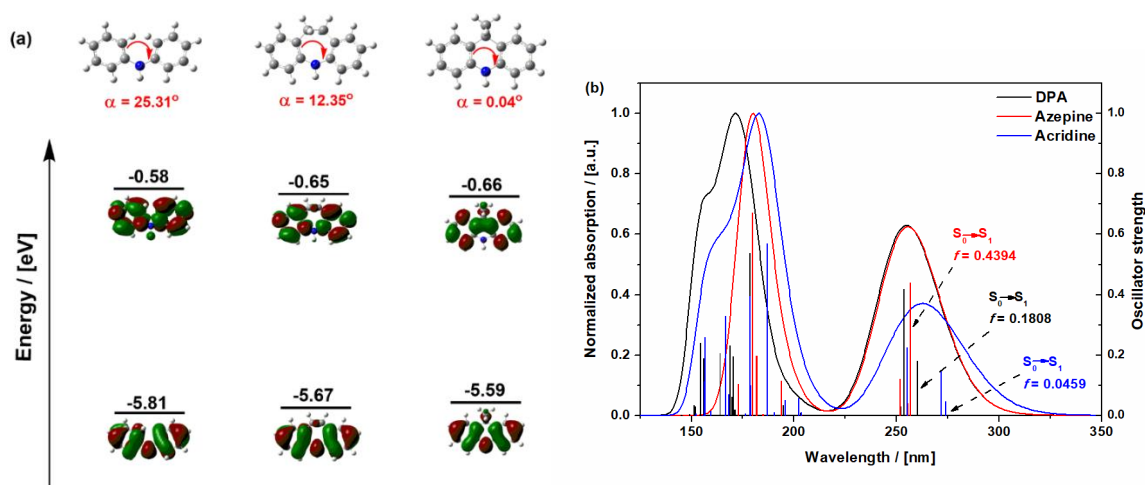


Figure S2. (a) The optimized structures along with profiles, frontier orbitals and corresponding HOMO/LUMO values (rBMK/6.31G(d)); (b) UV/Vis spectra (TD rBMK/6-31G(d)) of diphenylamine (DPA), 10,11-dihydro-5H-dibenz[*b,f*]azepine (Az), and 9,9-dimethylacridine (Ac).

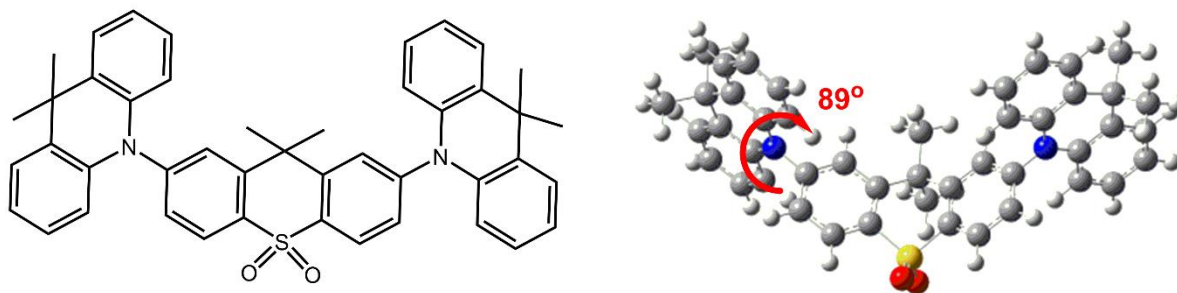
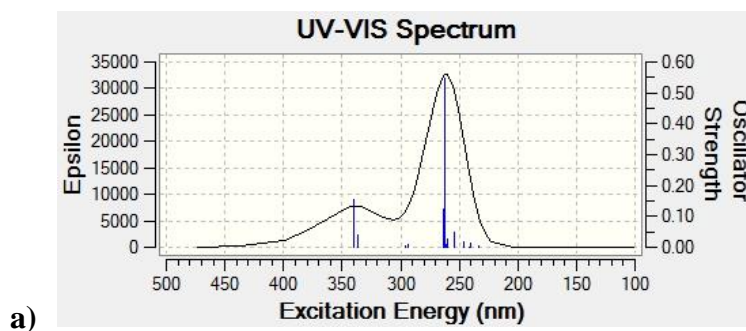


Figure S3. Chemical structure and the optimized structure (TD-DFT rBMK/6-31G(d)) of *p*-DDMAc-TXO2



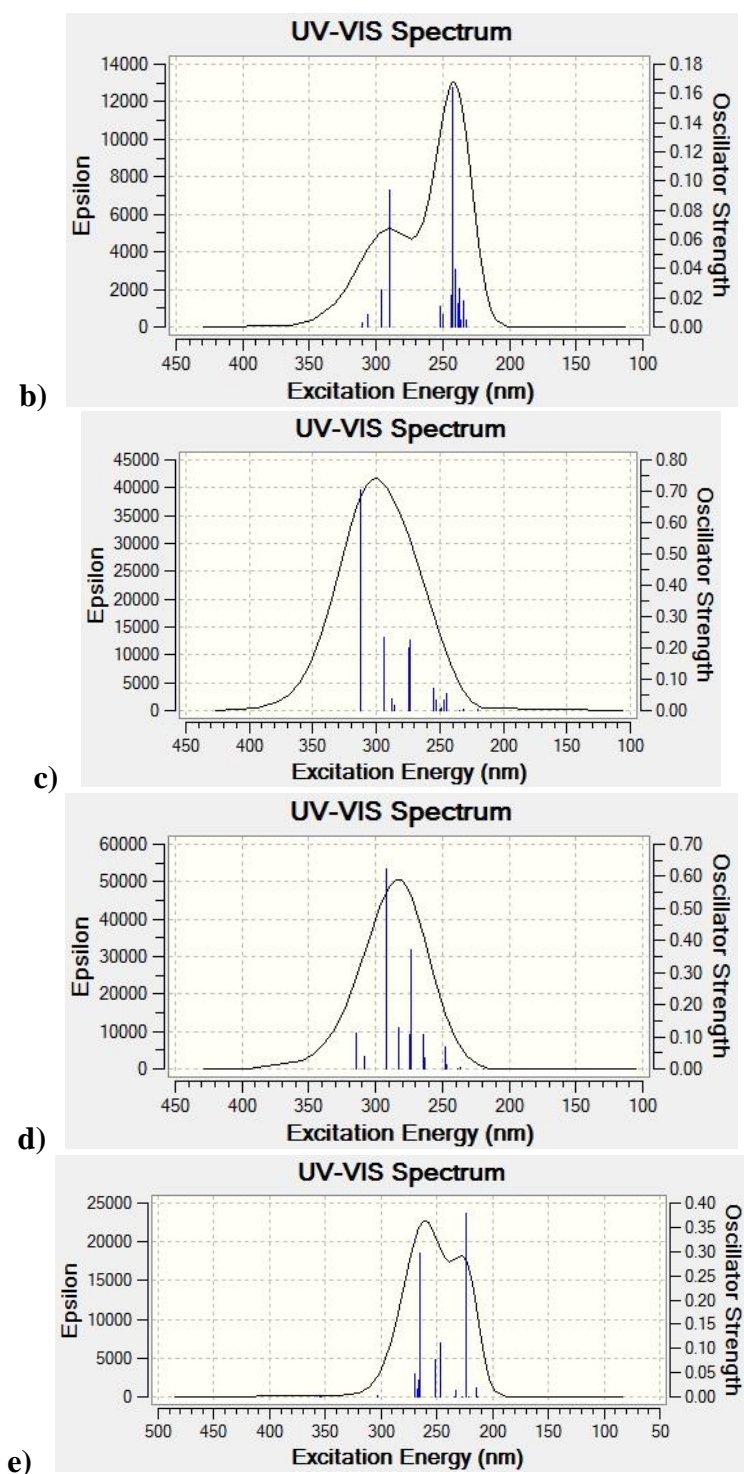


Figure S4. Theoretically predicted UV/Vis absorption spectra of *p*-DAz-TXO₂, *m*-DAz-TXO₂, *p*-DDPA-TXO₂, *m*-DDPA-TXO₂ and *p*-DDMAc-TXO₂ (TD-DFT rBMK/6-31G(d))

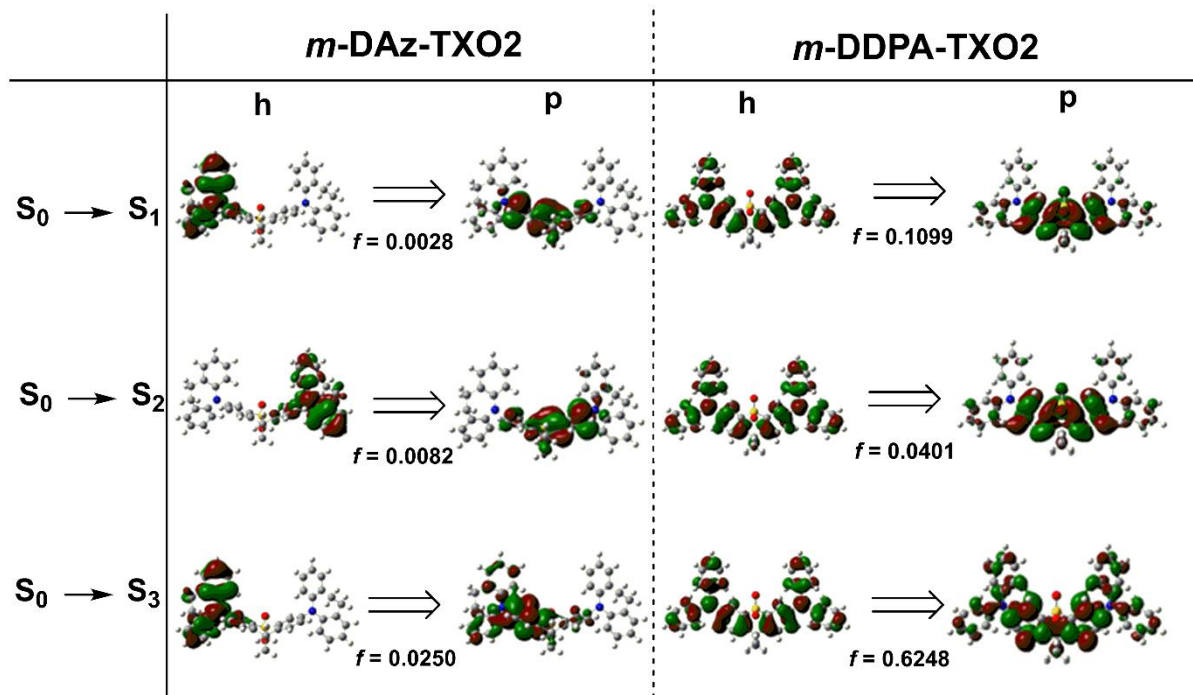


Figure S5. Natural transition orbitals (NTO) corresponding to the first three singlet transitions in the absorption of *m*-DAz-TXO2 and *m*-DDPA-TXO2 (TD-DFT rBMK/6-31G(d))

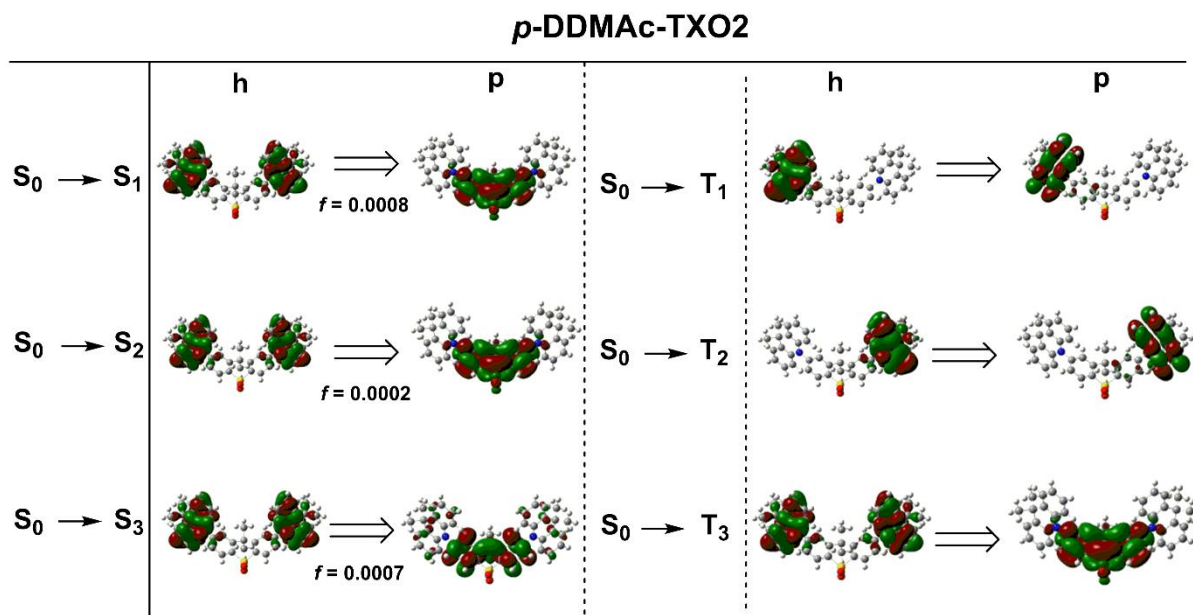


Figure S6. Natural transition orbitals (NTO) corresponding to the first three singlet and triplet transitions of *p*-DDMAc-TXO2 (TD-DFT rBMK/6-31G(d))

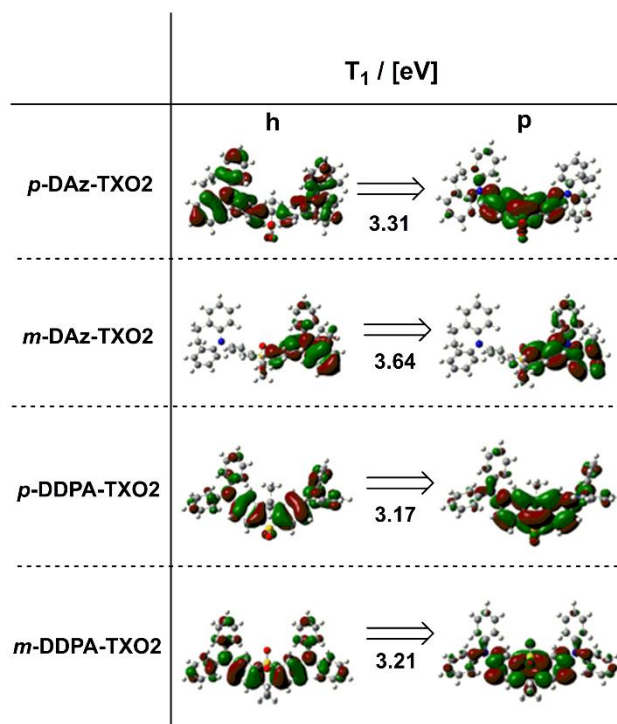
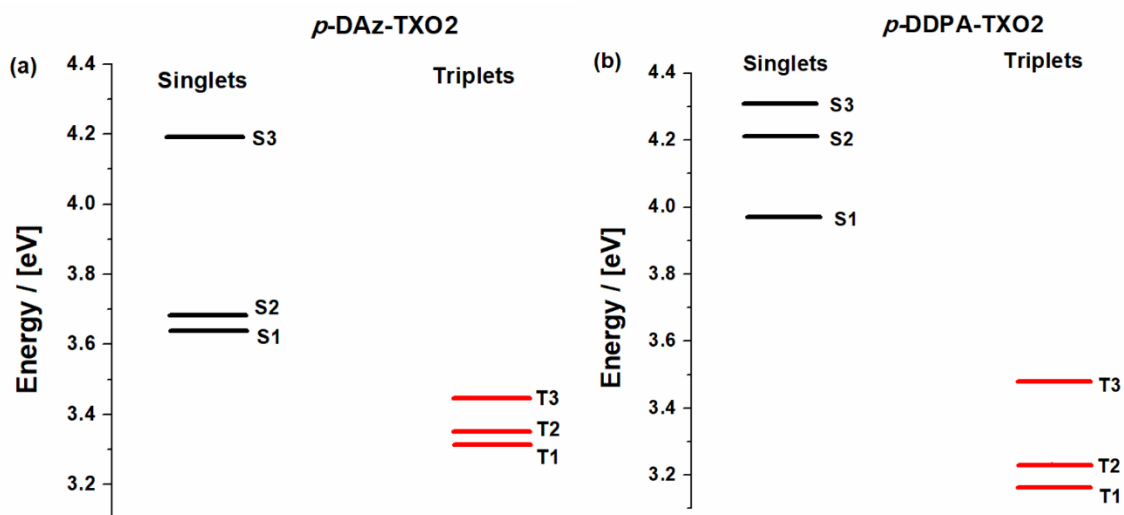


Figure S7. Natural transition orbitals (NTO) corresponding to the first triplet transitions of *p*-DAz-TXO2, *m*-DAz-TXO2, *p*-DDPA-TXO2 and *m*-DDPA-TXO2 (TD-DFT rBMK/6-31G(d))



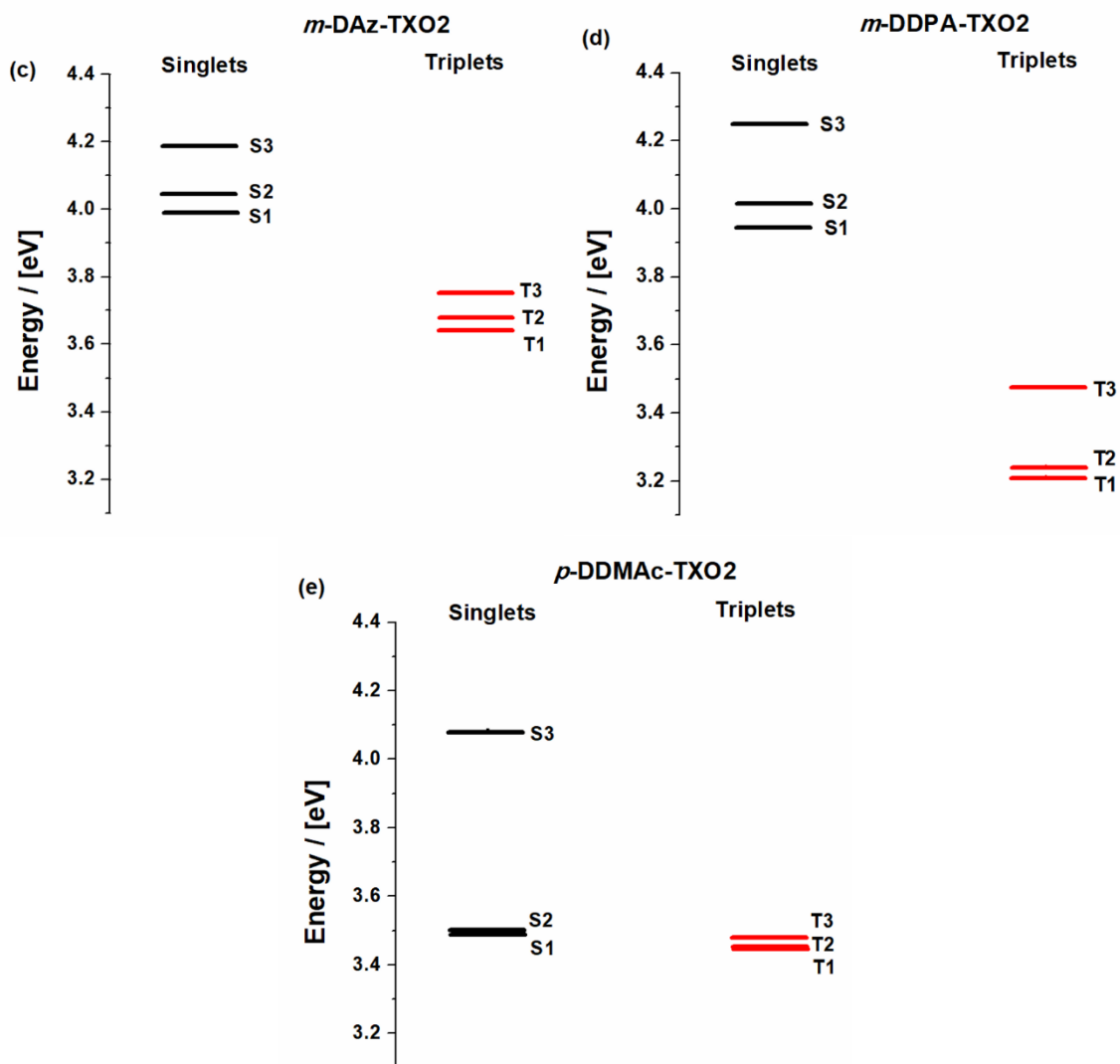
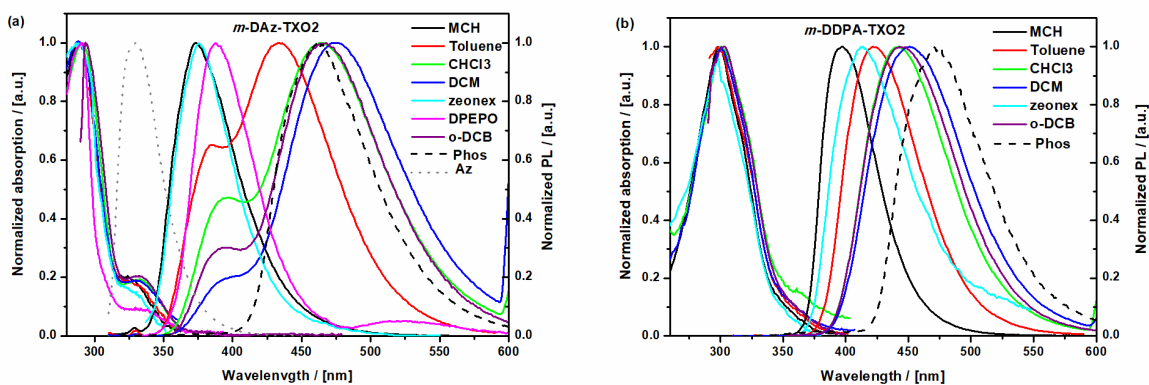


Figure S8. Energy diagrams depicting singlet/triplet energy distribution of *p*-DAz-TXO2, *p*-DDPA-TXO2, *m*-DAz-TXO2, *m*-DDPA-TXO2 and *p*-DDMAc-TXO2 (TD-DFT rBMK/6-31G(d))

S3. Optical and photophysical properties



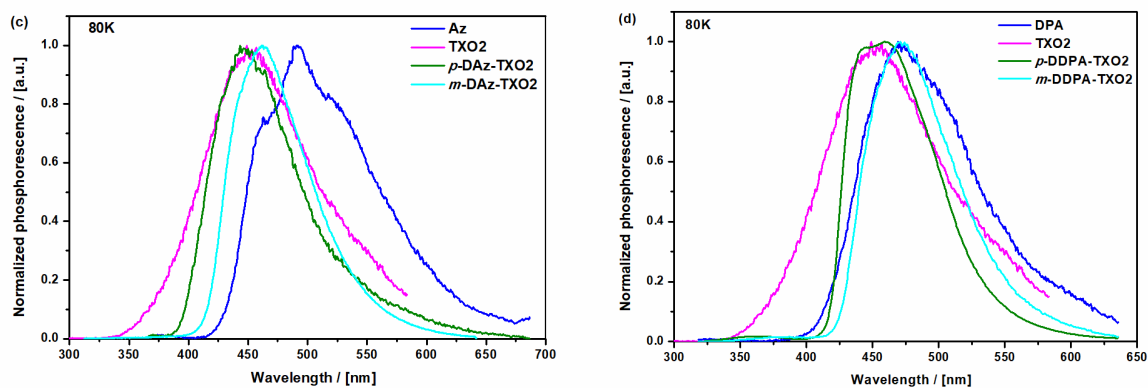
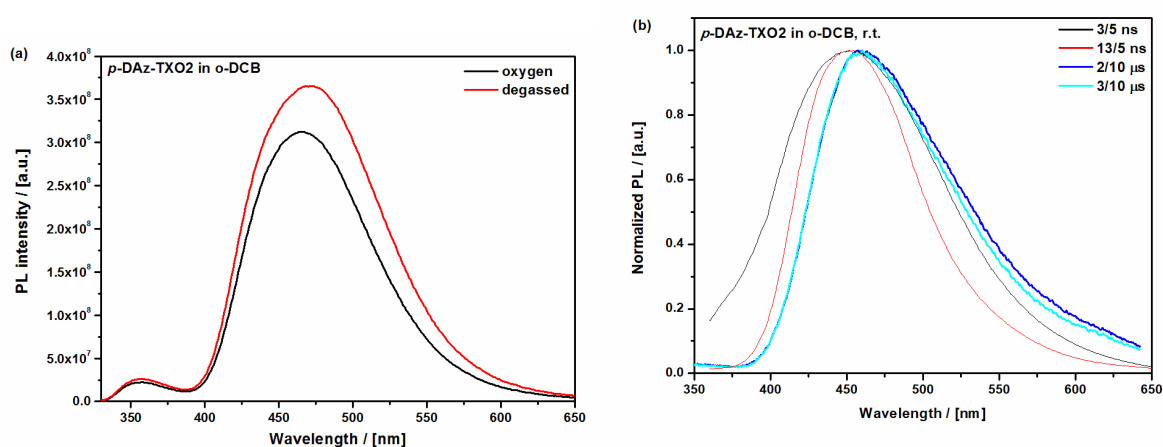


Figure S9. (a, b) UV/Vis absorption and photoluminescence of *m*-DAz-TXO2 and *m*-DDPA-TXO2 measured in various solvents ($\lambda_{\text{ex}} = 310 \text{ nm}$); (c, d) phosphorescence spectra of the D–A–D derivatives and the individual donor/acceptor units recorded at 80 K (delay 10 ms, integration time 10 ms).

Table S2. Degassing increments of *p*-DAz-TXO2, *p*-DDPA-TXO2, *m*-DAz-TXO2 and *m*-DDPA-TXO2, measured in various solvents.

Compound	CHCl ₃	DCM	<i>o</i> -DCB	Toluene
<i>p</i> -DAz-TXO2	1.57	1.46	1.31	2.1
<i>m</i> -DAz-TXO2	1.51	1.17	1.08	1.71
<i>p</i> -DDPA-TXO2	1.07	1.13	1.01	1.06
<i>m</i> -DDPA-TXO2	1.12	1.18	1.11	1.08



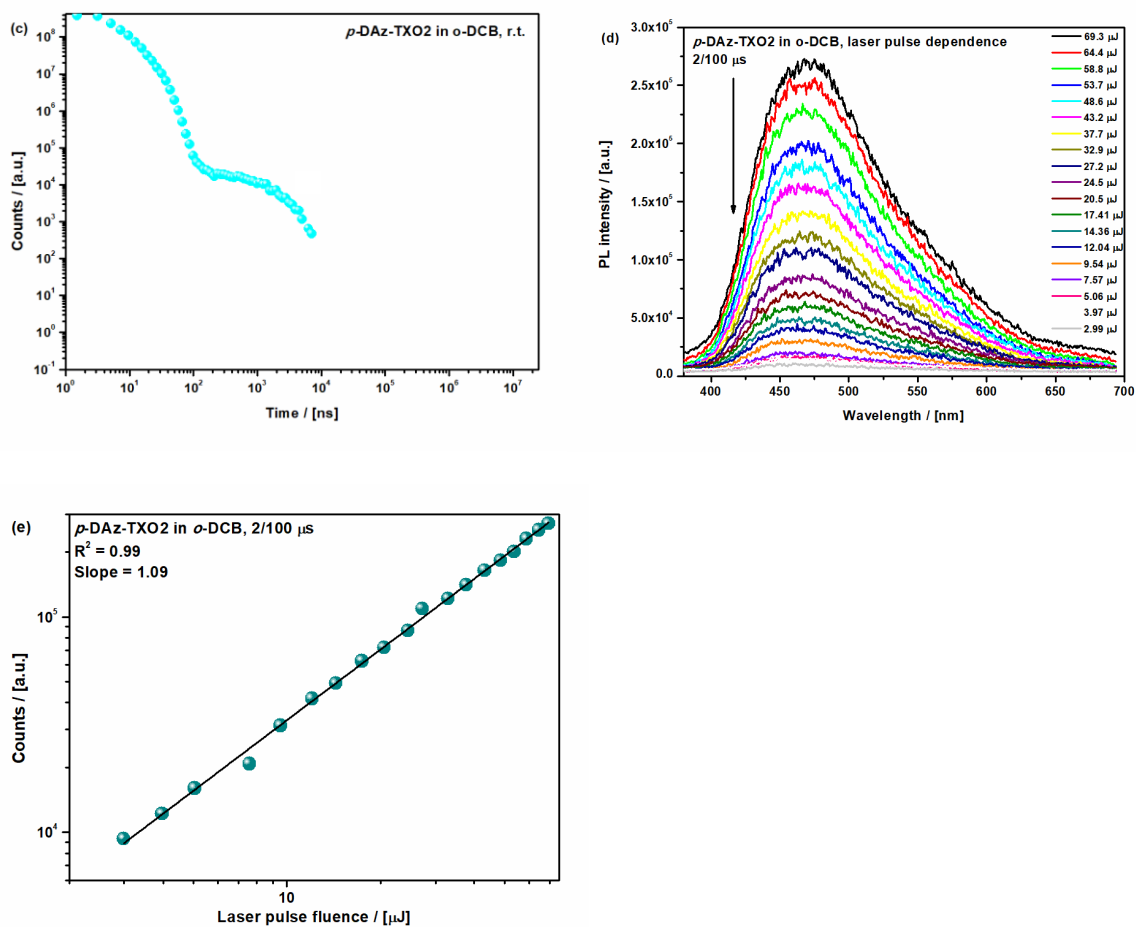


Figure S10. (a) Steady-state PL spectra of oxygen equilibrated and deoxygenated o -DCB solutions of p -DAz-TXO2; (b) time-resolved (Nd-YAG laser, $\lambda_{\text{ex}} = 355$ nm) PL spectra (c) PL decay curve; (d, e) dependence of the PL intensity on the excitation laser fluence.

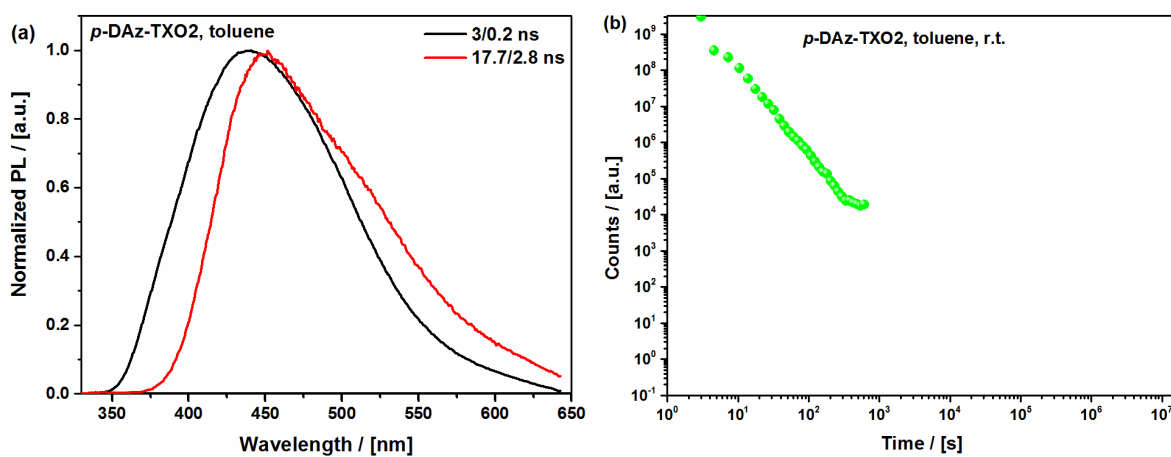


Figure S11. (a) time-resolved (Nd-YAG laser, $\lambda_{\text{ex}} = 355$ nm) PL spectra (b) PL decay curve of the degassed toluene solution of p -DAz-TXO2.

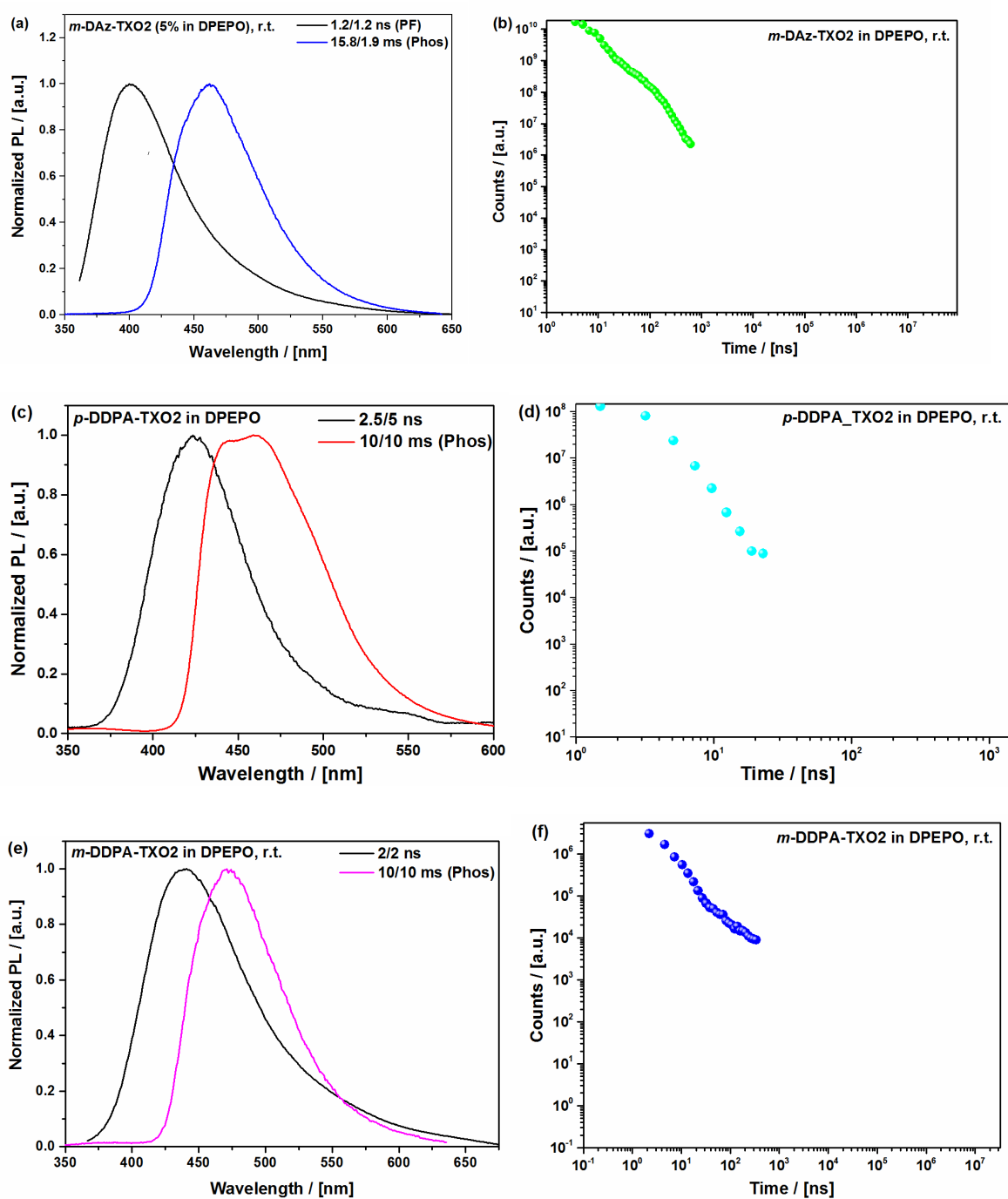


Figure S12. (a, c, e) Time-resolved (Nd-YAG laser, $\lambda_{\text{ex}} = 355$ nm) PL spectra; (b, d, f) PL decay curves of *m*-DAz-TXO2, *p*-DDPA-TXO2, *m*-DDPA-TXO2 measured in DPEPO at room temperature.

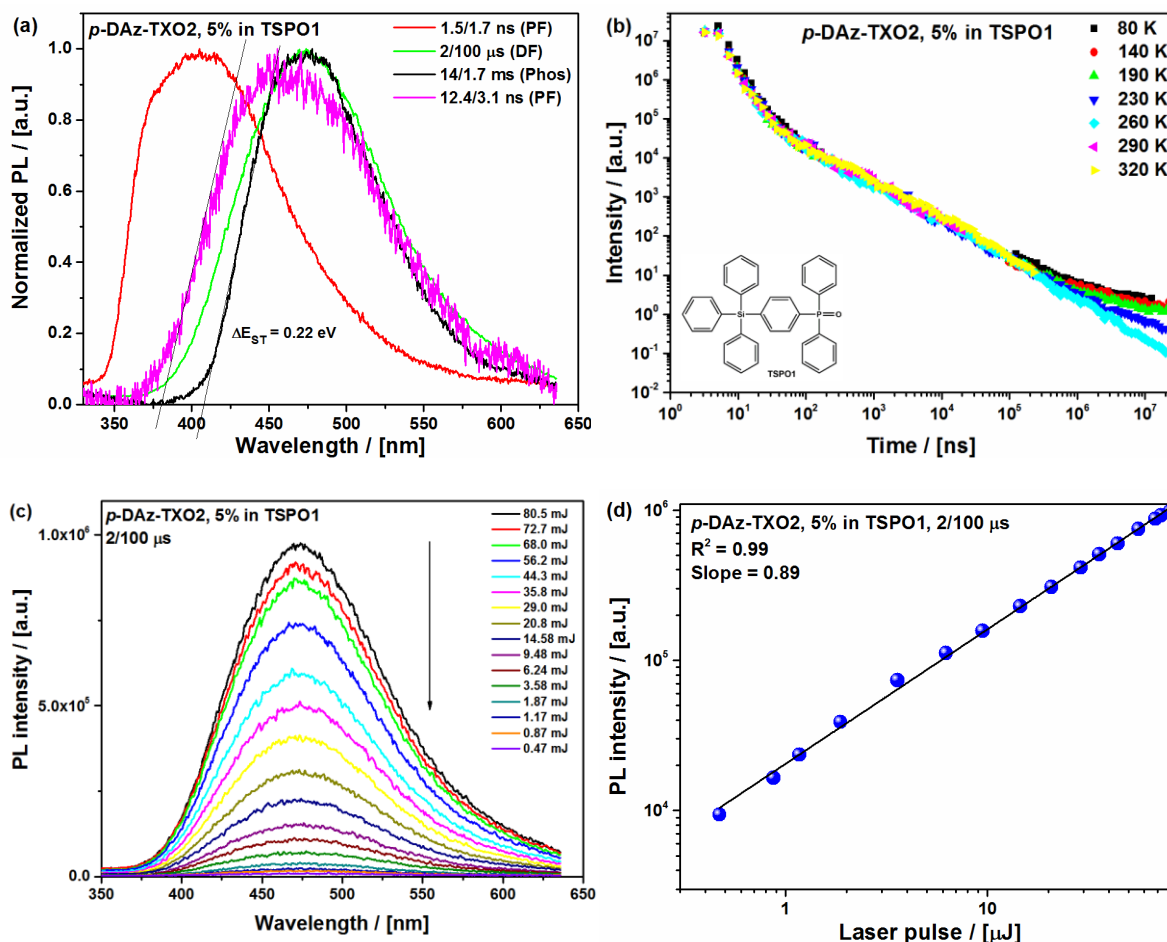


Figure S13. (a) Time-resolved (Nd-YAG laser, $\lambda_{\text{ex}} = 355$ nm) PL spectra (c) PL decay curve along with the chemical structure of TSP01; (d, e) dependence of the PL intensity on the excitation laser fluence of the deoxygenated film of *p*-DAz-TXO2 in TSP01

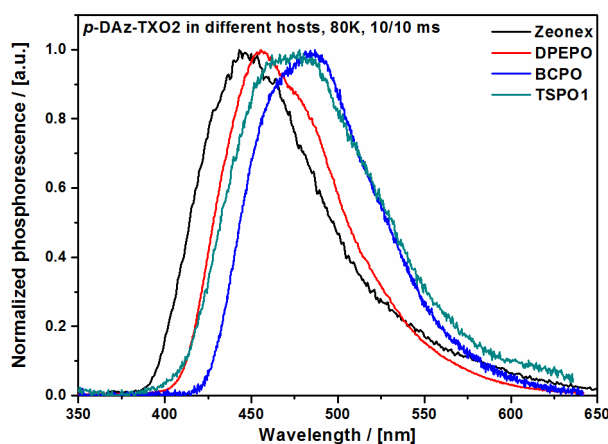
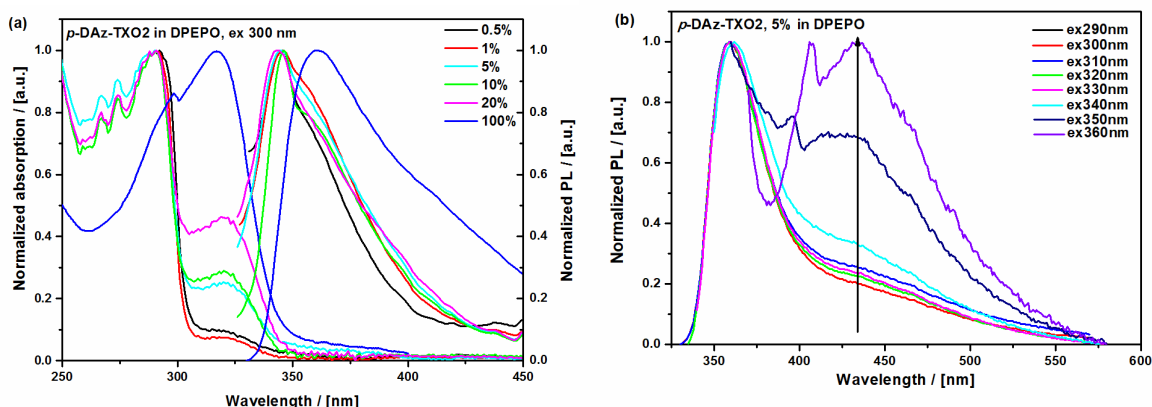


Figure S14. Phosphorescence spectra of *p*-DAz-TXO2 recorded in hosts of different polarity (Nd-YAG laser, $\lambda_{\text{ex}} = 355$ nm). BCPO is 9,9'-(4,4'-(phenylphosphoryl)bis(4,1-phenylene))bis(9*H*-carbazole).

S4. Possibility of the ground state dimers

The possible presence of ground state dimers of the azepine derivatives *p*- and *m*-DAz-TXO2 was investigated by concentration dependent studies. Solid-state films (Zeonex and DPEPO) of *p*-DAz-TXO2 were chosen for the investigation. With the increasing concentration the LEB enhancement can be observed for *p*-DAz-TXO2 dispersed both in DPEPO (Figure S15) and Zeonex (Figure S16). However, the steady-state PL, which features the vibronic structure in the case of both Zeonex and DPEPO films, does not show drastic changes with the increase of concentration, which would be expected for the dimeric species. The red shift of the neat film emission can be attributed solely to the change of the dipole moment of the film. Interestingly, the steady-state PL of the DPEPO film shows dependence on the excitation wavelength: the higher the excitation wavelength, the more intense is the PL of the low energy peak (Figure S15 (b)). We assume that direct excitation of the CT state is facilitated at lower energies. Examination of the time-resolved spectra of the DPEPO films (Figure S15 (c-e)) suggests the presence of several conformers in the PF. A similar situation was observed in Zeonex (Figure S16). The DF was observed in DPEPO films at all concentrations of the dopant. Noteworthy, the intensity of the DF increased with the increase of the guest concentration, being the most intense in the neat film. Additionally, the DF of the neat film is red-shifted by 10-20 nm compared to the DF of DPEPO films at various concentrations. The above results lead us to speculate that the intensity of the conformers with higher CT character giving rise to the DF strongly depends on the polarity of the surrounding media (as was observed in solvatochromism, Figures 4 (c) and S9 (a)). While no DF can be observed in non-polar Zeonex, the DF is present in DPEPO.

Concentration tests were also carried out in solutions (Figure S17). Similarly to the solid state, the increase of LEB intensity was observed in absorption with the increase of concentration; however, only a minor red shift occurs in emission with the spectral profile retained. Given the molecular packing in the crystals of the azepine derivatives (Figure S1), where the distance between the donors is much longer than described in the literature for a simple azepine system,⁶ we further conclude that for the current compounds the presence of dimers is unlikely.



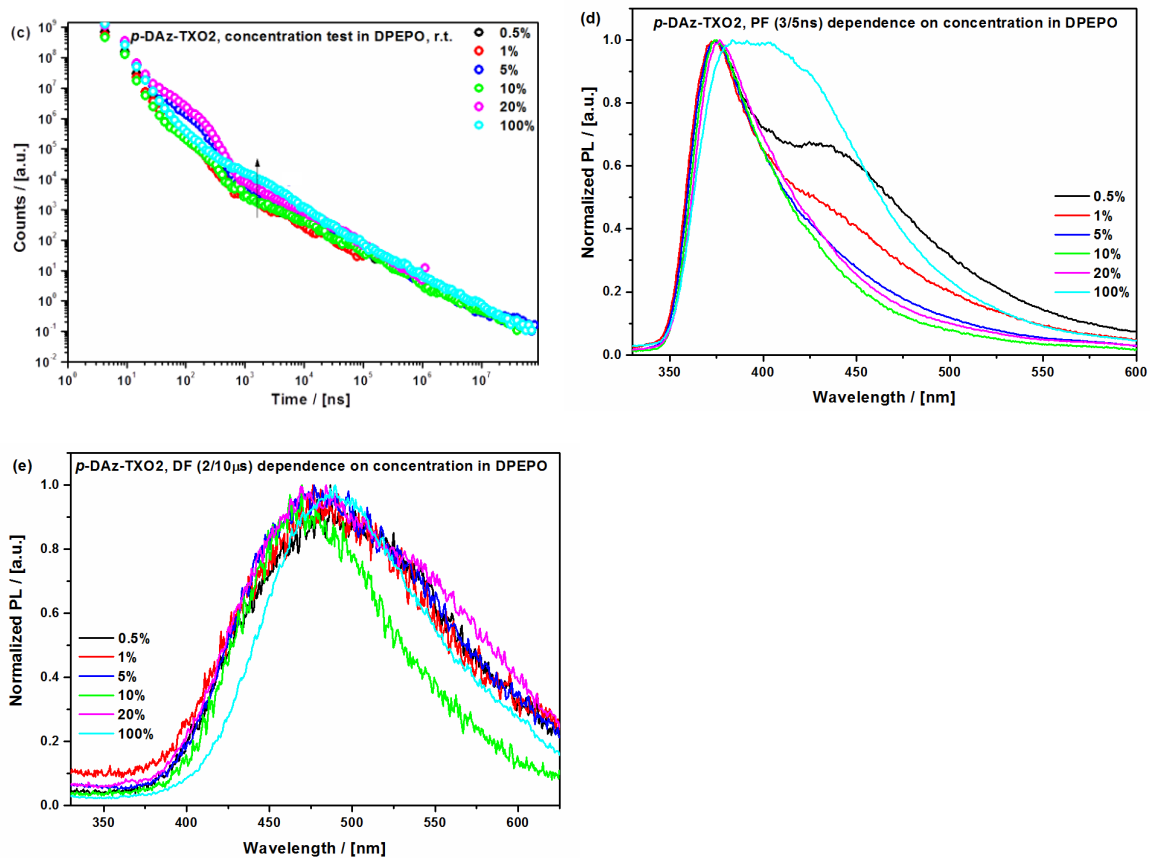
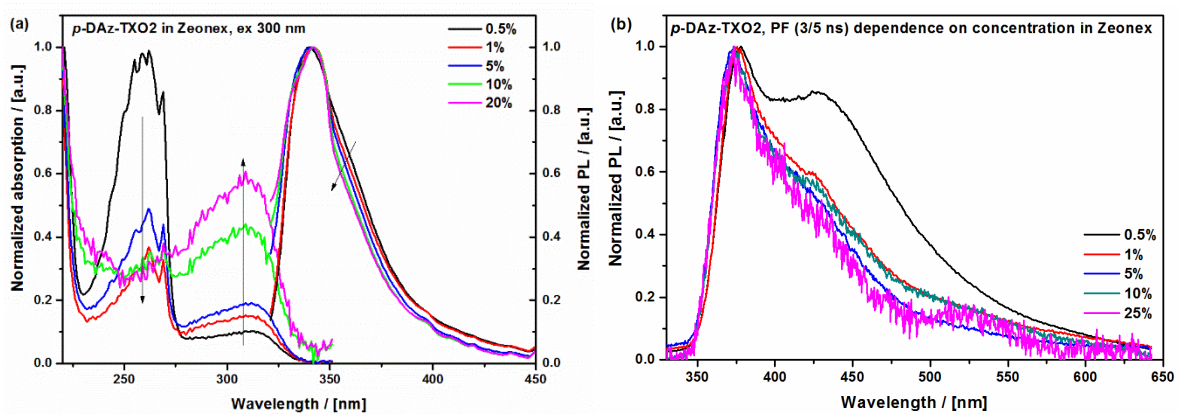


Figure S15. (a) Absorption and SS-PL; (b) PL decay curves; (c) decays; (d) PF; (e) DF of *p*-DAz-TXO2 at various concentrations in DPEPO.



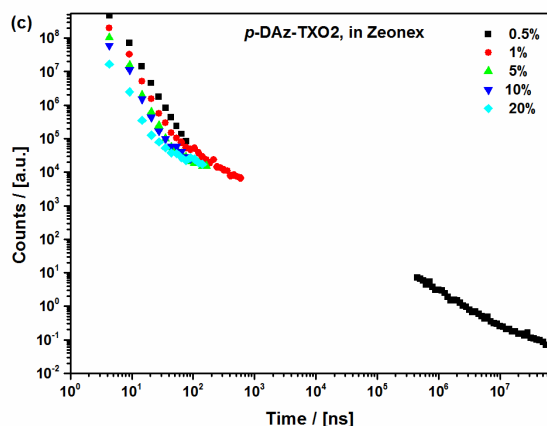


Figure S16. (a) Dependence of the absorption (left) and photoluminescence (right) of *p*-DAz-TXO2 on the concentration in Zeonex; (b) PF; (c) PL decay curves of *p*-DAz-TXO2 at various concentrations in Zeonex.

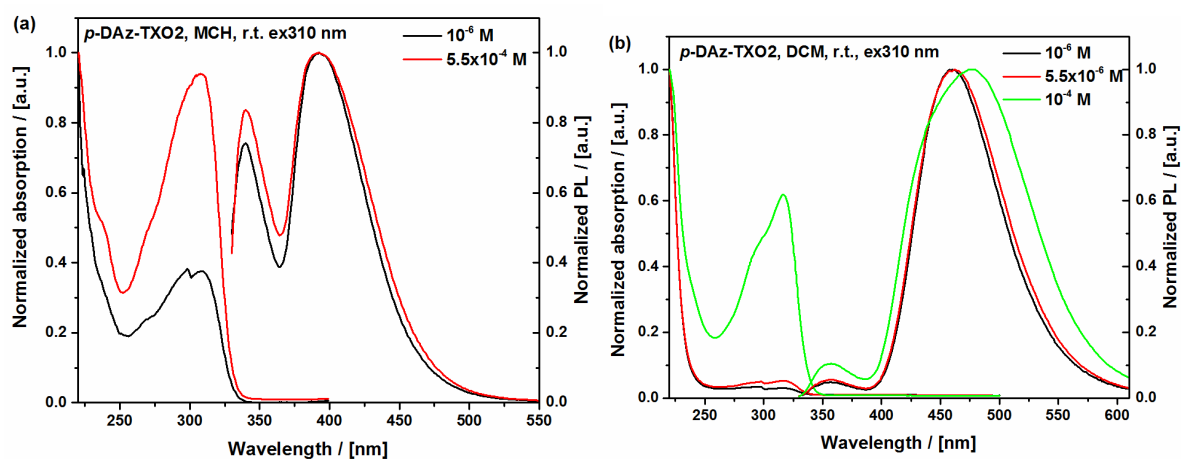


Figure S17. Dependence of the absorption (left) and photoluminescence (right) of *p*-DAz-TXO2 on the concentration in (a) MCH; (b) DCM.

S4. Computational atomic coordinates (xyz).

1. *p*-DAz-TXO2

0 1

C	-3.55240500	-1.24770200	-1.63444800
C	-2.43446500	-1.98935100	-2.03278000
C	-1.31933700	-2.01665300	-1.19506700
C	-1.22173200	-1.32883300	0.02902700
C	-2.35714200	-0.57593000	0.38936800
C	-3.50610000	-0.53991800	-0.42179300
C	0.04821500	-1.40186400	0.91851100
C	1.32407000	-1.24308200	0.04882700
C	1.48664100	-1.92339500	-1.17325700
C	2.61050300	-1.82182900	-1.99319900

C	3.66774700	-1.00222900	-1.58155800
C	3.55794600	-0.30457400	-0.36778000
C	2.40464400	-0.42372900	0.43035400
H	-4.44205400	-1.19537000	-2.25564900
H	-2.40563600	-2.52724100	-2.97767400
H	-2.37443900	0.00542900	1.30381700
H	4.56249500	-0.89227900	-2.18765900
H	2.37099700	0.15781900	1.34427100
C	0.00319100	-0.32515900	2.03169200
H	0.87673300	-0.42837600	2.68444200
H	-0.01978300	0.69435000	1.62593400
H	-0.87901800	-0.47879300	2.66224600
C	0.08764600	-2.79870300	1.63637800
H	0.12087100	-3.63458800	0.92831000
H	0.97659500	-2.84329000	2.27935800
H	-0.80662600	-2.90177900	2.26487400
S	0.12293300	-3.00165900	-1.79812900
H	2.62797800	-2.35316600	-2.94209800
O	0.13478000	-2.96310700	-3.43533000
O	0.16646900	-4.50008400	-1.11811200
N	-4.63999200	0.24252600	0.00850600
C	-4.90388700	1.42838100	-0.75294600
C	-5.35912700	-0.32549200	1.11400300
C	-6.08982800	2.21521200	-0.66867700
C	-3.90202400	1.85156100	-1.67016200
C	-6.14653400	0.41892300	2.03332200
C	-5.23833000	-1.72483500	1.32369800
C	-6.23831100	3.31840000	-1.53371400
C	-7.15312100	2.01806400	0.39497100
C	-4.08255900	2.94802300	-2.51745800
H	-2.96228500	1.31703200	-1.72549900
C	-6.73734000	-0.24774100	3.12438200
C	-6.49662500	1.87119100	1.79880300
C	-5.82805000	-2.35981200	2.42091400
H	-4.67992100	-2.32707300	0.61637500
C	-5.26977700	3.68767600	-2.47158500
H	-7.15113800	3.90534800	-1.44663700
H	-7.77504600	1.13200000	0.20339800
H	-7.82043200	2.88928900	0.37811600
H	-3.28440900	3.21970400	-3.20458700
H	-7.34184900	0.34172500	3.81183200
C	-6.57613100	-1.61980800	3.34533700
H	-7.19315300	2.19751600	2.58145700
H	-5.61492300	2.52569700	1.85137100
H	-5.70680200	-3.43407600	2.53876500
H	-5.42850000	4.54009100	-3.12670800
H	-7.03743800	-2.09956800	4.20465500
N	4.62165900	0.56921600	0.06577300
C	5.82460200	-0.09223300	0.48105400
C	4.30905800	1.96817600	-0.00276900

C	7.09295700	0.53566900	0.63961600
C	5.74460400	-1.48810800	0.73874600
C	4.96748200	2.98684300	0.74095900
C	3.24020000	2.35910700	-0.85400500
C	8.20735100	-0.25531400	0.98279100
C	7.28312100	2.03799800	0.59568300
C	6.86998800	-2.24739300	1.07158900
H	4.78674100	-1.99036400	0.67887900
C	4.50443900	4.31360100	0.64248500
C	6.23991900	2.73277900	1.51966700
C	2.79696600	3.68322000	-0.92541400
H	2.74883000	1.62007900	-1.47553500
C	8.12552900	-1.63725000	1.18045000
H	9.16473300	0.24925700	1.10224300
H	7.17870500	2.44085200	-0.42184800
H	8.30177200	2.26867900	0.93241500
H	6.75356400	-3.31366100	1.25145100
H	5.02870300	5.07527900	1.21723400
C	3.41800200	4.67769400	-0.15967100
H	6.62861800	3.69457700	1.87765200
H	6.07075200	2.10023100	2.40258600
H	1.97207200	3.92922700	-1.59017600
H	9.01098900	-2.21446300	1.43284500
H	3.08173100	5.71032400	-0.20087400

2. *m*-DAz-TXO2

0 1

C	-3.62169600	-0.27603700	0.41076000
C	-2.52343900	-0.51990200	-0.43303400
C	-1.40201700	-1.15484400	0.09557500
C	-1.25811900	-1.55832700	1.43514200
C	-2.36578800	-1.27440300	2.26262500
C	-3.52027200	-0.65549400	1.76018600
C	0.01630700	-2.27737400	1.95253000
C	1.29469000	-1.58669000	1.40815500
C	1.41179700	-1.17255600	0.07004100
C	2.53080100	-0.55507100	-0.48346000
C	3.64870400	-0.32059400	0.33614000
C	3.58444800	-0.73593200	1.67867500
C	2.43586600	-1.34590800	2.20414300
H	-2.51923600	-0.19471000	-1.47093700
H	-2.33604100	-1.53116600	3.31536900
H	2.43345300	-1.62018900	3.25291400
C	0.03239600	-2.31526800	3.50124000
H	0.90673100	-2.87395100	3.85190200
H	0.04968700	-1.30980000	3.94118500
H	-0.84821600	-2.85214200	3.87014100
C	-0.00635300	-3.76881700	1.45940900
H	-0.01656100	-3.84560400	0.36643900

H	0.88342300	-4.28559500	1.84271300
H	-0.90171400	-4.26405400	1.85782700
S	-0.00720200	-1.43558100	-1.08541300
H	2.52048700	-0.26930100	-1.53164700
O	-0.00722500	-0.23470900	-2.19971300
O	-0.02356600	-2.96758400	-1.68788200
H	-4.35961700	-0.45274400	2.42077100
H	4.44752600	-0.56402000	2.31718400
N	-4.82954700	0.34334500	-0.06082800
C	-5.79004800	-0.51986500	-0.69367900
C	-4.95202600	1.76665300	0.03872700
C	-7.11550800	-0.58319200	-0.20907700
C	-5.39957500	-1.35405000	-1.76036000
C	-6.18205500	2.45296800	0.24409100
C	-3.75986300	2.52965700	-0.05752100
C	-8.02784600	-1.46055100	-0.82285000
C	-7.54468600	0.33762400	0.91035100
C	-6.31447300	-2.23909400	-2.34678100
H	-4.38136300	-1.31301800	-2.13416100
C	-6.15415500	3.86383100	0.31074300
C	-7.55536800	1.80770100	0.42885400
C	-3.76519400	3.92336300	0.02838800
H	-2.81639100	2.01742800	-0.21382300
C	-7.63682900	-2.29214000	-1.88139800
H	-9.05101400	-1.49665300	-0.45173100
H	-6.86811700	0.24096500	1.77238400
H	-8.55227700	0.06136900	1.24746000
H	-5.99365400	-2.87415000	-3.16898700
H	-7.09943600	4.38201300	0.46897800
C	-4.97606800	4.60742300	0.20522300
H	-8.10971200	2.41983200	1.15471800
H	-8.12081200	1.85181700	-0.51562100
H	-2.82727200	4.46756600	-0.05561900
H	-8.35350800	-2.97175000	-2.33624500
H	-5.00123000	5.69239900	0.26755500
N	4.83411900	0.32647400	-0.14957000
C	4.80212700	1.75707000	-0.29458100
C	5.94776100	-0.49470200	-0.52049900
C	5.72787800	2.55218100	0.41797300
C	3.82464300	2.37787400	-1.09708000
C	7.30941900	-0.13434900	-0.32361000
C	5.65376000	-1.75144100	-1.10813000
C	5.67010000	3.95163400	0.29148700
C	6.79893100	1.88035300	1.24769700
C	3.76543500	3.77547300	-1.19412200
H	3.11050000	1.77641900	-1.65003200
C	8.30519900	-1.03967100	-0.75419400
C	7.81438800	1.14757000	0.33908900
C	6.66144900	-2.63234100	-1.50585500
H	4.61615500	-2.03092200	-1.26280000

C	4.69274700	4.56828000	-0.50229800
H	6.39305400	4.55855500	0.83458500
H	6.34803500	1.15917000	1.94519200
H	7.32908200	2.63348500	1.84510400
H	3.00388000	4.23665800	-1.81838000
H	9.34667300	-0.75778100	-0.60248400
C	8.00702700	-2.27353500	-1.33831000
H	8.70171400	0.88317200	0.93253800
H	8.15361500	1.85663200	-0.43307200
H	6.39255100	-3.58563800	-1.95498800
H	4.65627300	5.65241200	-0.57896700
H	8.80592700	-2.94283800	-1.64775000

3. *p*-DDPA-TXO2

0 1

C	3.54120500	-1.93027100	0.51067100
C	2.41098400	-2.73609800	0.36101500
C	1.29460400	-2.22658800	-0.30139900
C	1.22016800	-0.91851300	-0.81811300
C	2.36223300	-0.12025000	-0.63584000
C	3.52534400	-0.61012300	0.00839700
C	-0.04783500	-0.39543900	-1.54822100
C	-1.32820000	-0.81014300	-0.77347000
C	-1.50249700	-2.11400800	-0.27113600
C	-2.64296900	-2.53528300	0.41253500
C	-3.68945800	-1.63412100	0.61297000
C	-3.57118000	-0.31137600	0.12919700
C	-2.39335900	0.07984400	-0.55493100
H	4.42474300	-2.31264900	1.01164300
H	2.38169800	-3.74956400	0.75401200
H	2.36864800	0.90743700	-0.97616200
H	-4.58011900	-1.93983900	1.15230400
H	-2.33147800	1.10121600	-0.90711800
C	0.01408000	1.14110000	-1.73493100
H	-0.85671600	1.48307700	-2.30461000
H	0.04408000	1.67662900	-0.77748900
H	0.89749300	1.41099400	-2.32324800
C	-0.09791700	-1.02435200	-2.98709400
H	-0.13935900	-2.11924300	-2.96568300
H	-0.98589800	-0.64565000	-3.51051700
H	0.79734900	-0.71425500	-3.54232300
S	-0.15391000	-3.35301300	-0.45955500
H	-2.68155600	-3.54758500	0.80826800
O	-0.18511500	-4.36407700	0.82993400
O	-0.19437700	-4.09056400	-1.93206100
N	4.65249800	0.22787600	0.15931100
C	5.49239100	0.10912900	1.31036200
C	4.98208400	1.19197200	-0.84255000
C	6.89464800	0.12295300	1.16869900
C	4.92528800	-0.00929100	2.59596900

C	5.38568600	2.49014500	-0.46921900
C	4.92400500	0.84975200	-2.20964700
C	7.71487500	0.02299900	2.30117800
C	5.75328500	-0.12540000	3.72084100
H	3.84356400	-0.01310800	2.70502900
C	5.72820000	3.42865500	-1.45267000
C	5.25236700	1.80012200	-3.18626400
H	4.62559600	-0.15505300	-2.49798300
C	7.15078500	-0.10606900	3.58099500
H	8.79577600	0.03351500	2.18027400
H	5.30469200	-0.21817900	4.70728000
H	6.04003600	4.42649200	-1.15243900
C	5.65913700	3.09216300	-2.81444600
H	5.20532400	1.52330400	-4.23701800
H	7.79032800	-0.19127300	4.45596600
H	5.92084300	3.82434200	-3.57437700
N	-4.61139000	0.62145500	0.33281700
C	-5.97345400	0.18984600	0.38711000
C	-4.32300800	2.01090000	0.50468800
C	-6.83534200	0.69726500	1.38010300
C	-6.46933800	-0.73176800	-0.55744000
C	-5.09406900	2.98007800	-0.16818800
C	-3.28083600	2.42478500	1.35977900
C	-8.17554100	0.28855800	1.42225200
C	-7.80664300	-1.14734300	-0.49751200
H	-5.80721700	-1.11763000	-1.32873800
C	-4.82388800	4.34332700	0.01460800
C	-3.00716400	3.78962900	1.52366600
H	-2.69508100	1.67711000	1.88897900
C	-8.66754600	-0.63799700	0.48860600
H	-8.83054000	0.68710300	2.19373800
H	-8.17715300	-1.86005400	-1.23076100
H	-5.42639300	5.08219800	-0.50899500
C	-3.77729700	4.75585700	0.85535400
H	-2.20046100	4.09672300	2.18558600
H	-9.70564000	-0.95822900	0.52808000
H	-3.56584700	5.81392200	0.98938500
H	7.32973700	0.21246500	0.17662000
H	5.43241100	2.75210400	0.58468600
H	-5.89997900	2.65869800	-0.82317000
H	-6.45111100	1.40712200	2.10821800

4. *m*-DDPA-TXO2

0 1

C	3.65055700	-0.46904500	-0.19738700
C	2.52888700	-0.05737900	0.55413900
C	1.40984100	-0.88210700	0.58827900
C	1.27643400	-2.11449200	-0.07524200
C	2.41075400	-2.49084400	-0.82709600
C	3.56263300	-1.69724400	-0.89022100

C	0.00002300	-2.98814400	0.03314500
C	-1.27639100	-2.11449900	-0.07526000
C	-1.40981400	-0.88210800	0.58824600
C	-2.52885700	-0.05737800	0.55407500
C	-3.65052100	-0.46904800	-0.19746200
C	-3.56257900	-1.69726100	-0.89027700
C	-2.41069900	-2.49085600	-0.82712800
H	2.51209300	0.88789900	1.09117200
H	2.40082100	-3.41215600	-1.39884500
H	-2.40076100	-3.41217000	-1.39887200
C	0.00003200	-4.08984000	-1.05704000
H	-0.87806200	-4.73372100	-0.93749900
H	0.00004100	-3.66948500	-2.07112100
H	0.87811800	-4.73372700	-0.93748400
C	0.00002200	-3.72084600	1.42273300
H	0.00002100	-3.01557100	2.26175400
H	-0.89299300	-4.35628200	1.49372100
H	0.89303400	-4.35628600	1.49372200
S	0.00000000	-0.25980200	1.61291600
H	-2.51207100	0.88790300	1.09110000
O	0.00000900	1.37701600	1.57725000
O	-0.00003000	-0.94450300	3.11053400
H	4.40497000	-2.02860500	-1.49059100
H	-4.40490600	-2.02863100	-1.49065700
N	4.81865000	0.32037000	-0.26014100
C	6.10016700	-0.30011700	-0.37922700
C	4.74156300	1.74586500	-0.18287500
C	7.05719300	0.22288200	-1.27258900
C	6.42519400	-1.42749600	0.40304000
C	5.66200500	2.45859000	0.61199700
C	3.75861000	2.45016700	-0.90712300
C	8.32166500	-0.37312600	-1.37591500
C	7.68637700	-2.02706200	0.28050400
H	5.69227900	-1.82349500	1.10165500
C	5.60114500	3.85721700	0.67238300
C	3.69403100	3.84796000	-0.82580000
H	3.04825300	1.90276400	-1.52171000
C	8.64219600	-1.50279400	-0.60535600
H	9.05258300	0.04202400	-2.06617400
H	7.92556900	-2.89486100	0.89102400
H	6.31634600	4.39587900	1.28995700
C	4.61640200	4.55928800	-0.04176800
H	2.92583600	4.37931100	-1.38256500
H	9.62256000	-1.96500900	-0.69039400
H	4.56674000	5.64379000	0.01441300
N	-4.81861700	0.32034500	-0.26024800
C	-4.74159100	1.74583800	-0.18278100
C	-6.10012800	-0.30015600	-0.37936600
C	-3.75868000	2.45027200	-0.90696100
C	-5.66206400	2.45841900	0.61217100

C	-7.05714100	0.22285500	-1.27272900
C	-6.42515600	-1.42753800	0.40290300
C	-3.69416400	3.84805300	-0.82546800
C	-5.60126800	3.85704700	0.67273100
H	-6.41613100	1.91365500	1.17424200
C	-8.32162200	-0.37314400	-1.37606300
C	-7.68634100	-2.02708800	0.28036300
H	-5.69222100	-1.82353300	1.10150100
C	-4.61656000	4.55924500	-0.04133600
H	-2.92600100	4.37950700	-1.38217900
H	-6.31648700	4.39559700	1.29038100
H	-9.05253600	0.04200900	-2.06632500
C	-8.64215300	-1.50280600	-0.60550400
H	-7.92555600	-2.89488500	0.89087400
H	-4.56694700	5.64374300	0.01497400
H	-9.62251700	-1.96502200	-0.69053800
H	-6.80590200	1.09324700	-1.87338500
H	-3.04831300	1.90296800	-1.52162700
H	6.80597400	1.09327400	-1.87325300
H	6.41609700	1.91392600	1.17413100

5. *p*-DDMAc-TXO2

0 1

C	3.63539500	-1.31229300	1.69819100
C	1.37599600	-2.06439400	1.30899100
C	1.27369600	-1.35869400	0.09179100
C	2.40709500	-0.61979300	-0.28650900
C	3.57109500	-0.60099300	0.49599100
C	-0.00000400	-1.41449500	-0.78740900
C	-1.27370400	-1.35869600	0.09179100
C	-1.37600400	-2.06439600	1.30899100
C	-3.63540500	-1.31229700	1.69819100
C	-3.57110500	-0.60099700	0.49599100
C	-2.40710500	-0.61979600	-0.28650900
H	2.41289500	-0.02919300	-1.19650900
H	-2.41290500	-0.02919600	-1.19650900
C	-0.00000500	-0.27249500	-1.83080900
H	-0.87660500	-0.35789500	-2.48120900
H	-0.00000600	0.72050500	-1.36380900
H	0.87659500	-0.35789400	-2.48120900
C	-0.00000400	-2.75799500	-1.59000900
H	-0.00000300	-3.63179500	-0.93270900
H	-0.89120400	-2.79649600	-2.22980900
H	0.89129600	-2.79649400	-2.22980900
S	-0.00000300	-3.05469500	1.90909100
C	2.51939600	-2.04099300	2.11279100
C	-2.51940400	-2.04099700	2.11279100
H	-2.51730400	-2.58049700	3.05739100
H	2.51729600	-2.58039300	3.05739100
O	-0.00000300	-4.35129500	1.24179100

O	-0.00000300	-3.02129500	3.36359100
H	4.54159500	-1.27629200	2.29819100
H	-4.54160500	-1.27629800	2.29819100
N	-4.69280500	0.16990200	0.06059100
C	-5.64540500	-0.43099800	-0.77890900
C	-4.81020600	1.50400200	0.48389100
C	-5.47760400	-1.77449800	-1.18400900
C	-6.77410600	0.29460100	-1.22190900
C	-5.91230700	2.29190100	0.08129100
C	-3.81890700	2.06930300	1.31859100
C	-6.40900400	-2.39259900	-2.01610900
H	-4.61470400	-2.33589800	-0.84070900
C	-7.69220500	-0.36080000	-2.05830900
C	-7.03750600	1.75200100	-0.81420900
C	-5.97680800	3.61970100	0.53489100
H	-2.97130600	1.47060300	1.63489100
C	-3.91540700	3.39150300	1.74809100
C	-7.52950400	-1.68660000	-2.46300900
H	-6.25310300	-3.42869900	-2.31080900
H	-8.56700500	0.18820000	-2.40200900
C	-8.38330600	1.82380000	-0.03500900
C	-7.14020700	2.63220100	-2.09360900
C	-5.00000800	4.18170200	1.35799100
H	-6.82500800	4.23110100	0.23279100
H	-3.13610800	3.79860300	2.38969100
H	-8.26540400	-2.15750000	-3.11070900
H	-8.60780700	2.85630000	0.26129100
H	-9.21190600	1.45939900	-0.65550900
H	-8.33440600	1.20790000	0.87149100
H	-7.95480700	2.28590000	-2.74170900
H	-7.34140800	3.67820000	-1.83140900
H	-6.20400700	2.59280100	-2.66400900
H	-5.08630900	5.21460200	1.68749100
N	4.69279500	0.16990800	0.06059100
C	4.81019400	1.50400800	0.48389100
C	5.64539500	-0.43099100	-0.77890900
C	3.81899300	2.06930700	1.31859100
C	5.91239300	2.29190900	0.08129100
C	6.77409400	0.29460900	-1.22190900
C	5.47759600	-1.77449200	-1.18390900
C	3.91549300	3.39150800	1.74809100
H	2.97129400	1.47060700	1.63499100
C	5.97679200	3.61970900	0.53489100
C	7.03749400	1.75200900	-0.81430900
C	7.69219500	-0.36079000	-2.05830900
H	4.61469600	-2.33589200	-0.84060900
C	6.40899600	-2.39269100	-2.01610900
C	5.00009200	4.18170800	1.35799100
H	3.13609200	3.79860700	2.38969100
H	6.82509200	4.23110900	0.23279100

C	8.38329400	1.82381000	-0.03500900
C	7.14009300	2.63221000	-2.09360900
C	7.52949600	-1.68669000	-2.46290900
H	8.56699500	0.18811000	-2.40200900
H	6.25309700	-3.42879100	-2.31070900
H	5.08629100	5.21460800	1.68749100
H	9.21189400	1.45951100	-0.65560900
H	8.60779300	2.85631000	0.26119100
H	8.33449400	1.20791000	0.87139100
H	7.34119200	3.67821000	-1.83140900
H	7.95469300	2.28601000	-2.74170900
H	6.20399300	2.59270900	-2.66410900
H	8.26549600	-2.15759000	-3.11060900

References

- (1) Fulmer, G. R.; Miller, A. J. M.; Sherden, N. H.; Gottlieb, H. E.; Nudelman, A.; Stoltz, B. M.; Bercaw, J. E.; Goldberg, K. I. NMR Chemical Shifts of Trace Impurities: Common Laboratory Solvents, Organics, and Gases in Deuterated Solvents Relevant to the Organometallic Chemist. *Organometallics* **2010**, *29*, 2176–2179.
- (2) dos Santos, P. L.; Ward, J. S.; Data, P.; Batsanov, A. S.; Bryce, M. R.; Dias, F. B.; Monkman, A. P. Engineering the Singlet-Triplet Energy Splitting in a TADF Molecule. *J. Mater. Chem. C* **2016**, *4*, 3815–3824.
- (3) Emslie, D. J. H.; Blackwell, J. M.; Britten, J. F.; Harrington, L. E. A Zwitterionic Palladium(II) H₃-Boratoxypentadienyl Complex: Cooperative Activation of Dibenzylideneacetone Between Palladium and a Phosphine/Thioether/Borane Ligand. *Organometallics*, **2006**, *25*, 2412–2414.
- (4) dos Santos, P. L.; Ward, J. S.; Data, P.; Batsanov, A.; Bryce, M. R.; Dias, F.; Monkman, A. P. Engineering the Singlet-Triplet Energy Splitting in a TADF Molecule. *J. Mater. Chem. C* **2016**, *4*, 3815–3824.
- (5) Polymer Containing Dibenzo Six-Membered Sulfonyl Condensed Ring Unit and Application Thereof. CN 201611125565. **2016**.
- (6) Sun, C.; Ran, X.; Wang, X.; Cheng, Z.; Wu, Q.; Cai, S.; Gu, L.; Gan, N.; Shi, H.; An, Z.; et al. Twisted Molecular Structure on Tuning Ultralong Organic Phosphorescence. *J. Phys. Chem. Lett.* **2018**, *9*, 335–339.